6-29-2018

System Modeling, Performance Evaluation, and Control of Battery System Charge Balance

Weiji Han
University of Connecticut - Storrs, weiji.han@uconn.edu

System Modeling, Performance Evaluation, and Control of Battery System Charge Balance

Weiji Han, Ph.D.

University of Connecticut, 2018

ABSTRACT

As the major energy storage device and power supply source in numerous energy applications, battery systems often face the issue of charge imbalance among battery cells/modules/packs, which can accelerate battery degradation, cause more energy loss, and even incur fire hazard. This thesis is focused on the system modeling, performance evaluation, and control of battery systems with various charge balancing circuits. Specifically, based on the proposed mathematical models for battery charge equalization systems, computationally efficient methods are developed to estimate the evolution of battery state of charge and to evaluate critical system performance measures. Then, near-optimal battery cell/module reconfiguration algorithms are proposed to expedite the battery charge equalization process. Besides, for the battery power modules, a new current allocation method based on charging/discharging spaces is derived for the coordinated control of module charge balance and total power efficiency. Extensive numerical experiments are carried out and the results are compared with those obtained from computer simulations and/or circuit experiments to justify the estimation accuracy and computational efficiency of the proposed methods.

System Modeling, Performance Evaluation, and Control of Battery System Charge Balance

Weiji Han

M.E., University of Connecticut, 2015

B.E., Shandong University, 2009

A Dissertation

Submitted in Partial Fulfillment of the

Requirements for the Degree of

Doctor of Philosophy

at the

University of Connecticut

2018

APPROVAL PAGE

Doctor of Philosophy Dissertation

System Modeling, Performance Evaluation, and Control of Battery System Charge Balance

Presented by

Weiji Han, B.E., M.E.

Major Advisor _____
Liang Zhang

Associate Advisor _____
Shalabh Gupta

Associate Advisor _____
Peng Zhang

University of Connecticut

2018

ACKNOWLEDGMENTS

Firstly, I would like to express my sincere gratitude to my advisor Prof. Liang Zhang for the continuous support of my Ph.D study and related research, as well as his great patience and immense knowledge.

Besides, I would like to thank the rest of my thesis committee: Prof. Gupta and Prof. Peng Zhang, for their insightful comments and encouragement, which help me widen my research from various perspectives.

My sincere thanks also goes to Prof. Luh, who provided me the opportunity to join his team and start my Ph.D. study in UCONN, and Prof. Bazzi, who helped me a lot on the research of photovoltaic systems.

Last but not the least, I would like to thank my parents, my wonderful wife, and two cute daughters for supporting me spiritually throughout the Ph.D. study and my life in general. Again, special gratitude is given to my wife. Without her great patience, tolerance, encouragement, support, and love in past years, I could have accomplished nothing.

Contents

Chapter 1

Mathematical modeling, performance evaluation, and control of battery system charge balance: review and recent developments

1.1 Introduction

The battery system is one of the key components in a number of modern power applications, such as electric vehicles (EVs), wind and solar power systems. For example, in the EVs, the battery system not only provides power to the engine but also maintains the normal operation of all on-board electronic appliances, e.g., audio/video systems, air-conditioning. Besides, as the most important resource for energy storage, an increasing number of large-scale battery systems are being applied to various grid-level services/uses such as electric energy time shift, microgrid capability, distri-

bution upgrade due to solar/wind energy penetration, and electric vehicle charging [1, 2, 3]. According to the global energy storage database run by the U.S. Department of Energy, a total of 309 operational battery energy storage projects in the U.S. were providing 692 MW rated power in 2017 [1]. In order to meet the high total voltage/current/capacity requirements, battery cells/modules/packs are usually connected in series and/or parallel in these large-scale battery systems. For example, one of these energy storage projects is the world's largest lithium-ion battery storage facility consisting of 400,000 batteries installed in about 20,000 modules and placed in 24 containers [4].

However, charge imbalance among battery cells/modules/packs is a very common issue, which may lead to serious problems in power efficiency, equipment reliability and safety, etc. In general, battery charge imbalance could be caused by internal or external factors [5, 6, 7, 8], such as manufacturing variations in physical volume, internal impedance, and self-discharging rate. Besides, the uneven thermal distribution across battery packs is another important factor. Due to the charge imbalance, individual battery cell voltages gradually differ over time and the available charge capacity of battery cells decreases quickly, which may even result in the failure of the entire battery system [9].

In order to alleviate the charge imbalance in a battery system, a number of circuit modules, referred to as *battery charge equalizers/balancer*, are developed and connected to the battery cells to form the *battery charge equalization (BCE) system*. The operation of the BCE system is usually controlled by the battery management system [10]. For the design of equalizers/balancers, two types of methods have been proposed: passive and active balancing. Based on these methods, various kinds of equalizers have been developed and summarized in [9, 11, 12, 13, 14, 15, 16]. Of all

the structures of BCE systems developed, a simple but widely-used one is the series-connected battery charge equalization (BCE) structure. In this structure, every two adjacent cells are connected with one equalizer. Each equalizer monitors the status of two adjacent cells and transfers charge from the one with higher state of charge (SOC) to the other one (see [17, 18, 19]), where the cell's SOC is usually defined as the ratio of the cell's remaining amount of charge and its rated charge capacity.

To further review the recent research contribution and development about the modeling, evaluation, and control of BCE systems from the system level, we conduct extensive review in [20]. The remainder of this chapter is organized as follows: In Section 1.2, we discuss the results on mathematical and computer modeling of BCE systems. Then the system performance evaluation and control strategies of BCE systems are reviewed in Section 1.3 and Section 1.4, respectively. Finally, the research framework of this thesis is given in Section 1.5.

1.2 Modeling of battery charge equalization systems

Developing a reliable mathematical or computer model of the physical system at hand is of critical importance in engineering research and development. The model developed can be used for verification and validation of product concept and design even before they are put into prototypes. In Systems and Control, a mathematical model for the system under consideration must be developed first before any quantitative analysis can be carried out, such as parameter design, optimization, and feedback control. In the cases, where an analytical model is all but impossible to derive, computer simulation models can be used as an alternative. The model constructed should

be able to qualitatively and quantitatively characterize the dynamics and statics of the system. Since modeling is the foundation for all types of rigorous quantitative analysis, we devote the first technical section of this chapter to review the results on this topic.

1.2.1 Circuit analysis-based modeling

Since BCE systems are naturally electrical circuit systems, direct circuit analysis techniques have been applied to derive their mathematical models. This approach typically uses an equivalent circuit model to describe each battery cell (e.g., simple capacitor model, capacitor-resistor model). Then, based on the operating modes of the circuit (e.g., the state of the switches), a set of differential equations are derived to characterize the behavior of the system during specific periods of time. This approach is straightforward and is used in the majority of results reported in the literature. Its advantage is that the resulting formulas can characterize the dynamics of the circuit systems in great details, thus, allowing design engineers to directly relate the parameters of the electronic components with the circuit performance. The drawback of this approach is also obvious: it is typically applicable for small-size systems. In fact, most of the results obtained following this approach only apply to two-cell systems. For larger size systems, complete circuit analysis of the entire system is usually very complex and, thus, is only carried out under certain restrictive conditions.

For instance, paper [7] performs the circuit analysis of BCE system with switching super capacitors and creates a model that only applies to the operation of two adjacent cells, while no analysis of the entire system operation is carried out. In addition,

assuming each cell as an ideal capacitor and constant input and output currents within the system, paper [19] models the equalization process when only one cell is undercharged. In paper [21], circuit analysis is carried out to describe the dynamics of two cells through the operation of the equalizer in between and to derive the condition for ripple-free inductor current. Although the paper later studies a three-cell system as an experiment, no analytical results beyond the two-cell system are reported. Similar approach is also used in [22], which proposes a 4-cell BCE system and derives the circuit model assuming the voltage of each cell remains constant during one switching period. Based on the model, feasible range of the duty cycle is obtained to ensure that the current of the inductor reaches zero by the end of a switching cycle. In addition, paper [23] uses a similar approach to study the relationship between the duty ratios of the dc-dc converters and the balancing currents to the battery cells. Papers [24, 25] perform a complete circuit analysis of a two-cell BCE system with bi-directional C$\hat{u}$k converter and obtain the close-form formulas for the balancing circuits. Finally, paper [26] studies the topology of BCE systems based on the graph theoretic properties. It is assumed that the charge transfers are implemented using an intermediate transformer. Then, differential equations describing the dynamics of individual cells and those describing the charge transfers are derived. To illustrate the typical analysis performed using this approach, the circuit diagram studied in [24, 25] is given in Figure 1.2.1 and the solution of currents $i_1(t)$ and $i_2(t)$ derived in [24] are given below:

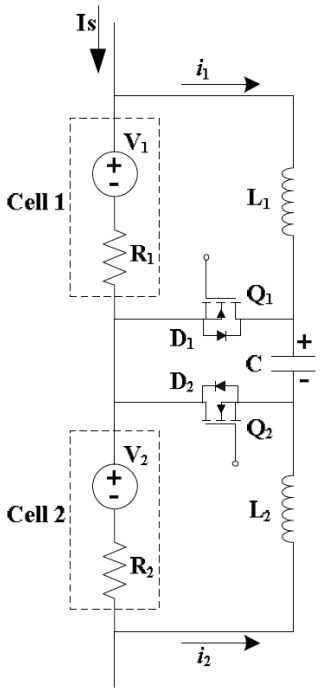

FIGURE 1.2.1: Illustration of circuit analysis-based BCE modeling.

$$i_1(t) = \begin{cases} \frac{V_1}{R_1} - \frac{V_1}{R_1} e^{-\frac{R_1}{L_1}t}, & t \in [0, T_0], \\ e^{\alpha_1 t}[b_1 \cos(\beta_1 t) + b_2 \sin(\beta_1 t)], & t \in (T_0, T_{11}], \\ 0, & t \in (T_{11}, T_s], \end{cases} \tag{1.2.1}$$

$$i_2(t) = \begin{cases} e^{\alpha_2 t} \frac{V_1}{\beta_2 L_2} \sin(\beta_2 t), & t \in [0, T_0], \\ \frac{V_2}{R_2} + A e^{\frac{R_2}{L_2}t}, & t \in (T_0, T_{12}], \\ 0, & t \in (T_{12}, T_s], \end{cases} \tag{1.2.2}$$

where the switches have control frequency f_s and duty cycle D, and

$$T_s = \frac{1}{f_s}, \quad T_0 = DT_0,$$
$$\alpha_1 = -\frac{R_1}{2L_1}, \quad \alpha_2 = -\frac{R_2}{2L_2},$$

$$\beta_1 = \frac{\sqrt{4CL_1 - R_1^2C^2}}{2CL_1}, \quad \beta_2 = \frac{\sqrt{4CL_2 - R_2^2C^2}}{2CL_2},$$
$$b_1 = \frac{\beta_1 i_1(T_0)\cos(\beta_1 T_0) - i'(T_0)\sin(\beta_1 T_0) + \alpha_1 i_1(T_0)\sin(\beta_1 T_0)}{\beta_1 e^{\alpha 1 T_0}},$$
$$b_2 = \frac{\beta_1 i_1(T_0)\sin(\beta_1 T_0) + i'(T_0)\cos(\beta_1 T_0) - \alpha_1 i_1(T_0)\cos(\beta_1 T_0)}{\beta_1 e^{\alpha 1 T_0}},$$
$$T_{11} = \frac{1}{\beta_1}\arctan\left(\frac{-b_1}{b_2}\right), \quad T_{12} = T_0 + \frac{L_2}{R_2}\ln\frac{-V_2}{R_2 i_2(T_0) - V_2},$$
$$A = e^{-\frac{R_2}{L_2}T_0}\left[i_2(T_0) - \frac{V_2}{R_2}\right].$$

As one can see from these equations, the parameters of the circuit components appear explicitly in the equations obtained. The evaluation of the currents can be used in component parameters selection, power ratings design, etc.

As mentioned above, there are numerous results that apply the circuit analysis approach to study local dynamics of a BCE system (see [17, 27, 28, 29, 30, 31, 32, 33, 34, 35]). A comprehensive survey is given by [16], which summarizes a number of realizations of BCE system and provides the circuit analysis on the power loss, efficiency, etc.

1.2.2 System analysis-based modeling

While the direct circuit analysis-based approach is capable to deliver a detailed model of the system under consideration, the complexity involved usually prohibits the implementation for the entire system. As a result, the model developed is usually only capable to describe a small part of the BCE system studied. This, obviously, is not desirable. As an alternative, system analysis-based approach has been used in a few recent publications. The system models constructed using this approach are based on circuit operation. However, certain simplifications are usually introduced so that the

dynamics of the system can be formulated as a continuous- or discrete-time control system:

- Continuous-time model: $\dot{\mathbf{x}}(t) = \mathbf{\Phi}(\mathbf{x}(t), \mathbf{u}(t), t)$, $t \geq 0$,
- Discrete-time model: $\mathbf{x}(t+1) = \mathbf{\Psi}(\mathbf{x}(t), \mathbf{u}(t), t)$, $t = 0, 1, 2, \ldots$,

where $\mathbf{x}(t)$ represent the system state (e.g., SOCs of the battery cells), $\mathbf{u}(t)$ represent the control actions (e.g., on/off of the MOSFET switches). It should be noted that this approach aims to model the behavior of the balancing process rather than dynamics of the power electronics or the battery chemistry. Representative results using this approach are reported in papers [36, 37, 38, 39, 40, 41, 42].

Specifically, papers [36, 37, 38, 39] model the battery cells using simple discrete-time integrator dynamics. The resulting system is a discrete-time linear system defined as follows:

$$\mathbf{x}(t+1) = \mathbf{x}(t) + \mathbf{Q}^{-1}\mathbf{B}\mathbf{u}(t), \tag{1.2.3}$$

where $\mathbf{x}(t)$ corresponds to the cell SOCs, $\mathbf{Q}$ represents the capacity of the cells, B denotes the directions of energy transfers through the equalizers, and $\mathbf{u}(t)$ indicates the amount of energy transfers through the equalizers. The model, however, does not consider energy losses during the equalization process. It is claimed that the method is applicable to all battery equalization topologies. Using a similar approach, paper [40] proposes a system model with parameters having more detailed connections with the underlying circuit and the electrical components involved.

In paper [41], three equalization structures are discussed (see Figure 1.2.2). In these figures, b_i's represent battery cells, while e_j's represent individual equalizers.

It is assumed that each equalizer is responsible to balance the two individual cells or two groups of battery cells that are connected with it. Specifically, in the series-based equalization structure, e_i balances b_i and b_{i+1} by transferring charge from the cell with higher SOC to the other; in the layer-based structure, for instance, $e_{B/2+1}$ compares the sum of SOCs of b_1 and b_2 with that of b_3 and b_4 and transfers equal amount of charge from b_1, b_2 (respectively, b_3, b_4) to b_3, b_4 (respectively, b_1, b_2) also evenly if b_1 and b_2 (respectively, b_3, b_4) have a higher SOC sum. The equalizers in the module-based structure work in a similar manner. The system dynamics of the series-based BCE system are given by [41]:

$$\begin{aligned} x_1(n+1) &= x_1(n) + \mathrm{sgn}(x_2(n) - x_1(n)) \cdot r, \\ x_i(n+1) &= x_i(n) + \mathrm{sgn}(x_{i-1}(n) - x_i(n)) \cdot r + \\ &\quad \mathrm{sgn}(x_{i+1}(n) - x_i(n)) \cdot r, \quad i = 2, \ldots, B-1, \\ x_B(n+1) &= x_B(n) + \mathrm{sgn}(x_{B-1}(n) - x_B(n)) \cdot r, \end{aligned} \tag{1.2.4}$$

where r is a constant and represents the charge transfer amount of each equalizer in one switching cycle, and

$$\mathrm{sgn}(u) = \begin{cases} -1, & \text{if } u < 0, \\ 0, & \text{if } u = 0, \\ 1, & \text{if } u > 0. \end{cases}$$

Similar formulas are also given for the layer- and module-based equalization structures. This work is further extended in [42] by considering external charging and discharging as well as energy loss within the the equalization process. Finally, pa-

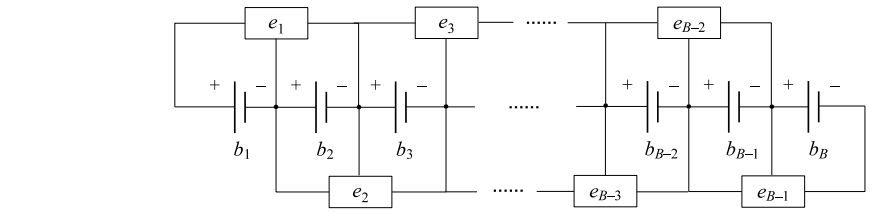

(a) Series-based equalization

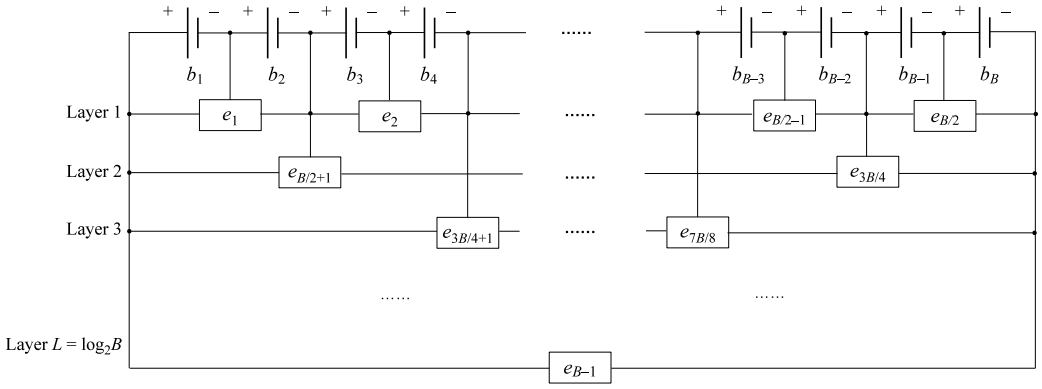

(b) Layer-based equalization

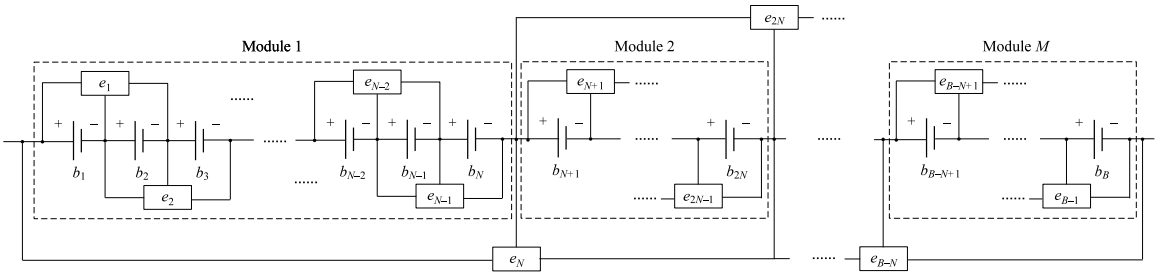

(c) Module-based equalization

FIGURE 1.2.2: Illustration of BCE systems studied in [41].

per [43] proposes a modularized global equalization structure (see Figure 1.2.3) and derives its mathematical model using a similar approach.

As one can see from system models (1.2.3) and (1.2.4), the mathematical models derived do not include any electrical components explicitly. Instead, new system parameters are introduced to characterize the system behavior. The focus of such models is to capture the higher-level interactions among all cells in the system, while

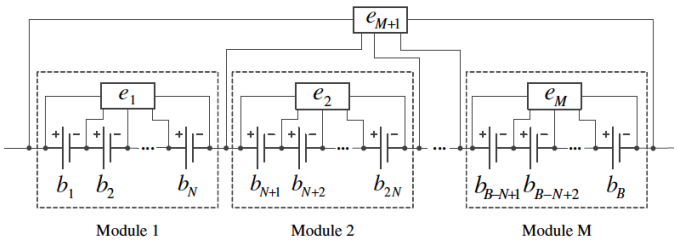

FIGURE 1.2.3: Illustration of equalization structure studied in [43].

the circuit level performance is not considered. Although this may slightly compromise the accuracy of the model, these models provide platforms and foundation for control engineers to design optimization and control algorithms for overall system operation. Indeed, these model simplifications can usually lead to analytical results, which are critical to understand the system properties as well as to design efficient optimization and control algorithms.

1.2.3 Computer simulation-based modeling

In addition to analytical modeling techniques based on circuit or system analysis, computer software tools are also used as a modeling alternative. As we have discussed above, while the outcomes of the former are usually analytical equations, the outcomes of the latter are computer programs. Indeed, it is usually difficult to apply the circuit analysis-based technique to derive the equations for large scale systems. To overcome this issue, computer software tools can be used to create the simulation model for the BCE systems at hand. Although computer simulations cannot provide close-form equations that characterize the system behavior, they can capture the circuit-level dynamics. Popular software tools used include MATLAB/Simulink, PSpice, etc. They usually have built-in libraries of electrical components that the users can

directly apply to create the simulation models that mimic the physical device (see, for instance, [15, 18, 44, 45, 46]). It should be noted that, although computer simulations provide the convenience of testing the system behavior without running the actual physical device, the model may become difficult to manage and time-consuming to run when the number of components in the system is large. Analytical models, on the other hand, are relatively more computationally efficient and easier to manipulate.

1.2.4 Future topics

So far, the mathematical models derived in the literature are developed from a series of simplifications. The simplifications do give the benefit of easier analysis. However, they also limit the scope of the models. To better capture the properties and characteristics of the system components, the models should include more details and the effects of other important factors (e.g., temperature) as well as the nonlinear and time-varying behavior of various electronic components. In fact, it is desirable that multiple models are developed for one physical system. The models should have different "resolutions" and can be used for different purposes. The higher resolution models should include more detailed considerations of the electronic components and are used to monitor the circuit dynamics. The output of these models will be used to supply parameters for the lower resolution ones, which are used for system-level analysis. It is also desired that the models to be developed are capable of handling random disturbances from both internal and external sources. Finally, it should be noted that although professional software tools (e.g., MATLAB/Simulink, PSpice) can be used as modeling alternatives, it is generally difficult if not impossible to incorporate the computer simulation models into the battery management systems

for real-time online monitoring and control purposes. On the other hand, analytical models can be easily converted to generic computer programs ready to be embedded into the battery management systems.

1.3 Performance evaluation of battery charge equalization systems

When designing a certain system, it is important to not only realize all the planned functionalities, but also achieve desired performance. In the case of BCE systems, the main efforts have been focused on the former, while the latter has not been thoroughly investigated. Clearly, while the purpose of a BCE system is to balance the charge of all cells in a battery pack, the efficiency of the equalization functionality is of critical importance. This can be quantified as equalization time, i.e., the time duration for all cells to reach the balanced state. However, it is obvious that different initial cell SOCs will lead to different equalization times and the cell SOCs may take arbitrary values within their feasible ranges. Therefore, two questions immediately come to the attention: 1) Given the initial system state, how to find out the time duration for all cells to be balanced without running the physical system? 2) How to properly compare the performance of two different BCE systems (e.g., realized using different topologies)?

Clearly, the first question demands the capability of predicting the system performance. To answer the first question and the alike, a mathematical model (either analytical or computer simulation-based) must be in place.

For the second question, the main issue is to define appropriate metrics for comparisons. It should be noted that, in addition to the equalization speed, other factors,

such as sizing, cost, and efficiency of an BCE system should also be considered in practical applications. Paper [15] provides a qualitative comparison of various BCE systems considering factors of equalization speed, control complexity, implantation, size, cost, efficiency, voltage and current stress, etc. A similar comparison is given in paper [16] with a numerical scoring scale. Unfortunately, no rigorous discussions or quantification standard of the scoring systems are provided. In this section, we will focus on explicitly defined quantitative comparisons.

1.3.1 Circuit analysis-based approach

As mentioned in Subsection 1.2.1, circuit analysis can only produce mathematical models for small-scale systems. As a result, this approach can only provide very crude approximations of the overall system performance under very special conditions.

For instance, papers [19, 47, 48] derive the formula to calculate the equalization time by assuming that 1) the battery cells are viewed as ideal capacitors, 2) the input and output currents of the equalizer are constants, 3) only one cell is initially undercharged and it is the only cell that will be charged (by other cells) during the equalization process, and 4) the equalization is terminated when the charge of the initially undercharged cell reaches the average charge of the other cells. Obviously, the equalization time calculation formula cannot be applied to general cases due to the restrictive constraints above. Paper [27] attempts to approximate the capacity of the weak battery cells under equalization. However, the calculation fails to capture the effects on other cells in the pack as well as the dynamics of the cells during the equalization process. Moreover, the calculation formulas does not consider the energy loss during equalization. As a result, the calculation error may be significant

for certain cases. In paper [26], it is proposed to approximate the maximum voltage difference among all cells during the equalization process using an exponential function, and to evaluate the equalization performance based on the limiting value and decay rate of the exponential function. The method is then applied to an 8-cell pack to compare the performance of four different topologies through randomly generated initial charge values. It should be noted that to obtain the performance measures, it is still necessary to carry out simulations of the circuit model (differential equations), while no analytical algorithms for direct calculation are derived in the paper. Paper [49] introduces a modular battery system and evaluates the power efficiency of the integrated power modules with various input voltages and output currents by experiments.

Finally, as mentioned in the previous section, the performance analysis results using this approach are usually used for parameter selection (e.g., power ratings of electrical components [19, 47], duty ratios of the PWM signals [33]), instead of overall system performance evaluation.

1.3.2 System analysis-based approach

As it is discussed in the previous section, the system analysis approach aims to characterize the interactions and dynamics among all cells in a BCE system. Although there may exist certain compromise in accuracy, this approach does lead to a possibility to derive analytical results for evaluating the performance of the overall system. The notable papers in this direction include [38, 41, 42, 43].

More specifically, paper [38] studies the performance evaluation of several equalization structures (see Figure 1.3.1). The paper considers two performance measures:

time duration until balance and the total energy dissipated until balance. The paper formulates the performance evaluation problem as a linear programming problem. The results obtained mark the shortest possible time for all cells to be balanced given that the charge transfers of equalizers can be arbitrarily controlled within hardware limits. If the control policy of the equalizers are pre-defined, then the results can only be used as a lower bound. Moreover, the results only apply to scenarios without external charging or discharging and the effects of energy loss on equalization time are not considered. Finally, to compare the performance of different equalization topologies, the paper randomly generates a set of initial cell states with fixed cell number, evaluates the equalization time for all cases, and uses the longest equalization time among all cases as the basis for comparison.

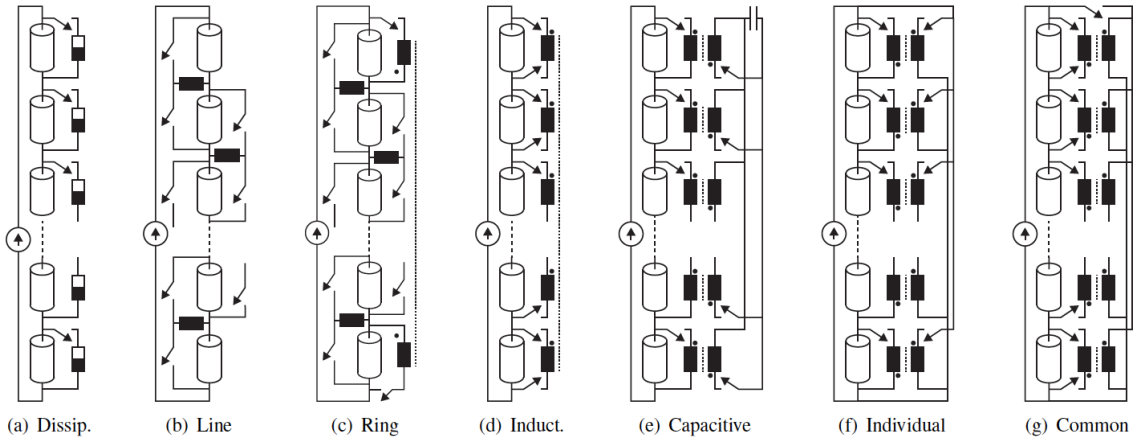

FIGURE 1.3.1: Battery equalization topologies considered in [38].

On the other hand, paper [41] studies the three equalization topologies of Figure 1.2.2 under fixed control policies described in (1.2.4). As a result, analytical algorithms are derived to directly calculate the equalization time given initial cell states. Then, an extensive Monte Carlo-based statistical analysis to compare the

performance of the three equalization structures considered. The performance evaluation algorithms are further generalized in [42], which analyzes BCE systems operating in various operation states and consider the effects of energy loss on overall system behavior. Computationally efficient algorithms and analytical formulas are derived to accurately estimate real-time individual cell SOCs during the system operation and some basic system performance measures such as equalization time, charging/discharging time, and maximum/minimum cell SOC. Based on these basic performance measures, other measures such as energy efficiency and real-time cell SOC range can also be evaluated. In paper [43], an analytical formula is derived to calculate the system equalization time assuming no energy loss. Then, the performance of the proposed structure is compared with the three equalization topologies of Figure 1.2.2 using numerical experiments.

1.3.3 Hardware experiment and computer simulation

Once the hardware realization of a new battery equalization topology is developed, experimentation with a prototype is usually carried out to test and demonstrate the performance of the design. Unfortunately, due to the lack of a standard benchmark, systematic comparisons among different designs cannot be carried out. Moreover, the long experiment time usually prohibits extensive evaluations and tests to reach a well justified conclusion. In fact, in the current literature, the efficacy of a newly developed BCE system is often demonstrated by only one or two specific examples. Apparently, this approach ignores the random variation of initial battery states as well as the sensitivity of system performance with respect to initial battery states. Although computer simulations may be used as an alternative, the experiments still

should be rigorously designed.

1.3.4 Future topics

An accurate performance evaluation method is the foundation for all subsequent tasks such as parameter optimization and controller design. In general, the performance evaluation algorithms can be applied either online (i.e., running together with the actual system in real time) or offline (i.e., running in isolation). When the algorithms are to be deployed online, their computational complexity and efficiency must be taken into consideration as they may draw extra power and take certain time to finish. At present, the most commonly used approach used in the literature is to directly perform the iterative calculation based on the equations of the system model to obtain the complete evolution of system states. Although this approach guarantees accuracy, it is also the least efficient. Therefore, developing computationally efficient algorithms for accurate performance evaluation is of great importance for designing and optimally operating BCE systems.

1.4 Control strategies for battery charge equalization systems

The basic idea of battery equalization is extracting the charge out of the stronger cells (i.e., the ones with higher SOC) and, in case of active balancing, transferring the charge to the weaker cells (i.e., the ones with lower SOC). To realize this idea, numerous topologies have been proposed (see review papers [15, 16]). When a battery equalization circuit is proposed, it is also accompanied with its own control strategy.

The control strategy should answer the following questions: 1) How often should the balancing actions be updated? 2) How to select the cells that will be discharged at a given time instant? 3) How to select the cells that will receive charge? 4) How much charge will be transferred?

In some control strategies of BCE systems, the control actions are formulated simply to realize the balancing functionality, while rigorous quantitative performance evaluations of the proposed strategies are rarely carried out. For the control strategies in more recent investigations, the control actions are more complex functions of certain measurements of the cells. These functions may be designed based on heuristics, fuzzy logic, circuit models, system models, etc. Certain experiments are usually performed to justify the effectiveness of the proposed methods. Clearly, the performance of a BCE system is heavily dependent upon the efficacy and efficiency of the control strategy applied. In this section, we provide a review on the control methods used in BCE systems.

1.4.1 Functionality-based simple control

For different battery charge balancing/equalization circuits, the functionality-based control methods may vary significantly. Next, several examples of functionality-based simple control methods are discussed.

A BCE system with modified buck-boost DC-DC converters as equalizers is introduced in [44] (see Figure 1.4.1). In this system, all the cells are connected in series and each cell is connected to an equalizer, referred to as the charge equalization module (CEM). All the equalizers are connected to a main DC bus. The control strategy is: during each control cycle, based on the monitored cell voltages, the energy is trans-

ferred from the cell with highest voltage to the cell with lowest voltage through the main bus. This control strategy has an advantage of reducing the cell voltage range directly by letting the cell with highest voltage charge the cell with lowest voltage.

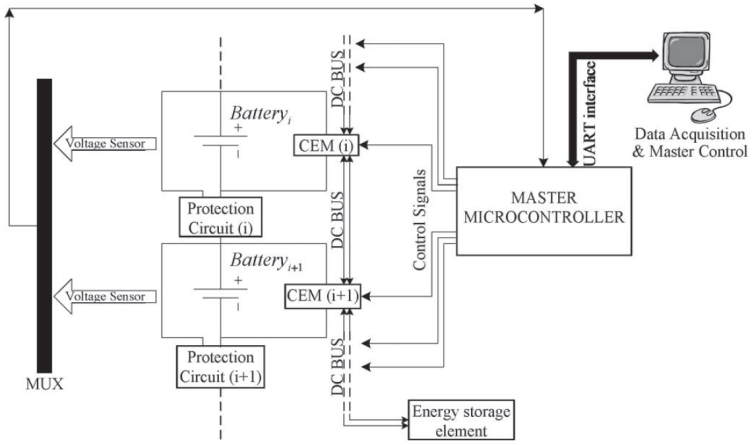

FIGURE 1.4.1: BCE system considered in [44].

A modularized two-stage BCE system designed for a series-connected battery system is introduced in [19]. Different from the module-based BCE structure discussed in last section, in this system each module has only one equalizer, which can be connected to any cell within the module by switch operations. All the modules also share a common equalizer. Thus, the required number of equalizers and the size of the BCE system are significantly reduced. For this system, the control strategy is: the controller detects all the undercharged cells with SOC smaller than the average cell SOC by 10%, then let the whole battery pack charge these undercharged cells. The general energy transfer efficiency of the two stages is about 61.5%. Clearly, this BCE system comes with reduced size and simple control strategy but it is not energy-efficient.

In addition, recently, a number of other battery charge equalization control methods have been developed (see, for instance, [22, 33, 46, 50, 51]). All these equal-

ization circuits have simple control mechanisms for easy implementation while the performance of these BCE system need to be quantitatively evaluated and further improved or optimized. A more comprehensive review of the functionality-based control methods can be found in [16].

1.4.2 Heuristics-based control

In functionality-based simple control strategies, the parameters of the systems are usually fixed or directly determined by the circuit designs. In fact, many equalization circuits possess the capability to be further improved by adjusting some parameter values of the systems based on the real-time battery cell states. To accomplish this, the idea of battery charge equalization is advanced so that the amount of charge transfers are dependent on the battery cells' states: larger SOC deviations from the pack average lead to larger amount of charge to be transferred. To implement this idea, a number of heuristics-based methods are proposed.

For instance, a series-connected battery string is designed with each cell associated with a dc-dc converter in [23]. The operation of the converters are controlled by PWM signals. To maintain a balanced discharging capability when connecting the battery string to a load, a heuristic method is proposed to adjust the duty ratios of the DC-DC converters based on SOCs and voltages of the battery cells.

In paper [52], a BCE system with multi-winding flyback converters is developed. The paper first gives the transfer function between the voltage at the secondary winding and the voltage of the battery cell. Then, the parameters of the inductors and capacitors are carefully selected such that frequency responses at the windings of different cells are different. Next, a unique switching frequency for each winding/cell

is identified such that the transfer function has the highest gain among all. This frequency will be applied as the system switching frequency if the corresponding cell is the most undercharged one. As a result, the overall charging speed can be improved.

Although the heuristics-based control has the potential to provide an improvement over the functionality-based simple control strategy, it should be noted that the significance of the potential improvement are not systematically studied or analytical proven. Therefore, quantitative performance evaluations of the heuristic methods are still necessary to justify the effectiveness of the propose control strategies.

1.4.3 Fuzzy logic-based control

Battery charge equalization is a complicated process since it is affected by various factors, such as the nonlinear characteristics of battery cells and electric elements, the connection structure of battery cells, the frequency of control, the stochastic change of ambient temperature. Thus, it is very difficult to develop a model that can accurately capture the influence of all these factors. Because of good adaptability, robustness, and efficiency for nonlinear control systems [21], fuzzy logic-based control methods have been applied to studying the nonlinear behavior of battery charge equalization by some researchers. These fuzzy logic-based control methods are developed based on either some specific circuits [34, 53] or some equalization models [21, 24, 54]. Besides, they can also be used in combination with other methods, such as proportional-integral (PI) control [34] or neural network [53]. Next, we will review some fuzzy logic-based control methods reported recently.

The series-based BCE structure in Figure 1.2.2(a) is studied in [21, 24], where modified C$\hat{u}$k DC-DC bidirectional converters are chosen as the equalizers and the

fuzzy logic controllers are applied to regulating the equalization current. It has been shown in several equalization circuits [21, 22, 24, 34, 40] that the equalization current is inversely proportional to the switch frequency, i.e., the lower switching frequency leads to the larger equalization current. This provides a way to control the equalization current by adjusting the switching frequency. Using this idea, the outputs of the fuzzy logic controllers in [21] and [24] are set as the switching frequency. The inputs of the fuzzy controller in [21] are selected as the voltage difference between every two adjacent cells and the individual cell voltages, while in [24] the inputs include the cell SOC difference between two adjacent cells, the average cell SOC and the total internal resistance. As a result, both fuzzy logic-based methods improve the equalization performance by reducing the equalization time to some extent.

The fuzzy logic-based control methods are also applied to other equalization structures or combined with other control methods. A dissipative BCE system is studied in [54], where the fuzzy logic-based control method is used to determine which cell should be dissipated during the charge equalization process. In [34], two kinds of controllers, a fuzzy logic-based controller and a proportional-integral controller, are used during different periods of the equalization process: The fuzzy controller is used to achieve quick equalization when cell voltage difference is large, while proportional-integral controller is selected to further reduce cell voltage difference during the final steady period. In oder to make the fuzzy logic-based control methods more adaptive to the dynamic process of battery equalization, combined control strategy based on fuzzy logic and neural network are developed in [53] to take advantage of the superior properties of neural network in learning and adaptation.

In general, the fuzzy logic-based control methods are independent of exact mathematical system model and good at modeling nonlinear behavior of the battery equal-

ization process. However, in the fuzzy logic-based control methods above, the rule base sets and the membership functions are defined based on experience and/or basic knowledge of cell equalization instead of first-principle formulas. Besides, the output of the controllers are usually qualitative description (e.g, small, medium, or large) instead of exactly defined quantitative values.

1.4.4 Model predictive control

While heuristics-based control and fuzzy logic-based control both aim to increase the equalization speed, the control rules are usually developed without having a system model in place. Moreover, the obtained control rules are based on intuition and experience, instead of rigorously formulated control or optimization problems.

In some recent publications [25, 39], model predictive control (MPC), which is an advanced method in Systems and Control, has been applied to BCE systems. To apply this method, a mathematical model characterizing the dynamics of the system at hand must be available. Using this model, the series of control actions that optimize the system performance over a finite time-horizon is identified. Then, the control action for the current time instant is implemented, while the optimization is carried out again from the new current state and with the time-horizon sliding forward for one time slot. The process will be repeated iteratively until the desired target is reached. It should be noted that the model predictive control approach is not necessarily optimal. However, in practice, it usually leads to high quality results.

As mentioned in Subsection 1.2.1, paper [25] studies a two-cell BCE system (see Figure 1.2.1) based on the circuit model derived in [24]. The control variables considered are the frequency and duty ratio of the PWM signals that regulate the MOSFET

switches. The control objective is to minimize the imbalance among all cell SOCs while minimizing the total balancing current at the same time. To accomplish this, a genetic algorithm is designed to solve the finite time-horizon optimization problem in each iteration so that the frequency and duty ratio can be dynamically adjusted based on the system operating status. An example is used to demonstrate the improvement over the case with constant frequency and duty ratio.

The MPC approach is applied in [39] based on a system model. Specifically, the paper considers the constrained flow control in storage network, in which the BCE system can be viewed as a special example. In this framework, each battery cell is viewed as a node and can dissipate energy by itself or transfer energy to any other cell. The control variable is the current flow between each pair of cells, while the control objective is to maximize the effective system capacity (the maximum charge by which each cell can be charged plus the maximum charge by which each cell can be discharged) or to achieve the battery equalization. Control algorithms based on a convex one-step model predictive controller are developed to solve the control problem under flow constraints.

1.4.5 Optimal control

Clearly, to achieve the best possible performance, optimal control of the equalization process is most desired. This, again, requires a well-defined system model to apply the optimal control methods.

Some preliminary work has been performed in [40], which develops a mathematical model for the BCE system by considering the dynamic property of the charge equalization current as well as the nonlinear behavior of SOC with respect to cell voltage.

The control variable for the system includes the balancing current and the duty ratio of the PWM signals, while the control objective is to minimize the imbalance among cell SOCs, the control efforts, and the total time until equalization. To obtain the optimal controller, a dynamic optimization algorithm is used. A numerical example is given to illustrate the efficacy of the control algorithm.

1.4.6 Future topics

It is obvious that the future work in this area should be centered at applying advanced control and optimization methods to BCE systems. Although some preliminary research results have been reported, they are all theoretical studies only with no implementation in actual electrical devices yet. Therefore, developing advanced theoretical control strategies and implementing them into actual battery management systems are both expected. It should be noted that since the mathematical model development research is still not fully established, both model-based control and non-model-based control (e.g., heuristics-based and functionality-based simple control) are strongly encouraged at this point. Meanwhile, it would be strongly beneficial to investigate the system-theoretic properties of different battery equalization topologies. This will provide understanding of the equalization processes, which can help design more effective heuristics and control policies.

1.5 Research framework

The BCE system is a great engineering innovation that has the potential to significantly improve the performance of battery systems with various connection topologies.

Up to today, extensive research and development efforts have been spent on various topologies and electrical circuit designs. The main focus of these efforts is the realization of the cell balancing functionality. On the other hand, the true potential of these systems has not been fully explored due to the lack of rigorous quantitative analysis of the performance at the system-level. In fact, while the "hardware" side has attracted significant research efforts and generated remarkable results, the "software" side has largely lagged behind. This includes not only the real-time control of the equalization process but also the optimal selection of the parameters of the electrical components. Although common-sense and intuition can help derive heuristics or empirical methods to facilitate these needs, rigorous engineering investigations are necessary to provide solutions with predictable and guaranteed results. To carry out such investigations, mathematical models must be formulated based on the characteristics of the battery cells, electrical components, and circuit operation. Certain simplifications may be needed in order to obtain a tractable model with sufficiently high fidelity. As of now, there has been some valuable results obtained on mathematical modeling of BCE systems through circuit analysis and systems analysis. When the complexity of the mathematical model becomes too high, computer simulations can be used as an alternative. To proceed with control and optimization based on the models developed, one must be able to evaluate the system's performance under any initial condition. In general, this can be accomplished by iterative calculations based on the equations of mathematical models. However, the computational efficiency of the calculation procedures needs to be taken into account for speed and energy consumption considerations. Accurate performance evaluation/estimation methods then can be used for system validation as well as selecting optimal component parameters and designing effective control policies. So far, the development of fast algorithms for

accurate performance prediction in BCE systems is still in its infancy and requires more research attention. Finally, the control and optimization algorithms developed need to be converted to software programs, embedded into the battery management systems, implemented through modern micro-controller technology. With more and more participation from systems and control scientists and engineers in recent years, it is expected that the design and development of BCE systems will have a transition from being hardware-heavy to hardware-software-balanced. This will lead to a more integrated battery management system that not only can track and monitor the status of the battery pack but also can actively and accurately predict the system performance and effectively and efficiently control the system operation in real time.

Based on the above review of BCE systems' mathematical modeling, performance evaluation, and charge equalization control, the following research topics will be studied in this thesis.

Firstly, despite the important and valuable research efforts in the development of BCE systems, so far, most of the results reported have only focused on the electrical hardware design and realization of the BCE systems, but investigations of the battery charge equalization process from the system's perspective have rarely been explored and a number of questions remain open. Different from the circuit designs, the system-level modeling and analysis can provide statistical evaluation results and analytical solutions to improve and even optimize the battery charge equalization/balance performance. Besides, to evaluate the BCE system performance and test/verify the proposed BCE system control methods, physical experiments by circuit devices and iterative computer simulations based on the mathematical BCE models remain as the main tools. These tools, however, could be energy- and time-consuming as the scale of the system becomes large. The low efficiency of these tools prohibits systematic

investigation and understanding of the charge transfer behavior during the battery equalization process. Therefore, in this thesis, system-level mathematical models of BCE systems are proposed, and then computationally efficient methods are developed for series-based and module-based BCE systems in Chapter 2 and Chapter 3, respectively, to estimate the cell SOC evolution throughout the charge balancing with charging/discharging process and to evaluate critical system performance measures such as the battery charge equalization time, charging time, discharging time. In addition to the system performance evaluation, these proposed analytical formulas proposed in Chapter 2 and Chapter 3 also provide some clues for improving the system performance. By combining the application of battery system reconfiguration, which is an emerging technique used to improve system reliability, energy efficiency, and charge balance, in Chapter 4, near-optimal battery cell/module reconfiguration algorithms are developed for fast charge equalization in series-based and module-based BCE systems.

In addition to the series-connected battery systems, the parallel-connected battery systems also suffer from the charge imbalance among battery cells/modules/packs. To alleviate the charge imbalance, biased battery current allocation during the charging/discharging process has been shown to be an effective way. The traditional current allocation method in proportion to battery voltage or SOC can only provide fixed system performance since it lacks controllability. In Chapter 5, a novel current allocation method based on the charging/discharging space is proposed to enable the flexible and dynamic control of multiple system performance measures such as the charge balance and total power efficiency.

Chapter 2

Series-based battery charge equalization system

2.1 Introduction

The battery system is one of the key components in a number of modern power applications, such as electric vehicles (EVs), wind and solar electric systems. However, charge imbalance among different cells is very common in a battery system, which may lead to serious problems in power efficiency, equipment reliability and safety, etc. Due to the charge imbalance, the voltages of individual cells gradually differ over time and the capacity of the battery pack decreases quickly, which may even result in the failure of the entire battery system [9].

In order to tackle the issue of charge imbalance among battery cells/modules/packs, a great number of circuit designs have been proposed and implemented by shunting resistors, switched capacitors, DC-DC converters, transformers, switches, and so on

[9, 14, 15, 16, 55, 56]. These electric devices developed for battery charge balance are usually called *battery equalizers* or *balancers*. Battery equalizers and their connection topology compose the *battery charge equalization (BCE) structure*. Some battery equalizers are designed for particular connection topologies, while others can be applied to various BCE structures [57, 58]. Specifically, cell-to-cell equalizers are designed to be connected to a pair of battery cells and, thus, can be flexibly arranged to set up different BCE structures. Among these structures, the series-based BCE structure [8, 11, 14, 20, 23, 41] and the module-based BCE structure [6, 19, 20, 41], have drawn plenty of research attention for their advantages such as convenient and flexible deployment. In this thesis, a battery system consisting of series-connected battery cells is referred to as a *series-connected battery system*. A series-connected battery system and the BCE structure mounted on it compose a *battery charge equalization (BCE) system*, which will be further specified according to the BCE structure applied. For example, if a module-based BCE structure is connected to a series-connected battery system, they form a module-based BCE system.

It should be noted that, despite the important and valuable research efforts in the development of battery equalization systems (see, for instance, [6, 22, 23, 27, 28, 52]), so far, most of the results reported have focused on the electrical hardware design and realization of the equalization systems. On the other hand, investigation of the battery equalization process from the system level has rarely been explored and a number of questions remain open. For example, given the initial SOC of each battery cell and all the system parameters, how long will it take to complete equalization, charging, and/or discharging? How to predict the SOC of each individual cell at any time instant during the equalization process (with or without charging or discharging)? To answer these questions, experiments with physical devices and computer simulations

of the circuit models remain as the main tools at present. These tools, however, could be costly and time-consuming as the scale of the system becomes large. The low efficiency of these tools prohibits systematic investigation and understanding of the system behavior during the battery equalization process. Therefore, in order to carry out comprehensive analysis of the system performance, accurate and computationally efficient tools are necessary, especially for larger-scale systems. Some preliminary results have been obtained in [41], including the mathematical models and calculation formulas of equalization time for different equalization structures. However, paper [41] still relies on the iterative of the mathematical models to obtain the SOC of each cell during the equalization process. Also, it does not consider the energy loss during the equalization process. In addition, the interactions of charging and discharging with the equalization process are not studied.

In this chapter, we focus on the analysis of battery equalization systems operating in various working states and consider the effects of energy loss on overall system behavior. Specifically, we consider the series-connected battery equalization system in the following parts of this chapter and assume that the battery system may operate in one of the three operating states: charging, discharging, or idle state. In addition, the battery equalization may occur in any operating state. Moreover, the energy loss during system operation is considered, which, in practice, may be caused by internal circuit resistance, conversion between chemical and electrical energy, etc.

To analyze systems with the above features, the remainder of this chapter is organized as follows: In Section 2.2, the mathematical model of the series-based BCE system considering charge transfer loss is introduced. Then, in Section 2.3, two important basic concepts, merging point and merging battery group (MBG), are defined and their properties are discussed. Based on the mathematical model

and the properties of merging point and MBG, computationally efficient algorithms are proposed in Section 2.4 to estimate each cell's SOC at any time instant of the equalization process and to calculate the system battery charge equalization (BCE) time. In Section 2.5, analytical formulas to calculate the maximum and minimum cell SOCs, charging time, and discharging time, are derived and validated by numerical experiments. Finally, conclusions and future work are provided in Section 2.6. All proofs are given in Section 7.1.

2.2 Mathematical modeling for the series-based BCE system

2.2.1 Model description and assumptions

Consider the BCE system with series-connected cells and equalizers shown in Figure 2.2.1 based on the following assumptions:

(i) The battery system consists of B cells, $b_1, b_2, \ldots, b_B$, connected in series, and the equalization system consists of $B-1$ equalizers, $e_1, e_2, \ldots, e_{B-1}$, connected with every two adjacent cells.

(ii) All cells have the same capacity, then the cell SOC can be used to characterize each cell's charge state. All equalizers have the same working cycle, τ, then the time axis is slotted with slot duration τ.

(iii) Each equalizer e_i is characterized by its equalization rate, $r_{e,i}$ units of SOC per working cycle, and energy loss rate $l_{e,i} \in (0,1)$, $i = 1, \ldots, B-1$. For simplicity, assume all the equalizers have identical and constant parameters, i.e., $r_{e,i} = r_e$

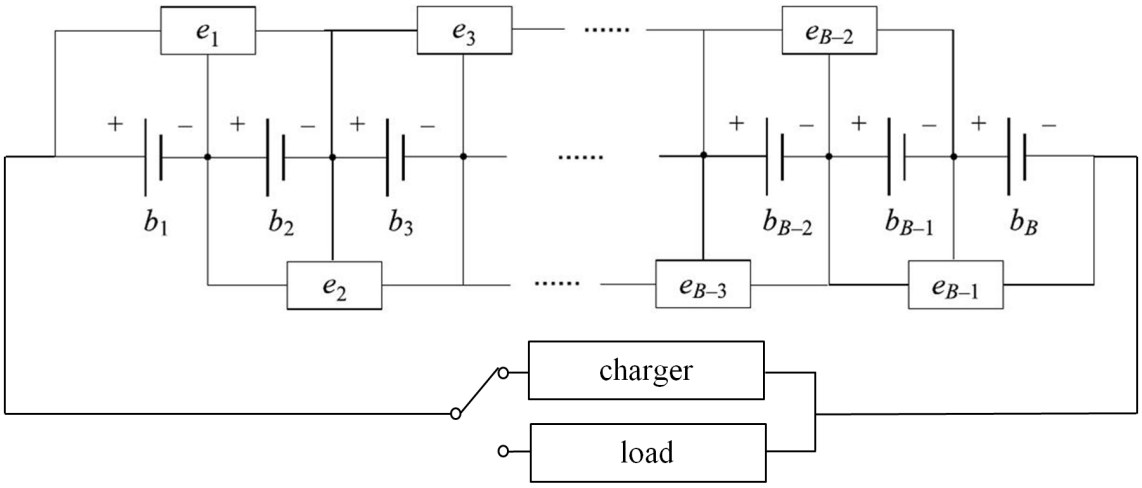

FIGURE 2.2.1: Series-based BCE system.

and $l_{e,i} = l_e$.

(iv) At the beginning of each working cycle, if cell b_i's SOC is higher than cell b_{i+1}'s SOC, then during this working cycle equalizer e_i takes r_e units of SOC away from b_i with constant rate and sends $(1 - l_e)r_e$ units of SOC to b_{i+1} also with constant rate. The remaining $l_e r_e$ units of SOC is consumed by the system as energy loss. Similarly, if cell b_i's SOC is smaller than cell b_{i+1}'s SOC, then equalizer e_i takes r_e units of SOC away from b_{i+1} and sends $(1 - l_e)r_e$ units of SOC to b_i with the rest $l_e r_e$ units of SOC consumed as energy loss. If b_i and b_{i+1} have equal SOC, then during the working cycle no charge transfer takes place between them.

(v) The external charging/discharging of the battery system is characterized by a constant parameter r_g. During the system operation, each cell receives r_g units of SOC per working cycle with constant rate. Clearly, $r_g > 0$ indicates the charging state, $r_g < 0$ indicates the discharging state, and $r_g = 0$ indicates the

idle state.

(vi) The SOC of each cell cannot exceed the upper SOC limit x_{ub} or lower SOC limit x_{lb}, $0 \leq x_{lb} < x_{ub} \leq 1$. In other words, as soon as any cell's SOC reaches x_{ub} or x_{lb}, all the processes, including equalization, charging, and discharging, will be terminated.

Remark 2.2.1. The model defined by the above assumptions describes the operation of series-based BCE systems from the system level. Under this framework, battery charge balancing/equalization and charging/discharging may occur simultaneously. The battery charge equalizers applied in this system could be designed by various circuit technologies, such as switched capacitors [9, 14, 15, 16], multi switched inductors [15], C$\hat{u}$k-converter[14, 15, 16, 21, 24, 25]. In all these circuits, each equalizer is connected with two adjacent cells and transfers charge from the cell with higher SOC to the other one.

Remark 2.2.2. Since the working cycle is usually very short in practical situations (e.g., $\tau = 0.05\ ms$ in [21]), we assume the charge transfer is carried out with constant rate during each working cycle. In addition, energy loss is considered to account for the internal resistance of the battery cells and other energy losses through system components [24].

Remark 2.2.3. Although the model considered above does not include lower level electrical components, the main factors affecting the dynamics of the equalization system have been incorporated through the "higher" level system parameters r_e, r_g, and l_e. As shown in [41], this type of model is capable to capture the main system dynamics of SOC changes in battery equalization systems. System models with deeper circuit details will be considered in future work.

2.2.2 Mathematical model

Let $t_n = n\tau$, $n = 0, 1, 2, \ldots$, and denote the n-th working cycle as $[t_{n-1}, t_n)$, $n > 0$. Let $x_i(t) \in [0, 1]$, $i = 1, \ldots, B$, denote the SOC of cell b_i at time $t \geq 0$. Then, based on assumptions (i)-(vi), given the initial cell SOCs, $x_i(0)$, $i = 1, \ldots, B$, the evolution of the system state is given below:

$$x_i(t) = x_i(t_n) + k_i(t_n)(t - t_n),\ t \in (t_n, t_{n+1}],\ n \in \{0, 1, \ldots\}, \tag{2.2.1}$$

where $k_i(t_n)$ is the overall charge transfer rate of cell b_i during time interval $(t_n, t_{n+1}]$. According to assumptions (i)-(vi), we have

$$k_i(t_n) = \begin{cases} \frac{\text{sgnl}(x_2(t_n) - x_1(t_n), l_e) r_e + r_g}{\tau}, & \text{if } i = 1, \\ \frac{\text{sgnl}(x_{i-1}(t_n) - x_i(t_n), l_e) r_e + \text{sgnl}(x_{i+1}(t_n) - x_i(t_n), l_e) r_e + r_g}{\tau}, & \text{if } 1 < i < B, \\ \frac{\text{sgnl}(x_{B-1}(t_n) - x_B(t_n), l_e) r_e + r_g}{\tau}, & \text{if } i = B, \end{cases} \tag{2.2.2}$$

$$\text{sgnl}(u, l_e) = \begin{cases} -1, & \text{if } u < 0, \\ 0, & \text{if } u = 0, \\ 1 - l_e, & \text{if } u > 0. \end{cases} \tag{2.2.3}$$

It should be noted that, since the charging/discharging rate r_g for each battery cell is assumed to be identical, charging or discharging does not affect the SOC differences among cells. In other words, the equalization process, which operates based on cell SOC differences, is somewhat "independent" of the charging and discharging processes. Thus, the system evolution can be viewed as the superposition of both charge equalization and charging/discharging processes. Based on the mathematical model above, an illustration of the charging process, equalization process, and simultaneous

charging and charge equalization processes for a 4-cell battery system is shown in Figure 2.2.2. The same initial cell SOC set is used in all three cases.

In Figure 2.2.2a, only charging is present without equalization (i.e., $r_e = 0$). As we can see, the SOCs of all cells increase with the same rate ($r_g = 10^{-4}$) and the process is terminated when cell b_4 is fully charged during the 2000-th working cycle. However, due to the imbalance of initial cell SOC, the other three cells are still under-charged. In Figure 2.2.2b, only charge equalization is present without charging and discharging (i.e., $r_g = 0$) and the equalizers (with $r_e = 10^{-4}$) manage to balance the cell SOCs of the battery. Finally, in Figure 2.2.2c, when both charging and equalization run simultaneously, the SOCs of all the cells are equalized at the same time as that in Figure 2.2.2b, since the equalization process is not affected by the charging process. Besides, during the first 2000 working cycles, if the cell SOC increments caused by charging in Figure 2.2.2a are superposed to the equalization process in Figure 2.2.2b, the superposed system evolution is exactly same as that in Figure 2.2.2c.

Clearly, based on the mathematical model, we can obtain the SOCs of all cells at any time instant by iterative calculation using equations (2.2.1)-(2.2.3). We refer to this approach as *iterative simulation*. The computational time of the iterative simulation approach depends on not only the initial SOCs and the number of cells, but also the values of r_e and r_g. Smaller values of r_e and r_g lead to more iterations and longer computational time. Therefore, the goal of this work is to study the properties of the charge equalization, charging, and discharging processes, and to develop computationally efficient methods for fast and accurate evaluation of system states and performance measures.

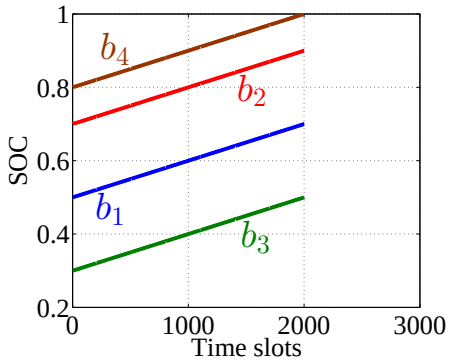

(A)

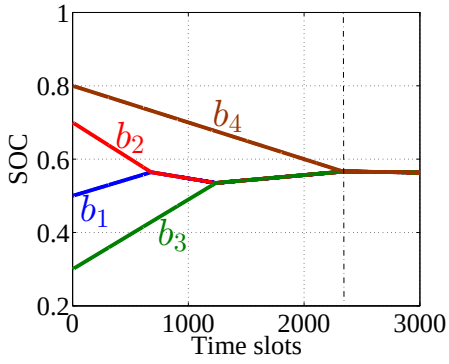

(B)

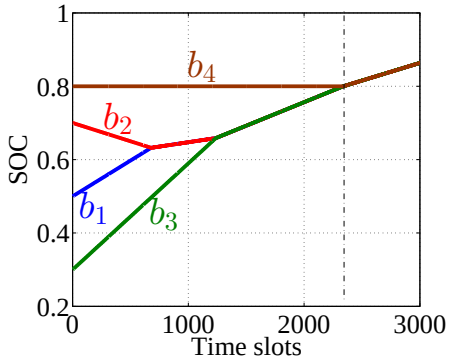

(C)

FIGURE 2.2.2: Illustration of a 4-cell battery system with $\{x_1(0), x_2(0), x_3(0), x_4(0)\} = \{0.5, 0.7, 0.3, 0.8\}$. (A) Charging process without equalization. (B) Equalization process without charging and discharging. (C) Simultaneous charging and equalization processes.

2.3 System-theoretic analysis of the equalization process

In this section, we discuss the system's properties in the idle state, i.e., when the charge equalization is present ($r_e > 0$) but there is no charging/discharging ($r_g = 0$).

2.3.1 Merging point

Definition 2.3.1. During the equalization process, the merging point of two adjacent cells b_i and b_{i+1} is defined as the time instant when $x_i(t) = x_{i+1}(t)$ is observed for the first time.

Denote the merging point of two adjacent cells b_i and b_{i+1} as $t_{merge}(i) \geq 0$, $i \in \{1, \ldots, B-1\}$. If cells b_i and b_{i+1} have equal initial SOCs, then $t_{merge}(i) = 0$. If $t_{merge}(i) > 0$, then according to assumption (iv), the charge transfer direction and rate between b_i and b_{i+1} are constant for $0 \leq t < t_{merge}(i)$, and only depend on their initial SOCs, r_e, and l_e.

Since every two adjacent cells have one merging point, the total number of merging points is $B-1$ for a B-cell battery system. As an illustration, the three merging points for the 4-cell battery system considered in Section 2.2 is shown in Figure 2.3.1.

According to the mathematical model, since each equalizer compares the two adjacent cells' SOCs at the beginning of each working cycle, i.e., only at some discrete time instants, the SOCs of two adjacent cells are not necessarily always equal if their merging point is not exactly at the beginning of a working cycle. This is illustrated in Figure 2.3.2, where we zoom in Figure 2.3.1 at the merging points. Fortunately, the SOC difference of any two adjacent cells is tightly bounded after their merging

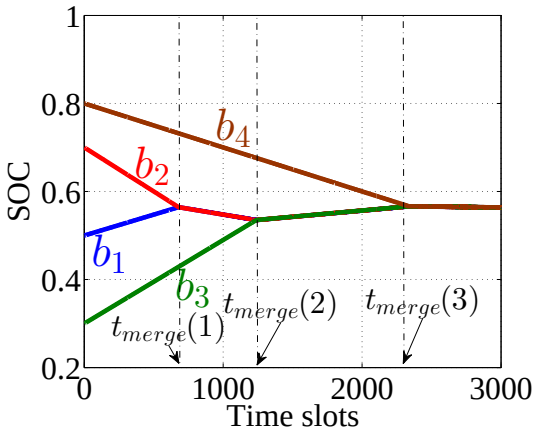

FIGURE 2.3.1: Illustration of merging points during the equalization process of a 4-cell battery system.

point thanks to the following property:

Proposition 2.3.2. *In the equalization process with $r_e > 0$ and $r_g = 0$, the SOC difference of any two adjacent cells will be always less than $(4 - 2l_e)r_e$ after their merging point is reached, i.e.,*

$$|x_i(t) - x_{i+1}(t)| < (4 - 2l_e)r_e, \ t \geq t_{merge}(i), \ i \in \{1, \ldots, B-1\}. \tag{2.3.1}$$

Proof: See Subsection 7.1.1.

According to this property, as soon as the SOCs of two adjacent cells have been equalized, they will not diverge but remain within a bounded neighborhood of each other. In the following discussions of the chapter, two adjacent cells are referred to as being *merged* or *equalized* after their merging point is reached. Moreover, it can

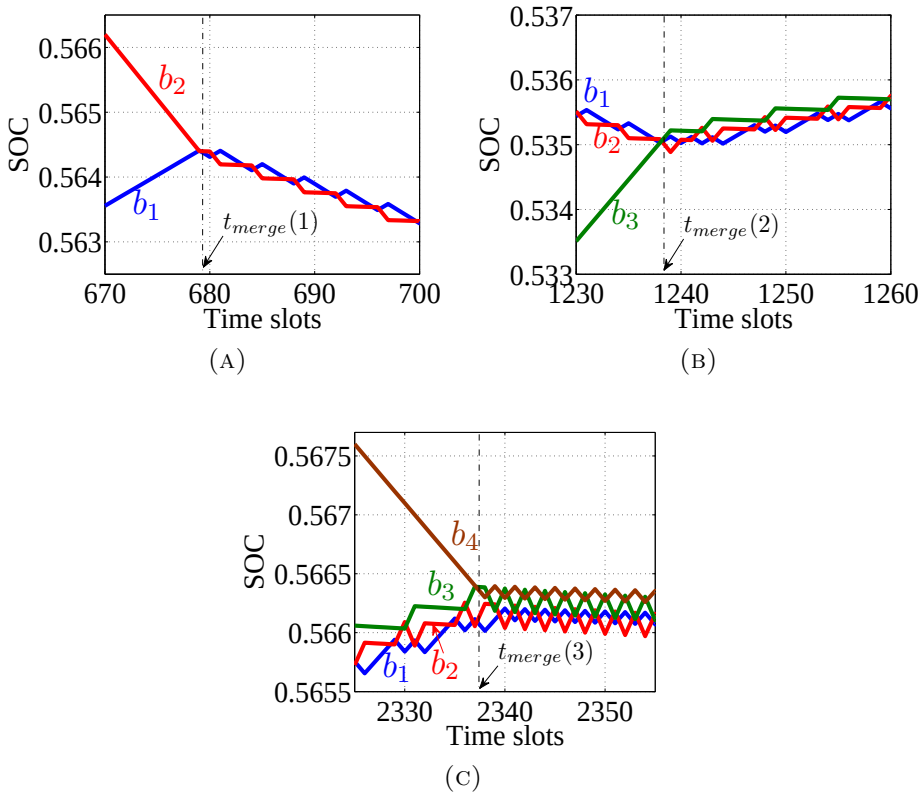

FIGURE 2.3.2: The cell SOCs evolution around the merging points of Figure 2.3.1.

be obtained from Proposition 2.3.2 that,

$$\max_{i\in\{1,\ldots,B\}} x_i(t) - \min_{i\in\{1,\ldots,B\}} x_i(t) < (B-1)(4-2l_e)r_e,\ t \geq \max_{i\in\{1,\ldots,B-1\}} t_{merge}(i).$$

In other words, all cell SOCs of the battery will remain equalized once the last merging point is reached. The battery charge equalization (BCE) time of the system is defined as the time instant when all cell SOCs are equalized for the first time, and denoted by T_e. Thus,

$$T_e = \max_{i\in\{1,\ldots,B-1\}} t_{merge}(i).$$

2.3.2 Merging battery group

To analyze BCE systems, the notion of battery group is introduced in [41]:

Definition 2.3.3. A *battery group* (BG) is a group of consecutively connected battery cells within a series-connected battery system.

In a B-cell series-connected battery system, if a battery group includes cell b_1 or cell b_B, it is called a *boundary battery group* (BBG); otherwise, it is called an *internal battery group* (IBG).

Let $BG(g,i)$, $g \in \{1,\ldots,B\}$, $i \in \{1,\ldots,B-g+1\}$, denote the g-cell BG starting with cell b_i, i.e., $BG(g,i)$ represents the cell sequence $\{b_i, b_{i+1}, \ldots, b_{i+g-1}\}$. The first cell b_i and last cell b_{i+g-1} of $BG(g,i)$ are called *boundary cell*s of $BG(g,i)$. Any cell not belonging to $BG(g,i)$ but connected with a boundary cell of $BG(g,i)$ is called a *neighboring cell* of $BG(g,i)$. For example, if $BG(g,i)$ is a BBG, then b_{i-1} (if $i-1 \geq 1$) or b_{i+g} (if $i+g \leq B$) is its neighboring cell; if $BG(g,i)$ is an IBG, then both b_{i-1} and b_{i+g} are its neighboring cells. In addition, two battery groups, $BG(g_1,i_1)$ and $BG(g_2,i_2)$ are referred to as being "neighboring" if they have no common cells and no cells in between, i.e., $i_1+g_1=i_2$ or $i_2+g_2=i_1$.

Let $x_{(g,i)}(t)$ denote the sum of SOCs of all cells in $BG(g,i)$ and $\bar{x}_{(g,i)}(t)$ denote the average cell SOC of $BG(g,i)$ at time t, i.e.,

$$x_{(g,i)}(t) = \sum_{j=i}^{i+g-1} x_j(t), \tag{2.3.2}$$

$$\bar{x}_{(g,i)}(t) = \frac{x_{(g,i)}(t)}{g} = \frac{1}{g}\sum_{j=i}^{i+g-1} x_j(t). \tag{2.3.3}$$

According to Proposition 2.3.2, for any two adjacent cells, b_i and b_{i+1}, with $x_i(0) \neq$

$x_{i+1}(0)$, their SOCs, $x_i(t)$ and $x_{i+1}(t)$, are not necessarily equal even after they have been equalized. Without loss of generality, we assume that the SOCs of any two adjacent cells are always unequal at the beginning of each working cycle. Thus, during each working cycle, the loss caused by charge transfer between every two adjacent cells is $l_e r_e$ units of SOC. For a B-cell battery system, the total loss during one working cycle is $(B-1)l_e r_e$ units of SOC.

For battery group $BG(g,i)$, the change of its sum SOC $x_{(g,i)}(t)$ or average cell SOC $\bar{x}_{(g,i)}(t)$ consists of two parts: the charge transfers with its neighboring cells and the energy loss caused by charge transfers within $BG(g,i)$. During each working cycle, the latter is a constant, $(g-1)l_e r_e$, while the former depends upon the SOC difference of its boundary cells and neighboring cells. To quantify this part of the charge transfer, we note that the fastest way for battery group $BG(g,i)$ to lose charge is to have all its neighboring cells continuously draw charge from the battery group's boundary cells. Thus, the lower bound of the average cell SOC of $BG(g,i)$ at time t is given by

$$\begin{aligned} &\bar{x}^l_{(g,i)}(t) = \bar{x}_{(g,i)}(0) + \frac{-\rho_{(g,i)} - (g-1)l_e}{g\tau} r_e t, \\ &g \in \{1,\ldots,B\},\ i \in \{1,\ldots,B-g+1\}, \end{aligned} \tag{2.3.4}$$

where $\rho_{(g,i)}$ is the number of neighboring cells of $BG(g,i)$ given by:

$$\rho_{(g,i)} = \begin{cases} 0, & \text{if } BG(g,i) \text{ is the entire battery,} \\ 1, & \text{if } BG(g,i) \text{ is a BBG with } g < B, \\ 2, & \text{if } BG(g,i) \text{ is an IBG.} \end{cases} \tag{2.3.5}$$

Similarly, the upper bound of the average cell SOC of $BG(g,i)$ at time t can be expressed as

$$\bar{x}^u_{(g,i)}(t) = \bar{x}_{(g,i)}(0) + \frac{\rho_{(g,i)}(1-l_e) - (g-1)l_e}{g\tau} r_e t, \tag{2.3.6}$$
$$g \in \{1,\ldots,B\},\ i \in \{1,\ldots,B-g+1\}.$$

Thus, the average cell SOC of $BG(g,i)$ satisfies the following inequality:

$$\bar{x}^l_{(g,i)}(t) \le \bar{x}_{(g,i)}(t) \le \bar{x}^u_{(g,i)}(t), \tag{2.3.7}$$
$$g \in \{1,\ldots,B\},\ i \in \{1,\ldots,B-g+1\},\ t \ge 0.$$

In particular, for $BG(B,1)$, i.e., the entire B-cell battery, we have

$$\bar{x}_{(B,1)}(t) = \bar{x}^l_{(B,1)}(t) = \bar{x}^u_{(B,1)}(t) = \bar{x}_{(B,1)}(0) - \frac{(B-1)l_e r_e}{B\tau} t. \tag{2.3.8}$$

During the equalization process, the time instant, when all the cells within $BG(g,i)$ merge together for the first time, is referred to as $BG(g,i)$'s *internal equalization time*, denoted as $t^{int}_e(g,i)$. Based on the definition of merging point, clearly,

$$t^{int}_e(g,i) = \begin{cases} 0, & \text{if } g = 1, \\ \max\limits_{j\in\{i,\ldots,i+g-2\}} t_{merge}(j), & \text{if } 2 \le g \le B. \end{cases} \tag{2.3.9}$$

For example, for the 4-cell battery system shown in Figure 2.3.1, $t^{int}_e(1,1) = 0$, $t^{int}_e(2,1) = t_{merge}(1)$, $t^{int}_e(2,2) = t_{merge}(2)$, and $t^{int}_e(4,1) = t_{merge}(3)$. Based on Proposition 2.3.2, from $t = t^{int}_e(g,i)$, all cells in $BG(g,i)$ will remain equalized and their

cell SOC range is bounded, i.e.,

$$\max_{j\in\{i,\ldots,i+g-1\}} x_j(t) - \min_{j\in\{i,\ldots,i+g-1\}} x_j(t) \le (g-1)(4-2l_e)r_e, \tag{2.3.10}$$
$$t \ge t_e^{int}(g,i),\ g\in\{1,\ldots,B\},\ i\in\{1,\ldots,B-g+1\}.$$

Therefore, if r_e is sufficiently small, the SOC of each cell in $BG(g,i)$ can be approximated by $BG(g,i)$'s average cell SOC $\bar{x}_{(g,i)}(t)$ for $t \ge t_e^{int}(g,i)$.

On the other hand, when $BG(g,i)$ merges with any of its neighboring cells for the first time, the time instant is referred to as $BG(g,i)$'s *external equalization time*, denoted as $t_e^{ext}(g,i)$,

$$t_e^{ext}(g,i) = \begin{cases} t_{merge}(g), & \text{if } g<B,\ i=1,\\ \min\{t_{merge}(i-1), t_{merge}(i+g-1)\}, & \text{if } g<B,\ 1<i<B-g+1,\\ t_{merge}(i-1), & \text{if } g<B,\ i=B-g+1,\\ \infty, & \text{if } g=B. \end{cases} \tag{2.3.11}$$

For example, for the 4-cell battery system shown in Figure 2.3.1, $t_e^{ext}(1,1) = t_{merge}(1)$, $t_e^{ext}(1,2) = t_{merge}(1)$, $t_e^{ext}(2,3) = t_{merge}(2)$, and $t_e^{ext}(4,1) = \infty$. Since $BG(g,i)$'s boundary cells do not merge with its neighboring cells until $t = t_e^{ext}(g,i)$, the charge transfer direction and rate between $BG(g,i)$'s boundary cells and neighboring cells are constant for $t < t_e^{ext}(g,i)$. Thus, for $t \in [0, t_e^{ext}(g,i))$, $BG(g,i)$'s average cell SOC, $\bar{x}_{(g,i)}(t)$, can be calculated based on the following result:

Proposition 2.3.4. *In the equalization process with $r_e > 0$ and $r_g = 0$, before a battery group $BG(g,i)$ merges with any of its neighboring cells at $t = t_e^{ext}(g,i)$, its*

average cell SOC can be calculated as

$$\bar{x}_{(g,i)}(t) = \bar{x}_{(g,i)}(0) + \frac{k_{(g,i)}}{g}t, \tag{2.3.12}$$
$$g \in \{1, \ldots, B\},\ i \in \{1, \ldots, B-g+1\},\ t \in [0, t_e^{ext}(g,i)],$$

where

$$k_{(g,i)} = \begin{cases} \frac{(sgnl(x_{i+g}(0)-x_{i+g-1}(0),l_e)-(g-1)l_e)r_e}{\tau},\ \textit{if } g < B,\ i = 1; \\ \frac{(sgnl(x_{i-1}(0)-x_i(0),l_e)r_e+sgnl(x_{i+g}(0)-x_{i+g-1}(0),l_e)r_e-(g-1)l_e r_e}{\tau}, \\ \qquad\qquad \textit{if } g < B,\ 1 < i < B-g+1; \\ \frac{(sgnl(x_{i-1}(0)-x_i(0),l_e)-(g-1)l_e)r_e}{\tau}, \quad \textit{if } g < B,\ i = B-g+1; \\ \frac{-(g-1)l_e r_e}{\tau}, \qquad \textit{if } g = B. \end{cases} \tag{2.3.13}$$

Proof: See Subsection 7.1.2.

As we can see, before a battery group's external equalization time is reached, its average cell SOC is a linear function with parameters determined only by the initial cell SOCs, the equalization rate, and the loss rate. Next, based on the above discussion regarding the internal and external equalization times of a battery group, we introduce a class of special battery groups as follows:

Definition 2.3.5. A merging battery group (MBG) is a battery group $BG(g,i)$ with $t_e^{int}(g,i) < t_e^{ext}(g,i)$.

For a merging battery group $BG(g,i)$, the time interval $[t_e^{int}(g,i), t_e^{ext}(g,i)]$ is referred to as its *active period*. A merging battery group is referred to as being *active* during its active period and *inactive* otherwise. Then, from inequality (2.3.10) and

Proposition 2.3.4, the SOC of each cell in merging battery group $BG(g,i)$ during the active period can be approximated as follows:

$$x_j(t) \approx \bar{x}_{(g,i)}(t) = \bar{x}_{(g,i)}(0) + \frac{k_{(g,i)}}{g}t, \tag{2.3.14}$$
$$i \le j \le i+g-1,\ t_e^{int}(g,i) \le t \le t_e^{ext}(g,i),$$

where $k_{(g,i)}$ is calculated from (2.3.13). The error of this approximation is bounded by:

$$|x_j(t) - \bar{x}_{(g,i)}(t)| < (g-1)(4-2l_e)r_e, \tag{2.3.15}$$
$$i \le j \le i+g-1,\ t_e^{int}(g,i) \le t \le t_e^{ext}(g,i).$$

To illustrate the implications of merging battery groups and its active period, consider again the 4-cell battery system in Figure 2.3.1. At $t = 0$, all individual cells can be viewed as active MBGs. Then, at $t = t_{merge}(1)$, cells b_1 and b_2 merge together and form battery group $BG(2,1)$ (i.e., $\{b_1, b_2\}$). According to Definition 2.3.5, $BG(2,1)$ is an MBG with its active period starting at this merging point, $t_{merge}(1)$. Next, at $t = t_{merge}(2)$, $BG(2,1)$ merges with cell b_3 into the battery group $BG(3,1)$ (i.e., $\{b_1, b_2, b_3\}$), which is an MBG again. Similarly to the previous case, the active period of $BG(3,1)$ starts at the merging point $t_{merge}(2)$. Meanwhile, this merging point also marks the end of the active period of merging battery group $BG(2,1)$ ($\{b_1, b_2\}$). As this procedure goes on, one can easily find out that:

- Each merging point during the equalization process deactivates two MBGs and activates a new MBG at the same time.

- At any time instant during the equalization process, each cell belongs to one and only one active MBG.

Therefore, it is possible to "construct" the entire equalization process by identifying all MBGs with their corresponding active periods and applying approximation formula (2.3.15). This idea can also be observed from Figure 2.3.3, in which each linear segment corresponds to the active period of an MBG. Finally, since, in general, there exist a total of $B-1$ merging points and the system has B initial single-cell active MBGs, the total number of MBGs is $2B-1$.

Next, we will develop an algorithm to approximate each cell's SOC during the equalization process based on the ideas illustrated above.

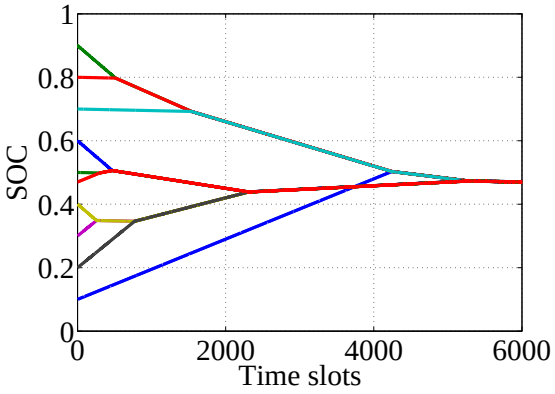

FIGURE 2.3.3: The equalization process of a 10-cell battery system.

2.4 SOC evolution estimation and system performance evaluation of battery equalization process

The previous section discusses the system properties during equalization based on the notions of merging point and merging battery group. In this section, we develop effective and computationally efficient methods to estimate the cell SOC evolution and to evaluate one critical system performance measure (i.e., the battery charge equalization time) when only charge equalization is in place (i.e., $r_e > 0$ and $r_g = 0$).

2.4.1 Estimation of the cell SOC evolution during equalization

The basic idea of the approximation algorithm comes from the properties of the merging points and merging battery groups discussed in the previous subsection. The steps of the algorithm is outlined as follows:

Series-based SOC Estimation Algorithm:

Step 0: Let $s = 0$.

Step 1: Identify all initially active MBGs: For all $i \in \{1, \ldots, B-1\}$, if $x_i(0) = x_{i+1}(0)$, then b_i and b_{i+1} belong to the same initial active MBG; otherwise, b_i and b_{i+1} belong to different initial active MBGs.

Step 2: Using formula (2.3.13), calculate the SOC change rate, $k_{(g,i)}$, for each MBG that is currently active. This leads to a linear function of t for each active MBG:

$$y_{(g,i)}(t) = \bar{x}_{(g,i)}(0) + \frac{k_{(g,i)}}{g}t. \tag{2.4.1}$$

Step 3: Identify the next merging point: For every pair of neighboring MBGs that are currently active, calculate the intersection of the linear functions $y_{(g,i)}(t)$'s obtained in Step 2. Specifically, for active neighboring MBGs, $BG(g_1, i_1)$ and $BG(g_2, i_2)$, their intersection time can be obtained by equating $y_{(g_1,i_1)}(t)$ and $y_{(g_2,i_2)}(t)$ as follows:

$$\begin{aligned} &\bar{x}_{(g_1,i_1)}(0) + \frac{k_{(g_1,i_1)}}{g_1}t = \bar{x}_{(g_2,i_2)}(0) + \frac{k_{(g_2,i_2)}}{g_2}t \\ &\Rightarrow t = g_1 g_2 \frac{\bar{x}_{(g_1,i_1)}(0) - \bar{x}_{(g_2,i_2)}(0)}{g_1 k_{(g_2,i_2)} - g_2 k_{(g_1,i_1)}}. \end{aligned} \tag{2.4.2}$$

Among all intersection times, let $t_m^{(s)}$ denote the smallest one, which results from merging battery groups $BG(g_1^{(s)}, i_1^{(s)})$ and $BG(g_2^{(s)}, i_2^{(s)})$. Without loss of generality, assume $i_1^{(s)} < i_2^{(s)}$.

Step 4: Update the active MBGs: After $t = t_m^{(s)}$, the MBGs $BG(g_1^{(s)}, i_1^{(s)})$ and $BG(g_2^{(s)}, i_2^{(s)})$ identified in Step 3 are both deactivated, while their combination, $BG(g_1^{(s)} + g_2^{(s)}, i_1^{(s)})$, becomes an active MBG. Other active MBGs remain active after $t = t_m^{(s)}$.

Step 5: For $t > t_m^{(s)}$, if there is only one MBG being active (i.e., all cells have merged), let $S = s$ and stop the algorithm; otherwise, let $s = s + 1$ and return to Step 2.

After the algorithm is terminated, we will obtain the (approximate) locations of all merging points, all merging battery groups, and their active periods. Assume cell b_j belongs to active merging battery group $BG(g, i)$ at time t. Then, the SOC of b_j

at time t can be approximated as:

$$\hat{x}_j(t) = \bar{x}_{(g,i)}(0) + \frac{k_{(g,i)}}{g}t, \ i \leq j \leq i+g-1. \tag{2.4.3}$$

Using this method, the equalization process shown in Figure 2.3.1 can be approximated as shown in Figure 2.4.1.

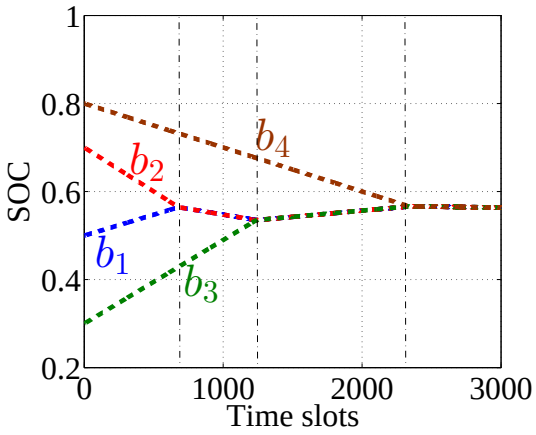

FIGURE 2.4.1: The approximation of the equalization process in Figure 2.3.1.

In order to test the accuracy of the above algorithm for approximating cell SOCs during the equalization process, iterative simulation is carried out based on the mathematical model described in Section 2.2. The number of cells in the system is selected from $B \in \{4, 8, 16, 32, 64, 128\}$. For each B, a total of 10,000 samples are studied with initial cell SOCs randomly generated based on uniform distribution $U(x_{lb}, x_{ub})$ with $x_{lb} = 0.05$ and $x_{ub} = 0.95$. The equalization rate and loss rate are selected as $r_e = 10^{-7}$ and $l_e = 0.05$. These parameters are used such that they reflect typical battery equalization systems in practice [21, 24, 59]. For instance, if an equalizer with a working cycle of 0.001 s (i.e., 1 kHz frequency) is capable of transferring 10%

SOC in 30 min, then the corresponding value of r_e in the mathematical model can be calculated as $0.1/(1800 \times 1000) = 0.56 \times 10^{-7}$.

For each sample generated above, we first "simulate" the system evolution by iteratively calculating all the cell SOCs $x_i(t_n)$ based on (2.2.1)-(2.2.3) until all the cells in the battery are equalized at its equalization time, T_e. Then, the proposed approximation algorithm is carried out under the same initial condition to calculate the approximated cell SOCs, $\hat{x}_i(t)$ for $t \in [0, T_e]$. Finally, for each B-cell sample, the mean absolute percentage error $\bar{\epsilon}_{soc}$ and maximum absolute percentage error ϵ_{soc}^{max} are calculated as follows:

$$\bar{\epsilon}_{soc} = \frac{\sum_{i=1}^{B} \sum_{n=0}^{\lfloor \frac{T_e}{\tau} \rfloor} \frac{|\hat{x}_i(t_n) - x_i(t_n)|}{x_i(t_n)}}{B(\lfloor \frac{T_e}{\tau} \rfloor + 1)} \times 100\%, \tag{2.4.4}$$

$$\epsilon_{soc}^{max} = \max_{\substack{i \in \{1, \ldots, B\} \\ n \in \{0, \ldots, \lfloor \frac{T_e}{\tau} \rfloor\}}} \frac{|\hat{x}_i(t_n) - x_i(t_n)|}{x_i(t_n)} \times 100\%, \tag{2.4.5}$$

where $t_n = n\tau$. For fixed B, let $\bar{\epsilon}_{soc}(B)$ and $\epsilon_{soc}^{max}(B)$ denote the average value of $\bar{\epsilon}_{soc}$ and the maximum value of ϵ_{soc}^{max}, respectively, from the 10,000 samples. In addition, the average iterative simulation time per sample and average approximation time per sample are denoted as $T_{sim}(B)$ and $T_{app}(B)$, respectively. The results are summarized in Table 2.4.1. As we can see, both $\bar{\epsilon}_{soc}(B)$ and $\epsilon_{soc}^{max}(B)$ are very small, i.e., the approximation of cell SOCs during the equalization process is very close to the iterative simulation results. However, when we compare the computational costs of approximation and iterative simulation, it is obvious that the approximation method is much more efficient than the iterative simulation. Therefore, we claim that the Series-based SOC Estimation Algorithm and equation (2.4.3) can be used to

effectively and efficiently evaluate the cell SOCs during the equalization process.

TABLE 2.4.1: Average $\bar{\epsilon}_{soc}$, maximum ϵ_{soc}^{max}, average iterative simulation time and average approximation time

B	$\bar{\epsilon}_{soc}(B)$	$\epsilon_{soc}^{max}(B)$	$T_{sim}(B)$	$T_{app}(B)$
4	<0.0001%	<0.0003%	0.6504 s	<0.0001 s
8	<0.0001%	<0.0003%	1.4818 s	<0.0001 s
16	<0.0001%	0.0003%	4.1559 s	<0.0001 s
32	<0.0001%	0.0005%	12.2191 s	0.0001 s
64	0.0001%	0.0011%	32.0580 s	0.0005 s
128	0.0002%	0.0028%	86.4782 s	0.0020 s

In addition to comparing the estimated cell SOCs with the results from iterative simulation, we also verify the accuracy of the proposed SOC estimation algorithm by the data from physical experiments. Consider a 5-cell series-based BCE system tested by the physical circuit experiment in [58]. We use the original initial cell SOCs, parameter values, and external charging/discharging profile provided in [58] to test the Series-based SOC Estimation Algorithm and the estimated cell SOC evolution is shown in Fig. 2.4.2, where the original experimental data is used as the background to facilitate the comparison of cell SOC evolution. As we can see from Fig. 2.4.2, when performing this estimation algorithm, the merging points, i.e., $T_{merge}(1)$, $T_{merge}(2)$, $T_{merge}(3)$, and $T_{merge}(4)$, are identified one by one, and then the cell SOC evolution between the initial points, merging points, final points are estimated using the derived cell SOC approximation formulas. In addition, as shown in Fig. 2.4.2, both the estimated cell SOC evolution (i.e., purple curves) and the estimated time instant when all cell SOCs get equalized (i.e., the last merging point $T_{merge}(4)$) well match the experimental data provided in [58] under the same initial cell SOCs, parameter values, and charging/discharging profile. This implies that the Series-based SOC Estimation Algorithm can be used to obtain an accurate estimation of the cell SOC

evolution in series-based BCE systems.

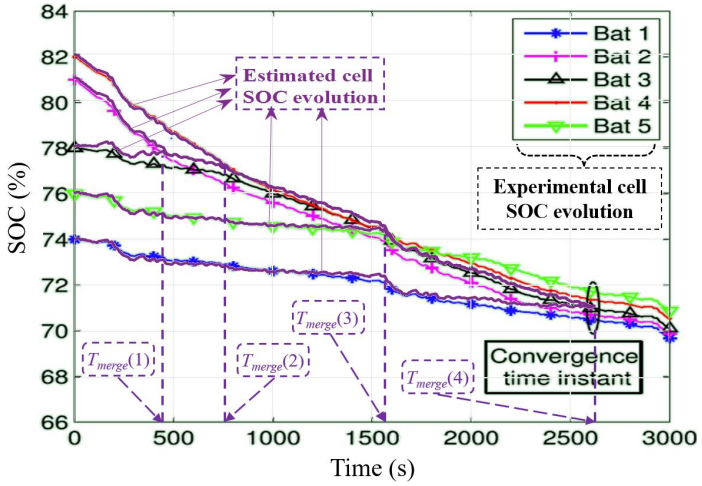

FIGURE 2.4.2: Comparison of the cell SOC evolution estimated by the Series-based SOC Estimation Algorithm and the experimental data from [58] for a 5-cell series-based BCE system.

2.4.2 Battery charge equalization time

As one can see, using the Series-based SOC Estimation Algorithm, the BCE time can be approximated as $\widehat{T}_e = t_m^{(S)}$, i.e., the last merging point identified by the algorithm before its termination. Note that, in some cases, we may be only interested in the BCE time of the system, instead of individual cell SOCs during the process. Therefore, it is desirable if $\widehat{T}_e$ can be calculated using a simpler approach without identifying all merging points and MBGs involved in the Series-based SOC Estimation Algorithm. Fortunately, as it turns out, $\widehat{T}_e$ can be obtained based on the following:

Proposition 2.4.1. *In the approximated equalization process generated by the Series-based SOC Estimation Algorithm, the approximated BCE time* $\widehat{T}_e$ *can be directly cal-*

culated by

$$\widehat{T}_e = \max_{g\in\{1,\ldots,B-1\}} t_{ideal}(g,1), \tag{2.4.6}$$

where

$$t_{ideal}(g,i) = \begin{cases} \frac{(\bar{x}_{(g,i)}(0)-\bar{x}_{(B,1)}(0))\tau}{-((\frac{1}{g}-\frac{1}{B})l_e-\frac{\rho_{(g,i)}}{g})r_e}, & \text{if } \bar{x}_{(g,i)}(0) > \bar{x}_{(B,1)}(0), \\ \frac{(\bar{x}_{(g,i)}(0)-\bar{x}_{(B,1)}(0))\tau}{-((\frac{1}{g}-\frac{1}{B})l_e+\frac{\rho_{(g,i)}(1-l_e)}{g})r_e}, & \text{if } \bar{x}_{(g,i)}(0) < \bar{x}_{(B,1)}(0), \end{cases} \tag{2.4.7}$$

$g \in \{1,\ldots,B-1\},\ i \in \{1,\ldots,B-g+1\}.$

Proof: See Subsection 7.1.3.

Note that the $t_{ideal}(g,i)$ defined in (2.4.7) indicates the shortest time for the average cell SOC of $BG(g,i)$ to reach the average cell SOC of the entire battery system. Specifically, if $\bar{x}_{(g,i)}(0) > \bar{x}_{(B,1)}(0)$, in order to reach $\bar{x}_{(B,1)}(t)$ in the fastest possible manner, $BG(g,i)$ should always transfer charge to its neighboring cells. In other words, the average cell SOC of $BG(g,i)$ should be set to its lower bound defined in (2.3.4): $\bar{x}^l_{(g,i)}(t)$. It can be shown that $t_{ideal}(g,i)$ is the intersection time of $\bar{x}^l_{(g,i)}(t)$ and $\bar{x}_{(B,1)}(t)$. On the other hand, if $\bar{x}_{(g,i)}(0) < \bar{x}_{(B,1)}(0)$, in order to quickly reach $\bar{x}_{(B,1)}(t)$, $BG(g,i)$ should always receive charge from its neighboring cells. Thus, the average cell SOC of $BG(g,i)$ should be set to its upper bound defined in (2.3.6), and it can be shown that $t_{ideal}(g,i)$ is the intersection time of $\bar{x}^u_{(g,i)}(t)$ and $\bar{x}_{(B,1)}(t)$.

In order to study the accuracy of the formula (2.4.6) for equalization time approximation, the same data set and approach used in the justification of the accuracy of the Series-based SOC Estimation Algorithm is adopted again. The parameters are selected as follows: $B \in \{4,8,16,32,64,128\}$, $r_e \in \{10^{-5},10^{-6},10^{-7}\}$, and $l_e = 0.05$.

For each sample, we use iterative simulation to obtain its "true" equalization time T_e. Meanwhile, we calculate the approximated equalization time, $\widehat{T}_e$, using Proposition 2.4.1 under the same initial condition. Then for each sample, the error of the approximation is defined as

$$\epsilon_e = \frac{|\widehat{T}_e - T_e|}{T_e} \times 100\%. \tag{2.4.8}$$

The average values of ϵ_e for fixed B are summarized in Table 2.4.2. As one can see, the error is very small for all cases studied. In particular, for fixed B, if r_e is decreased by 10 times, then $\bar{\epsilon}_e$ is also reduced by about 10 times. This can be explained by Proposition 2.3.2: Since the decreasing r_e narrows down the cell SOC range after each merging point, the approximation error is reduced and, thus, the approximation of equalization time becomes more accurate. Note that, as discussed in Subsection 2.4.1, the practical equalization rate is typically very small (e.g., $r_e = 10^{-7}$ or smaller). Therefore, we claim that Proposition 2.4.1 can be used to effectively and efficiently evaluate the equalization time of the battery system under consideration.

TABLE 2.4.2: Average $\bar{\epsilon}_e$ for 10000 samples with different r_e

r_e	10^{-5}	10^{-6}	10^{-7}
$\bar{\epsilon}_e(4)$	0.0028%	0.0003%	<0.0001%
$\bar{\epsilon}_e(8)$	0.0103%	0.0010%	0.0001%
$\bar{\epsilon}_e(16)$	0.0334%	0.0033%	0.0003%
$\bar{\epsilon}_e(32)$	0.0968%	0.0097%	0.0010%
$\bar{\epsilon}_e(64)$	0.2718%	0.0272%	0.0027%
$\bar{\epsilon}_e(128)$	0.7594%	0.0763%	0.0076%

2.5 System performance evaluation under simultaneous equalization and charging/discharging

The previous sections discuss the system-theoretic properties and performance evaluation assuming $r_g = 0$, i.e., no charging/charging in place. In this section, we study the system behavior when equalization and charging/discharging occur simultaneously.

2.5.1 Approximation of cell SOCs

In Subsection 2.4.1, the Series-based SOC Estimation Algorithm has been developed to effectively and efficiently approximate the cell SOCs during equalization. In fact, based on the superposition of equalization process and charging/discharging process, the same method can be directly used to approximate the cell SOCs during simultaneous equalization and charging/discharging by only modifying approximation formula (2.4.3) into

$$\hat{x}_j(t) = \bar{x}_{(g,i)}(0) + \frac{k_{(g,i)}}{g}t + \frac{r_g}{\tau}t,\ i \leq j \leq i+g-1, \tag{2.5.1}$$

where $BG(g,i)$ is an active MBG at time t from the Series-based SOC Estimation Algorithm. The estimation accuracy of this algorithm is already verified in Fig. 2.4.2.

It should be noted that some $\hat{x}_j(t)$'s calculated above may have exceeded x_{ub} or x_{lb} before the final merging point identified by the Series-based SOC Estimation Algorithm. This implies that the system process is terminated because the upper limit or lower limit of SOC is reached before all cells are equalized. In this case, it is necessary to keep track of the *maximum* and *minimum cell SOCs* at any time of the system evolution. The calculation of these two can be directly carried out based on system initial condition thanks to the following:

Proposition 2.5.1. *In the simultaneous charging/discharging process and approximated equalization process generated by the Series-based SOC Estimation Algorithm and (2.5.1), the maximum and minimum of the approximated cell SOCs at time t can be calculated as*

$$\max_{j\,\in\,\{1,\ldots,B\}} \hat{x}_j(t) = \max_{\substack{g\,\in\,\{1,\ldots,B\}\\ i\,\in\,\{1,\ldots,B-g+1\}\\ \bar{x}_{(g,i)}(0)\,\geq\,\bar{x}_{(B,1)}(0)}} \bar{x}^l_{(g,i)}(t) + \frac{r_g}{\tau}t, \quad t \geq 0, \tag{2.5.2}$$

$$\min_{j\,\in\,\{1,\ldots,B\}} \hat{x}_j(t) = \min_{\substack{g\,\in\,\{1,\ldots,B\}\\ i\,\in\,\{1,\ldots,B-g+1\}\\ \bar{x}_{(g,i)}(0)\,\leq\,\bar{x}_{(B,1)}(0)}} \bar{x}^u_{(g,i)}(t) + \frac{r_g}{\tau}t, \quad t \geq 0, \tag{2.5.3}$$

where $\bar{x}^l_{(g,i)}(t)$ and $\bar{x}^u_{(g,i)}(t)$ are defined in (2.3.4) and (2.3.6), respectively.

Proof: See Subsection 7.1.4.

Since Proposition 2.5.1 is also derived in the approximated process based on MBGs and their properties, the approximated maximum and minimum cell SOCs obtained above have similar accuracy as that of cell SOC approximation summarized in Table 2.4.1.

2.5.2 Charging and discharging time

In the presence of charging or discharging (i.e., with $r_g \neq 0$), when any cell's SOC reaches the x_{ub} (respectively, x_{lb}) for the first time, the time instant is referred to as *charging time*, denoted as T_c, (respectively, *discharging time*, denoted as T_d). In addition, the balancing effect caused by equalizers will "prolong" the original charging or discharging process. Clearly, if the equalization process is fast enough, then the SOCs of all cells can reach x_{ub} (respectively, x_{lb}), which is the most desirable scenario.

For example, as shown in Figure 2.2.2, the charging time is extended from about 2000 working cycles without equalization to about 2340 working cycles with equalization. As a result, the battery system is able to make use of its whole capacity. On the other hand, the energy loss during the equalization process may cause the scenario that no cell SOC can reach x_{ub} even if $r_g > 0$. In other words, the charging time may not exist. Thus, Lemma 2.5.2 is introduced to help determine the existence of charging time or discharging time.

Lemma 2.5.2. *For the approximated equalization process of a battery system with* $x_i(0) \in (x_{lb}, x_{ub})$, $i = 1, \ldots, B$, T_c *exists if and only if* $r_g > \frac{B-1}{B} l_e r_e$; T_d *exists if and only if* $r_g < \frac{B-1}{B} l_e r_e$.

Proof: See Subsection 7.1.5.

Based on Lemma 2.5.2, we will discuss how to calculate the charging or discharging time next.

Consider the approximated cell SOCs obtained by the Series-based SOC Estimation Algorithm and formula (2.5.1). Without loss of generality, assume that $x_i(0) \in (x_{lb}, x_{ub})$ (otherwise, the system evolution is terminated at $t = 0$). Let $\widehat{T}_c$ (respectively, $\widehat{T}_d$) denote the time instant when any $\hat{x}_j(t)$ reaches x_{ub} (respectively, x_{lb}) for the first time during the process. Clearly, $\widehat{T}_c$ and $\widehat{T}_d$ are the solutions to the following equations:

$$\max_{j \in \{1,\ldots,B\}} \hat{x}_j(\widehat{T}_c) = x_{ub}, \ r_g > \frac{(B-1)}{B} l_e r_e, \tag{2.5.4}$$

$$\min_{j \in \{1,\ldots,B\}} \hat{x}_j(\widehat{T}_d) = x_{lb}, \ r_g < \frac{(B-1)}{B} l_e r_e. \tag{2.5.5}$$

Similar to Subsection 2.4.2, both $\widehat{T}_c$ and $\widehat{T}_d$ can be directly calculated based on

the system parameters and initial condition using the method below:

Proposition 2.5.3. *Consider the approximated cell SOCs obtained by the Series-based SOC Estimation Algorithm and formula (2.5.1). The approximated charging time $\widehat{T}_c$ and approximated discharging time $\widehat{T}_d$ can be calculated by*

$$\widehat{T}_c = \min_{\substack{g \in \{1,\dots,B\}, i \in \{1,\dots,B-g+1\} \\ \bar{x}_{(g,i)}(0) \geq \bar{x}_{(B,1)}(0) \\ gr_g > ((g-1)l_e + \rho_{(g,i)})r_e}} t_c^{(g,i)}, \ r_g > \frac{(B-1)}{B} l_e r_e, \tag{2.5.6}$$

$$\widehat{T}_d = \min_{\substack{g \in \{1,\dots,B\}, i \in \{1,\dots,B-g+1\} \\ \bar{x}_{(g,i)}(0) \leq \bar{x}_{(B,1)}(0) \\ gr_g < ((g-1)l_e - \rho_{(g,i)}(1-l_e))r_e}} t_d^{(g,i)}, \ r_g < \frac{(B-1)}{B} l_e r_e, \tag{2.5.7}$$

where

$$t_c^{(g,i)} = \frac{g(x_{ub} - \bar{x}_{(g,i)}(0))\tau}{gr_g - ((g-1)l_e + \rho_{(g,i)})r_e}, \ t_d^{(g,i)} = \frac{g(x_{lb} - \bar{x}_{(g,i)}(0))\tau}{gr_g - ((g-1)l_e - \rho_{(g,i)}(1-l_e))r_e},$$
$$g \in \{1,\dots,B\}, \ i \in \{1,\dots,B-g+1\}.$$

Proof: See Subsection 7.1.6.

To evaluate the accuracy of the approximation method described in Proposition 2.5.3, the same data set and approach used in the accuracy justifications in the previous section are used. The parameters are selected as follows: $B \in \{4, 8, 16, 32, 64, 128\}$, $r_e \in \{10^{-5}, 10^{-6}, 10^{-7}\}$, $l_e = 0.05$, $x_{lb} = 0.05$, and $x_{ub} = 0.95$.

For each sample, we use iterative simulation to obtain its "true" charging time T_c and discharging time T_d. Meanwhile, we calculate the approximated charging or discharging time, $\widehat{T}_c$ and $\widehat{T}_d$ using Proposition 2.5.3 under the same initial condition.

Then for each sample, the error of the approximation is defined as

$$\epsilon_c = \frac{|\widehat{T}_c - T_c|}{T_c} \times 100\%, \tag{2.5.8}$$

$$\epsilon_d = \frac{|\widehat{T}_d - T_d|}{T_d} \times 100\%. \tag{2.5.9}$$

The average values of ϵ_c and ϵ_d for fixed B are summarized in Table 2.5.1 and Table 2.5.2, respectively. As we can see, Proposition 2.5.3 can be used to evaluate the charging and discharging times of the considered battery equalization systems with high accuracy and the calculation results are more accurate with smaller r_e.

TABLE 2.5.1: Average $\bar{\epsilon}_c$ for 10000 samples with different r_g and r_e

r_e	10^{-5}	10^{-6}	10^{-7}
r_g	10^{-5}	10^{-6}	10^{-7}
$\bar{\epsilon}_c(4)$	0.0041%	0.0004%	<0.0001%
$\bar{\epsilon}_c(8)$	0.0067%	0.0007%	<0.0001%
$\bar{\epsilon}_c(16)$	0.0107%	0.0011%	0.0001%
$\bar{\epsilon}_c(32)$	0.0127%	0.0013%	0.0001%
$\bar{\epsilon}_c(64)$	0.0134%	0.0013%	0.0001%
$\bar{\epsilon}_c(128)$	0.0148%	0.0015%	0.0002%

TABLE 2.5.2: Average $\bar{\epsilon}_d$ for 10000 samples with different r_g and r_e

r_e	10^{-5}	10^{-6}	10^{-7}
r_g	-10^{-5}	-10^{-6}	-10^{-7}
$\bar{\epsilon}_d(4)$	0.0043%	0.0004%	<0.0001%
$\bar{\epsilon}_d(8)$	0.0070%	0.0007%	<0.0001%
$\bar{\epsilon}_d(16)$	0.0104%	0.0010%	0.0001%
$\bar{\epsilon}_d(32)$	0.0120%	0.0012%	0.0001%
$\bar{\epsilon}_d(64)$	0.0130%	0.0013%	0.0001%
$\bar{\epsilon}_d(128)$	0.0148%	0.0015%	0.0002%

2.6 Summary

In this chapter, we study the system-theoretic properties, cell SOC estimation, and performance evaluation of series-based BCE systems with energy loss during equalization, charging, and discharging processes. Specifically, a mathematical model is constructed to describe the system-level dynamics of charge transfers. Then, we analyze the equalization process based on the properties of merging points and merging battery groups. These analyses lead to the development of accurate and computationally efficient algorithms to approximate the cell SOCs during the charge equalization process and to calculate the time required to achieve complete charge balance under given initial conditions. Finally, the approach is extended to analyze the system with simultaneous equalization and charging/discharging. Algorithms are developed for approximating individual cell SOCs, maximum and minimum cell SOCs, and charging and discharging times. The accuracy of the algorithms proposed is validated using extensive numerical experiments and physical circuit experiments. It should be noted that a number of other system performance metrics (e.g., total energy loss, range of SOCs) can be calculated based on the ones studied in this chapter.

Chapter 3

Module-based battery charge equalization system

3.1 Introduction

Battery charge imbalance becomes a very common issue in multi-cell/module/pack battery systems especially large-scale battery systems [60, 61]. The battery charge imbalance could result in charge capacity reduction, early termination of charging or discharging, accelerated battery degradation, and even safety hazards such as fire and explosion [14, 16, 55, 62]. For example, severe charge imbalance among the series-connected lithium-ion battery cells in a laptop computer could drive permanent disabling of the entire battery pack [63]. In general, it is suggested that battery applications requiring high current or more than 12 battery cells should use a custom solution for safety and cell charge balancing [60].

In order to mitigate the charge imbalance in battery systems, a number of battery

charge equalizers are developed and applied to the battery charge equalization (BCE) systems. In Chapter 2, we have studied the mathematical modeling, estimation of cell SOC evolution, and evaluation of critical system performance measures in series-based BCE systems. In this chapter, we will investigate another widely-used BCE system, i.e.. the module-based BCE system. In this system, all series-connected battery cells are grouped into battery modules, and module-level charge equalizers are connected to every two adjacent battery modules to balance their charge. In addition, inside each battery module, a series-based BCE system is constructed.

The charge balance or equalization performance of a BCE system depends on its two components: the battery system and the BCE structure. While a number of charge equalizers and balance topologies have been developed in recent years, their charge balance or equalization performance measures are usually evaluated under only a small set of initial battery system states. In practice, battery charge imbalance may occur at any system state during system operation. Thus, the performance of a BCE system should be evaluated against a large number of diverse operational states. To achieve this, circuit experiments and model-based computer simulations are usually applied. However, to carry out extensive performance tests, especially for large-scale battery systems, circuit experiments usually consume a great amount of energy and time [14, 57]. Meanwhile, computer simulations may also be very time-consuming [20, 41, 42, 64]. Therefore, computationally efficient tools become of great importance for accurate estimation of the charge equalization behavior and performance under various battery system states.

Motivated by this, for the module-based BCE system, we develop computationally efficient methods to estimate the battery cell state evolution as well as to evaluate critical system performance measures, such as the charge equalization time and

charging/discharging time. While most methods reported recently focus on estimating *single* battery cell's state at the current moment based on some current physical measurements, e.g., those reviewed in [65, 66] and applied/proposed in [67, 68, 69, 70], the algorithm proposed in this chapter is aimed at quickly providing an accurate estimation of *all* battery cells' state evolution throughout the entire charge equalization process.

In addition, when cell-to-cell charge balancing and charging/discharging are implemented simultaneously, both the charge transfer rate and charging/discharging rate need to be coordinated to avoid overcharging/overdischarging issues. This is of great importance for the safe and efficient operation of battery systems, but has not been systematically investigated in the literature. Thus, in this study, constraints on charge transfer rates and charging rates are derived to ensure that the charge equalization outpaces charging/discharging, and, as a result, no battery cell suffers from overcharging/overdischarging.

The remainder of this chapter is organized as follows: The mathematical model of module-based BCE systems is formulated in Section 3.2. Based on this model, an computationally efficient algorithm for estimating the battery cell state evolution throughout the charge equalization process is proposed in Section 3.3. Next, the formulas for quickly calculating the battery charge equalization time are derived in Section 3.4. The analysis is extended to the charging/discharging process of module-based BCE systems in Section 3.5. Finally, conclusions and future work are summarized in Section 3.6. All proofs are given in Section 7.2.

3.2 Mathematical model of the module-based BCE system

3.2.1 Series-based BCE system and module-based BCE system

For series-connected battery systems, the module-based BCE structure has emerged as one promising solution to battery charge imbalance [6, 19, 20, 41] for its advantages such as low voltage stress, small size, and low cost [19]. A mathematical model of module-based BCE system using cell-to-cell charge equalizers was introduced in [41]. In this model, the charge transfer loss is not considered. In practice, however, such loss cannot be ignored and it reflects the energy efficiency of the battery charge balance process. Moreover, since the energy loss is usually dissipated as heat, it is closely related to the safe and reliable operation of battery systems. Thus, in this chapter, we will take into account the charge transfer loss when modeling the module-based BCE system.

To facilitate the model formulation for the module-based BCE system, we first briefly review the modeling of the series-based BCE system introduced in Chapter 2. As shown in Fig. 3.2.1, a series-based BCE system consists of a group of battery cells connected in series and a *cell-level series-based BCE structure* in which each cell-level equalizer is connected to two adjacent battery cells to balance their charge [41, 42]. A number of circuit designs of battery charge equalizers have been proposed in recent decades (see, for instance, our prior review in [20]). One commonly used cell-to-cell charge equalizer, designed in [24], is shown in Fig. 3.2.2. During each working cycle of such an equalizer, the charge is transferred from the cell with higher charge to the cell with lower charge through the two inductors and one capacitor so that their

charge can gradually get balanced.

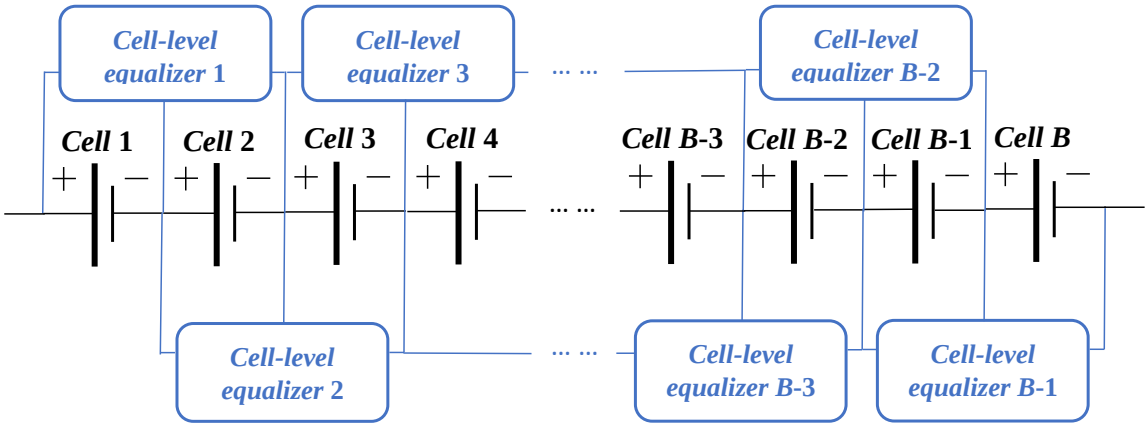

FIGURE 3.2.1: Series-based BCE system.

Now consider a battery system consisting of several series-based BCE systems connected in series, and each of these subsystems is referred to as a *battery module*. In order to perform charge balance among these battery modules, module-level equalizers are connected to each pair of consecutive battery modules, i.e., under a *module-level series-based BCE structure*. This leads to the module-based BCE system shown in Fig. 3.2.3.

Therefore, the module-based BCE system can be viewed as a series-connected battery system with both cell-level and module-level series-based BCE structures. Specifically, the module-based BCE system shown in Fig. 3.2.3 consists of M series-connected battery modules, to which $M-1$ module-level charge equalizers are connected. Inside each battery module, as shown in Fig. 3.2.1, there are B battery cells and $B-1$ associated cell-level charge equalizers. In other words, a module-based BCE system with M modules can be broken down into $M+1$ subsystems: one *module-level* series-based BCE system and M *cell-level* series-based BCE systems.

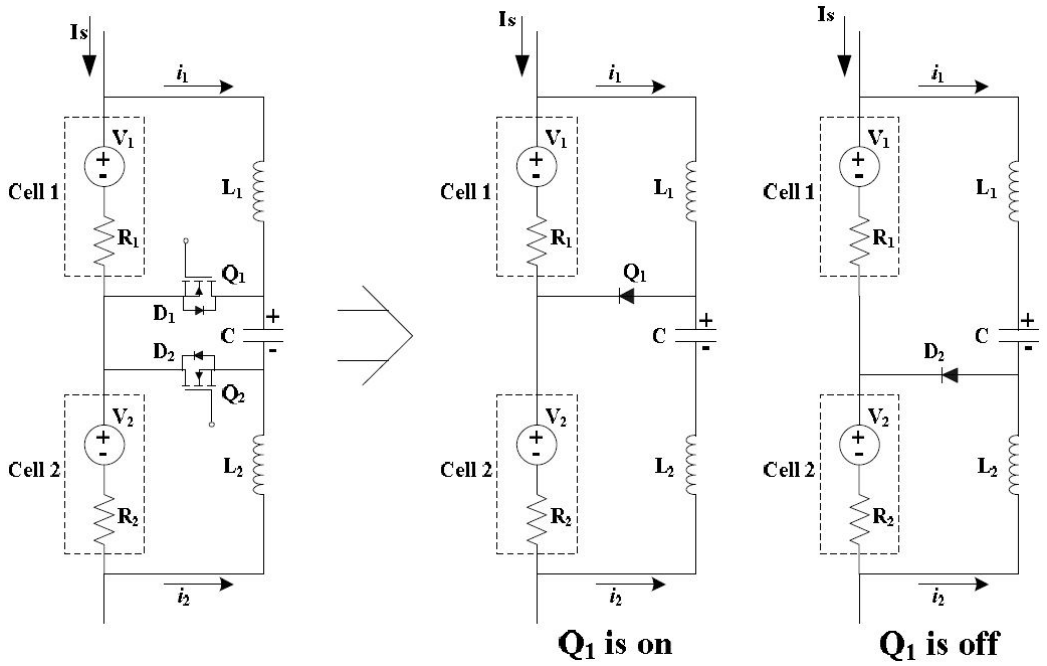

FIGURE 3.2.2: A cell-to-cell charge equalizer based on the modified bidirectional Cûk converter designed in [24].

3.2.2 Model formulation of the module-based BCE system

In practice, the state of charge (SOC) is commonly used to characterize the amount of charge in a battery cell. Again, a battery cell's SOC is defined by the ratio of the cell's present amount of charge to its rated charge capacity [71]. Series-connected battery cells usually have identical rated charge capacity, which is denoted by C_B. Then, battery cell SOCs can be used to represent and compare battery cells' amount of charge. Note that, in this chapter we mainly focus on modeling the interactive behavior of battery cells driven by cell-to-cell and module-to-module charge transfers. Besides, the charge equalization structures shown in Fig. 3.2.1 and Fig. 3.2.3 can be applied to various battery types. Thus, in order to simplify the mathematical modeling, a lumped model based on only SOC is used to characterize each battery cell's state

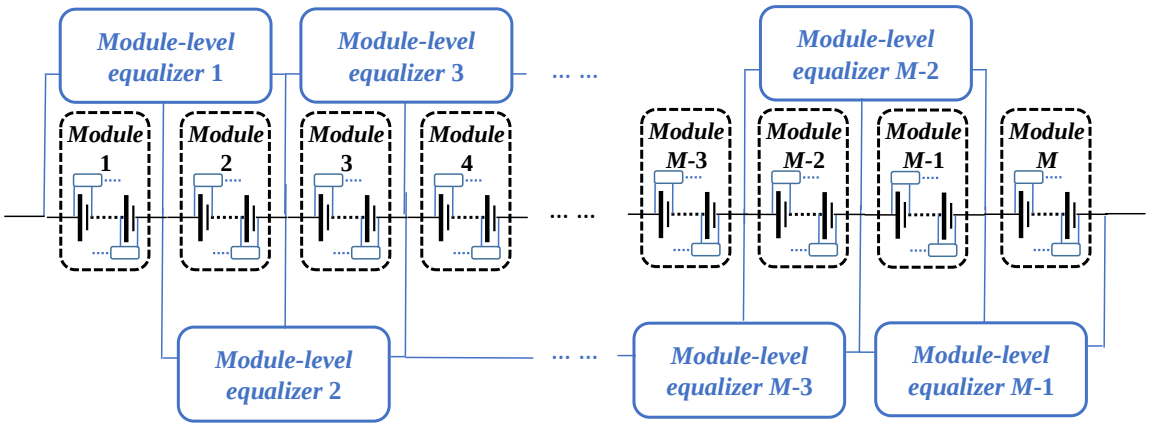

FIGURE 3.2.3: Module-based BCE system.

without considering the cell's internal distributed dynamics and polarization voltage.

Consider a module-based BCE system with M modules and B cells per module. Let $x_i(t) \in [x_{lb}, x_{ub}],\ i = 1, 2, \ldots, B \times M$, denote the i-th battery cell's SOC at any time instant $t \geq 0$, where $x_{lb} \geq 0$ and $x_{ub} \leq 1$ are the battery cell SOC's lower bound and upper bound, respectively.

In the module-based BCE system, charge equalization is typically performed periodically according to the *working cycle of charge equalizers*, i.e., the control period of charge equalization controllers. For instance, the working cycle of charge equalizers is about 30 to 160 μs in [21], while it is set to 1 s in [24]. For the module-based BCE systems considered here, we assume all module-level and cell-level equalizers are synchronized with identical working cycle, denoted by τ. Let $t_n = n\tau,\ n = 0, 1, 2, \ldots$ Then, $[t_{n-1}, t_n)$ is the time interval of the n-th working cycle for all charge equalizers.

To formulate the model, first consider the cell-level charge transfer behavior within each battery module. At the beginning of each working cycle, each cell-level equalizer compares the SOCs of the two adjacent cells connected to it, and then transfers charge

from the higher-charge cell to the lower-charge one. Specifically, during each working cycle, the higher-charge cell releases $r_c C_B$ units of charge and the lower-charge cell receives $(1-l_c)r_c C_B$ units of charge. Meanwhile, the rest $l_c r_c C_B$ units of charge is lost during the transfer. Here the parameters r_c and l_c are referred to as the *cell-level charge transfer rate* and *cell-level charge transfer loss rate*, respectively. As a result, at the end of each working cycle, the SOC of the higher-charge cell will decrease by r_c, while that of the lower-charge one will increase by $(1-l_c)r_c$. In a module-based BCE system, where each module includes B cells, the i-th battery cell belongs to the $\lceil \frac{i}{B} \rceil$-th module. Then, during the n-th working cycle, the SOC change of the i-th cell caused by the charge transfer with its left and right neighboring cells within the same module (in the sense as illustrated by Fig. 3.2.1 and Fig. 3.2.3) are denoted by $k_i^{cl}(n)$ and $k_i^{cr}(n)$, respectively, which can be calculated by

$$k_i^{cl}(n) = \begin{cases} \text{sgnl}\left(-\Delta_i^c(n-1), l_c\right) r_c, & \text{if } i-1 > \left(\lceil \frac{i}{B} \rceil - 1\right) B, \\ 0, & \text{otherwise}, \end{cases} \tag{3.2.1}$$

$$k_i^{cr}(n) = \begin{cases} \text{sgnl}\left(\Delta_{i+1}^c(n-1), l_c\right) r_c, & \text{if } i+1 \leq \lceil \frac{i}{B} \rceil B, \\ 0, & \text{otherwise}, \end{cases} \tag{3.2.2}$$

where

$$\text{sgnl}(u,v) = \begin{cases} -1, & \text{if } u < 0, \\ 0, & \text{if } u = 0, \\ 1-v, & \text{if } u > 0, \end{cases} \tag{3.2.3}$$

$$\Delta_h^c(n-1) = x_h(t_{n-1}) - x_{h-1}(t_{n-1}).$$

Clearly, $\Delta_h^c(n-1)$ is the SOC difference between the h-th cell and its left neighboring cell at $t = t_{n-1}$, while function $\mathrm{sgnl}(u, v)$ determines the charge transfer direction.

On the module level, the equalizers work in a similar manner except that they compare and transfer charge between every two adjacent modules with the module-level charge transfer rate, r_m, and module-level charge transfer loss rate, l_m. Since all cells are connected in series in each module, they always share the same module-level charge transfer current. As a result, at the end of each working cycle, the SOC of each cell in the higher-charge module will decrease by r_m, while those in the lower-charge module will increase by $(1-l_m)r_m$ each. Thus, during the n-th working cycle, the SOC change of the i-th cell caused by the charge transfer with its left and right neighboring modules (in the sense as illustrated by Fig. 3.2.3) are denoted by $k_i^{ml}(n)$ and $k_i^{mr}(n)$, respectively, which can be calculated by

$$k_i^{ml}(n) = \begin{cases} \mathrm{sgnl}\left(-\Delta_i^m(n-1), l_m\right) r_m, & \text{if } \lceil \frac{i}{B} \rceil - 1 > 0, \\ 0, & \text{otherwise}, \end{cases} \tag{3.2.4}$$

$$k_i^{mr}(n) = \begin{cases} \mathrm{sgnl}\left(\Delta_{i+B}^m(n-1), l_m\right) r_m, & \text{if } \lceil \frac{i}{B} \rceil + 1 \leq M, \\ 0, & \text{otherwise}, \end{cases} \tag{3.2.5}$$

$$\Delta_h^m(n-1) = \sum_{j=\left(\lceil \frac{h}{B} \rceil - 1\right)B+1}^{\lceil \frac{h}{B} \rceil B} x_j(t_{n-1}) - \sum_{j=\left(\lceil \frac{h}{B} \rceil - 2\right)B+1}^{\left(\lceil \frac{h}{B} \rceil - 1\right)B} x_j(t_{n-1}),$$

where $\mathrm{sgnl}(u, v)$ is defined by (3.2.3), and $\Delta_h^m(n-1)$ is the difference of the total cell SOCs between the module containing the h-th cell and its left neighboring module at $t = t_{n-1}$.

Based on the above, during the n-th working cycle, the net SOC change of the i-th cell caused by both cell-level and module-level charge transfers is denoted by $k_i^{net}(n)$,

and can be calculated as the sum of (3.2.1), (3.2.2), (3.2.4), and (3.2.5), i.e.,

$$k_i^{net}(n) = k_i^{cl}(n) + k_i^{cr}(n) + k_i^{ml}(n) + k_i^{mr}(n). \tag{3.2.6}$$

Finally, based on (3.2.6), the cell SOC evolution during each working cycle is given by

$$\begin{aligned} &x_i(t) = x_i(t_{n-1}) + \frac{k_i^{net}(n)}{\tau}\left(t - t_{n-1}\right), \\ &t \in (t_{n-1}, t_n],\ n = 1, 2, \ldots \end{aligned} \tag{3.2.7}$$

3.2.3 Independence of cell- and module-level charge equalizations

It follows from the above model formulation that both cell- and module-level charge equalizations are performed simultaneously in the module-based BCE system. In this subsection, we will discuss the relationship between them.

As mentioned above, for the cell-level charge equalization, the charge transfer direction of every two adjacent cells is updated only at the beginning of every working cycle, while the exact charge equalization almost always occurs within some working cycle, e.g., $t \in ((n-1)\tau, n\tau)$. Thus, without loss of generality, we can assume that the SOCs of two adjacent cells are never identical at the beginning of every working cycle. In this case, due to the cell-level charge transfer, the total cell SOC of each module decreases by an identical amount during every working cycle, i.e., the total cell-level charge transfer loss $(B-1)r_c l_c$. Therefore, the cell-level charge equalization does not change the difference in total SOCs between two adjacent modules, and,

thus, does not affect the module-level charge equalization.

On the other hand, the module-level charge transfer current is identical for all series-connected cells in the same module. Then, the module-level charge transfer does not change the SOC difference between any two adjacent cells within the same module. Thus, the module-level charge equalization does not affect the cell-level charge equalization as well.

In addition, since the cell-level charge transfer is performed only among cells within the same module, the cell-level charge equalization in each module is also independent of each other.

Therefore, in a module-based BCE system, the cell-level charge equalizations within all battery modules and the module-level charge equalization among battery modules can be studied independently.

3.2.4 Constraint on charge transfer rates to avoid overcharging and overdischarging

It has been shown in [42] that if only cell-level charge equalization is performed, i.e., $r_c > 0$ and $r_m = 0$, all cell SOCs can finally get equalized. However, when the module-level charge equalization is superposed, i.e., $r_c > 0$ and $r_m > 0$, the cell with the largest (smallest) SOC in some battery module may have positive (negative) *net* charge transfer rate. In this case, it is possible that the largest (smallest) cell SOC in some module exceeds the cell SOC upper bound x_{ub} (lower bound x_{lb}) before the charge equalization is reached. In other words, some cell(s) may be overcharged or overdischarged during the two-level charge equalization process of the module-based BCE system. Based on the mathematical model derived above, it can be shown that

such issues can be avoided if the module-level and cell-level charge transfer rates are selected based on:

Proposition 3.2.1. *Consider a module-based BCE system defined by (3.2.1)-(3.2.7) with* $x_i(0) \in (x_{lb}, x_{ub}),\ i = 1, 2, \ldots, B \times M$. *If*

$$0 \leq r_m \leq \frac{(1 - l_c) r_c}{2}, \tag{3.2.8}$$

all battery cell SOCs can get equalized before any cell SOC reaches x_{ub} *or* x_{lb}.

Proof: See Subsection 7.2.1.

Indeed, under condition (3.2.8), it is guaranteed that the largest (smallest) cell SOC does not increase (decrease) throughout the charge equalization process, when no external charging/discharging is applied. As a result, the SOC imbalance among all battery cells can be eliminated without any cell being overcharged or overdischarged in the process. Moreover, note that (3.2.8) is a sufficient (in other words, "conservative") condition instead of a necessary condition to avoid overcharging/overdischarging during the charge equalization process.

3.3 Estimation of battery cell SOC evolution

3.3.1 Motivation

To quantitatively analyze the charge equalization behavior and performance of a BCE system, it is of great importance to track the evolution of battery cell SOCs over time, since they provide all detailed information to characterize the charge equalization process. In addition, for large-scale systems, since there exist various possible initial

cell SOC combinations, a large number of system tests need to be performed to obtain statistically reliable performance evaluation. To accomplish these tasks, physical circuit experiments or computer simulations remain the main tools [14, 20, 41, 42, 57, 64].

While the circuit experiment is a straightforward approach for estimating the cell SOC evolution and evaluating system performance, it could consume a significant amount of time and energy, especially for large-scale battery systems. Besides, it is worth noting that battery cell SOCs cannot be directly measured and must be estimated through other physical measurements. To accomplish this, a number of battery cell SOC estimation methods have been proposed [65, 66]. In [65], these methods are divided into two categories: direct and indirect SOC estimations. The direct estimation methods are mainly based on direct measurements of battery current, voltage, or temperature, such as the Coulomb Counting and Open Circuit Voltage-Based Estimation, while the indirect estimation methods deploy more estimation techniques based on various battery models, adaptive filters, adaptive artificial intelligence, and so on. Most of these methods focus on estimating the individual battery cell SOC at the current moment. Then, to estimate the SOC evolution of all battery cells during the circuit experiment, the SOC estimation method needs to be applied to each individual battery cell during each working cycle, which may require a lot of computational efforts.

An alternative way for cell SOC estimation and system performance evaluation is the iterative computer simulation based on some mathematical BCE models, such as the model described by (3.2.1)-(3.2.7), which typically require a great amount of time, computing power, and storage space as the system scale gets large. For instance, as we will show later, to obtain the cell SOC evolution of a 64-cell module-

based BCE system throughout the charge equalization process, the average running time of iterative computer simulation is longer than 100 s.

Therefore, for large-scale battery systems, both physical circuit experiments and model-based iterative computer simulation become very energy- or time-consuming. Motivated by this, for the module-based BCE system, we propose computationally efficient algorithms to estimate the cell SOC evolution in this section and to evaluate some critical system performance measures in subsequent sections. Note that, these proposed methods are all carried out based on the given initial battery cell SOCs. Thus, accurate estimation of the initial cell SOCs is necessary to achieve the expected performance of these proposed methods.

3.3.2 Estimation algorithm

For series-based BCE systems, an algorithm was developed in Chapter 2 for fast estimation of the cell SOC evolution during the charge equalization process and it was referred to as the *Series-based SOC Estimation Algorithm*. This is a dynamic estimation/prediction algorithm since the cell SOCs to be estimated change over time. When applying this algorithm, the initial cell SOCs need to be estimated based on some physical measurements, and the charge transfer rate and charge transfer loss rate of the system need to be identified. Then, the algorithm can quickly generate the entire evolution of all cell SOCs based on the given initial cell SOCs, system parameters, and external time-varying charging/discharging profile.

As discussed in Section 3.2, in a module-based BCE system with M modules, there exists one module-level and M cell-level series-based BCE subsystems. Since the charge equalization in each subsystem is independently performed, the Series-

based SOC Estimation Algorithm can be applied to each subsystem. Thus, based on the mathematical model formulated in Section 3.2, and the Series-based SOC Estimation Algorithm, we propose the following *Module-based SOC Estimation Algorithm* to estimate the cell SOC evolution throughout the charge equalization process in the module-based BCE system:

Module-based SOC Estimation Algorithm:

Step 1: *Estimation of the cell-level charge equalization*: Consider a module-based BCE system with only cell-level charge equalization (i.e., $r_m = 0$). Then, the SOC of the i-th cell at time instant t, denoted by $x_i^{cel}(t)$, $i \in \{(m-1)B + 1, \ldots, mB\}$, $m \in \{1, 2, \ldots, M\}$, $t \geq 0$, can be estimated by applying the Series-based SOC Estimation Algorithm to the m-th cell-level series-based BCE subsystem.

Step 2: *Estimation of the module-level charge equalization*: Consider the same module-based BCE system but with only module-level charge equalization (i.e., $r_c = 0$). Then, the SOC sum of all cells in the m-th module at time instant t, denoted by $X_m^{mod}(t)$, $m \in \{1, 2, \ldots, M\}$, $t \geq 0$, can be estimated by applying the Series-based SOC Estimation Algorithm to the module-level series-based BCE subsystem.

Step 3: *Superposition of both cell-level and module-level charge equalizations*: Calculate the instantaneous cell SOC of the i-th cell, $x_i(t)$, $i = 1, 2, \ldots, B \times M$, $t \geq 0$, by the superposition of its initial cell SOC and both cell-level and module-

level charge transfers:

$$\begin{aligned} x_i(t) =& x_i(0) + \left(x_i^{cel}(t) - x_i(0)\right) + \frac{1}{B}\left(X^{mod}_{\lceil \frac{i}{B} \rceil}(t) - X^{mod}_{\lceil \frac{i}{B} \rceil}(0)\right) \\ =& x_i^{cel}(t) + \frac{1}{B}\left(X^{mod}_{\lceil \frac{i}{B} \rceil}(t) - X^{mod}_{\lceil \frac{i}{B} \rceil}(0)\right). \end{aligned} \tag{3.3.1}$$

3.3.3 Accuracy and computational efficiency of the algorithm

To verify the accuracy of the proposed estimation algorithm for module-based BCE systems, one can directly compare the estimated cell SOCs with those obtained from physical circuit experiments. On the other hand, since a module-based BCE system with M modules can be broken down into $M + 1$ independently operating series-based BCE subsystems, checking the estimation accuracy on the module-based BCE system amounts to testing it on each subsystem. As the estimation accuracy on the series-based BCE system has been verified by experimental data in Fig. 2.4.2, the accuracy of the proposed battery cell SOC estimation algorithm on the module-based BCE system is also verified.

In addition to the above verification based on the physical experimental data of series-based BCE systems. We also directly verify the accuracy of the proposed Module-based SOC Estimation Algorithm by the physical circuit experiment on the module-based BCE system. Consider a small module-based BCE system with 3 battery modules and 2 cells in each module. The initial cell SOCs are $\{0.8, 0.74, 0.78, 0.73, 0.76, 0.72\}$. Then, this system is tested using the same experimental bench introduced in [58]. Specifically, as shown in Fig. 3.3.1a, in this module-based BCE system, the Sony VTC4 18650 Lithium battery cell with the rated charge capacity 2100 mAh is applied. Besides, the battery charge equalizer is designed based on a modified

buck-boost converter as shown in Fig. 3.3.1b and Fig. 3.3.1c, which is composed of a 3.46 μH WE-FB Flyback transformer, two NTD6416AN-1G MOSFETs, and two 0.1 Ω current sense resistors. An illustration of the charge equalization current through the two battery cells is given in Fig. 3.3.1d. This charge equalizer is applied to both the cell-level and module-level charge transfers. Based on this circuit test bed, we can obtain the experimental data of the cell SOC evolution throughout the charge equalization process as shown in Fig. 3.3.2 (i.e., the blue solid curves).

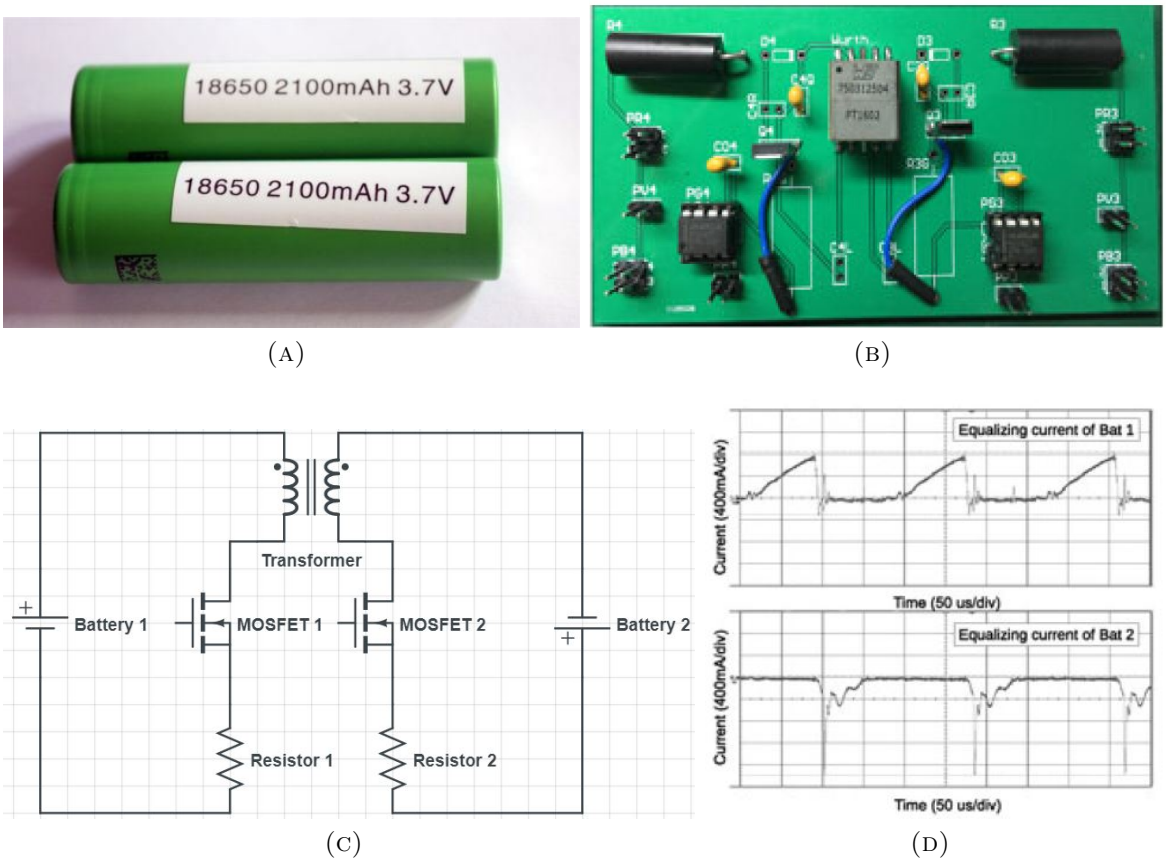

(A) (B)

(C) (D)

FIGURE 3.3.1: Battery cells and the cell-to-cell charge equalizer adapted from a modified buck boost converter designed in [58]. (A) Sony VTC4 18650 Lithium battery cells. (B) Circuit design of the charge equalizer. (C) Circuit diagram of the charge equalizer. (D) Charge equalization current.

According to the above experimental test, we can obtain the rated battery cell capacity $C_B = 2100$ mAh, the working cycle $\tau = 2$ s, the average cell-level charge transfer current from the high-SOC cell $I_c = 0.261290$ A, the average cell-level charge transfer efficiency $\eta_c = 90.05\%$, the average module-level charge transfer current from the high-SOC module $I_m = 0.261326$ A, the average module-level charge transfer efficiency $\eta_m = 87.87\%$. Then, the two-level charge transfer parameter values are:

$$r_c = \frac{I_c \tau}{C_B} = 6.9124 \times 10^{-5},\ l_c = 1 - \eta_c = 9.95\%,$$
$$r_m = \frac{I_m \tau}{C_B} = 1.3827 \times 10^{-4},\ l_m = 1 - \eta_m = 12.13\%.$$

Using these parameter values, the proposed Module-based SOC Estimation Algorithm is performed to estimate the cell SOC evolution, which is also shown in Fig. 3.3.2 for comparison. As one can see from Fig. 3.3.2, the estimated cell SOCs can well match the experimental data for most battery cells throughout the battery charge equalization process. Besides, the estimated BCE time is also very close to that observed in the physical circuit experiment. On the other hand, for such a small BCE system, it takes more than 900 s to complete the battery charge equalization in the circuit experiment, while the proposed estimation algorithm only needs less than 3 ms. Thus, to obtain the cell SOC evolution of this module-based BCE system, the proposed Module-based SOC Estimation Algorithm is much more computationally efficient than the circuit experiment.

In order to evaluate the estimation accuracy and computational efficiency of the proposed algorithm under various scenarios of initial cell SOC imbalance, a large number of tests need to be performed to get statistically reliable conclusions. In this case, physical circuit experiments are too time-consuming, and hence extensive

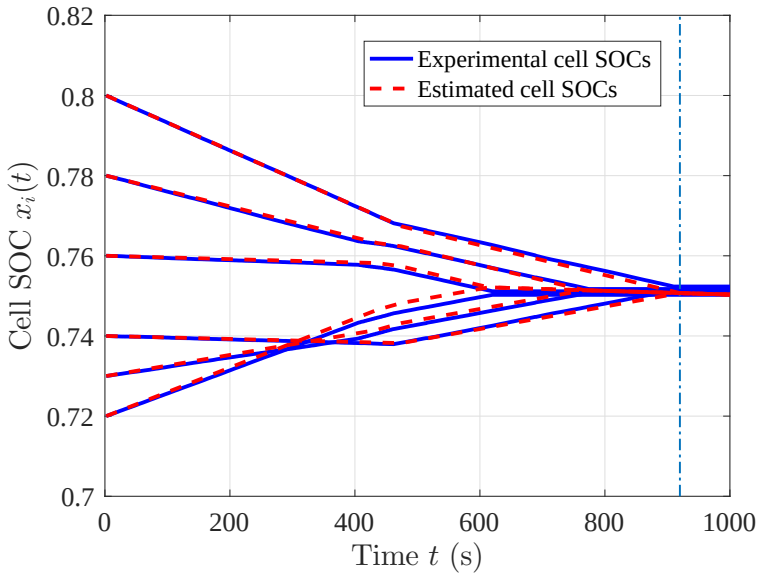

FIGURE 3.3.2: Verification of the proposed Module-based SOC Estimation Algorithm by experimental data.

numerical experiments are performed. Specifically, we study a module-based BCE system with $M = 8$ modules and $B = 8$ cells in each module, and generate a total of $S = 1000$ test cases for the 64-cell system. Each test case consists of a set of initial cell SOCs for the 64 cells in the system, and each initial cell SOC is randomly generated subject to the uniform distribution $U(0, 1)$. It can be shown that $S = 1000$ is a sufficiently large sample size to represent the initial cell SOC distribution. To illustrate these randomly generated test cases, the initial cell SOCs of the first three test cases are shown in Fig. 3.3.3.

For all these test cases, assume that the working cycle of all charge equalizers is $\tau = 0.1$ s and each battery cell has a rated charge capacity $C_B = 6$ Ah which is also used in [24]. The typical charge equalization current of cell-to-cell charge equalizers ranges from 0 A to 2.5 A in [21, 24]. Then, we can roughly estimate the cell-level

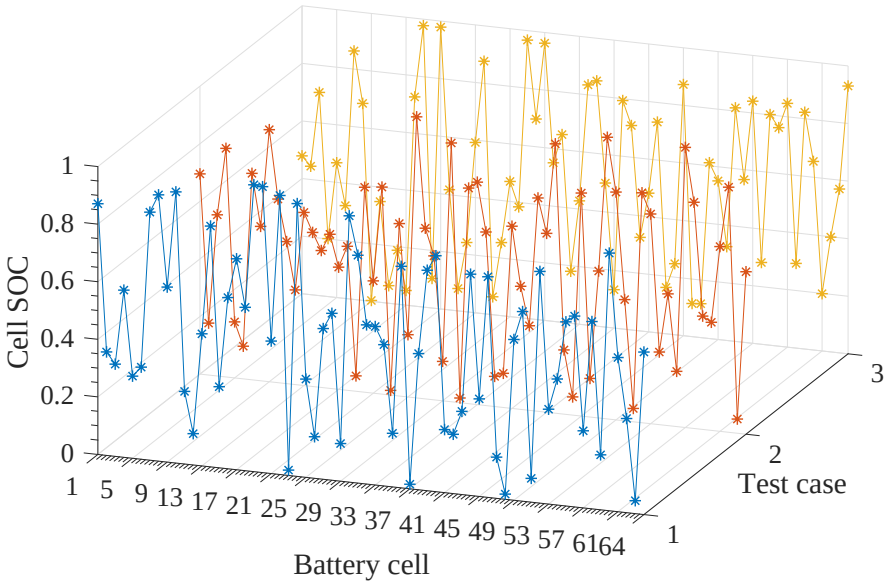

FIGURE 3.3.3: Illustration of the initial cell SOCs of the first three test cases generated subject to the uniform distribution.

charge transfer rate $r_c \leq (2.5\text{ A} \times 0.1\text{ s})\,/\,(6\text{ Ah}) \approx 1.157 \times 10^{-5}$. Thus, here the cell-level charge transfer rate is set to $r_c = 10^{-5}$. Accordingly, the cell-level charge transfer loss rate is selected as $l_c = 5\%$ according to [24, 72]. Besides, the module-level charge transfer rate is set to its upper bound according to Proposition 3.2.1, i.e., $r_m = (1 - l_c)r_c/2 = 4.75 \times 10^{-6}$. Finally, the module-level charge transfer loss rate is also set to $l_m = l_c = 5\%$.

For each test case, two methods are used to obtain the battery cell SOC evolution from the initial cell SOCs. The first method, referred to as *iterative simulation*, is to calculate the SOCs for each working cycle by iteratively evaluating equations (3.2.1)-(3.2.7). For the s-th test case, denote the i-th cell's SOC at the time instant t calculated by this method as $x_i^{sim}(s,t)$. Next, for each case, the proposed estimation algorithm is carried out to calculate the SOC evolution, and denote the instantaneous

cell SOC obtained from the proposed algorithm as $x_i^{est}(s,t)$. Then, for the s-th test case, we compare $x_i^{sim}(s,t)$ and $x_i^{est}(s,t)$ for all working cycles during the charge equalization process and calculate the mean and maximum absolute estimation errors by

$$\epsilon_{SOC}^{mean}(s) = \frac{\sum_{i=1}^{MB} \sum_{n=0}^{\lfloor \frac{T_e^{sim}(s)}{\tau} \rfloor} |x_i^{est}(s,n\tau) - x_i^{sim}(s,n\tau)|}{MB(\lfloor \frac{T_e^{sim}(s)}{\tau} \rfloor + 1)},$$
$$\epsilon_{SOC}^{max}(s) = \max_{\substack{i \in \{1,\ldots,MB\} \\ n \in \{0,\ldots,\lfloor \frac{T_e^{sim}(s)}{\tau} \rfloor\}}} |x_i^{est}(s,n\tau) - x_i^{sim}(s,n\tau)|,$$

where $T_e^{sim}(s)$ denotes the time instant when all cell SOCs in test case s get equalized in the iterative simulation.

For all 1000 randomly generated test cases above, the mean and maximum absolute estimation errors are calculated and illustrated in Fig. 3.3.4. It can be seen from the figure that for these 1000 test cases the mean absolute estimation errors are all close to 10^{-5} and the maximum absolute estimation errors are within $(4\times10^{-5}, 8\times10^{-5})$. Thus, we claim that the proposed cell SOC estimation algorithm can provide very accurate evaluation of the cell SOC evolution during the charge equalization process of module-based BCE systems.

Next, we analyze the computational effort required by the proposed algorithm to achieve the above accuracy. For the s-th test case, the computation times of the iterative simulation and proposed estimation algorithm are denoted by $T_{SOC}^{sim}(s)$ and $T_{SOC}^{est}(s)$, respectively. As shown in Fig. 3.3.5, the computation time ratio $T_{SOC}^{est}(s)/T_{SOC}^{sim}(s)$ for each test case is less than 0.5%. In addition, the mean computation time of the proposed algorithm across all 1000 test cases is only $\overline{T}_{SOC}^{est} = 0.3315$ s,

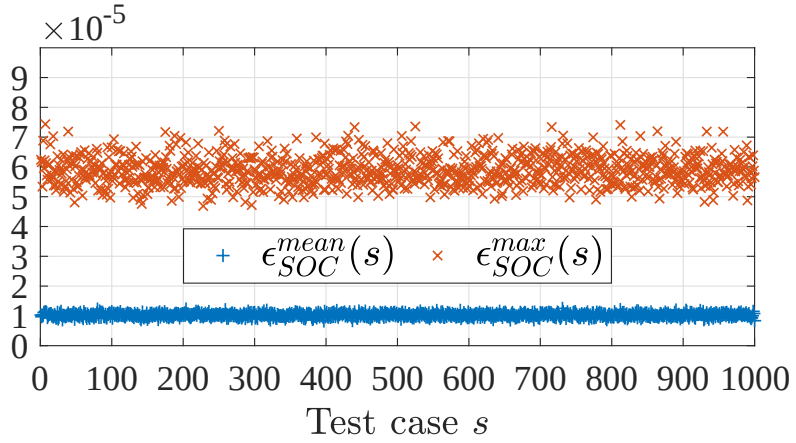

FIGURE 3.3.4: Mean and maximum absolute estimation errors for 1000 randomly generated test cases of a 64-cell module-based BCE system.

while that of the iterative simulation method is $\overline{T}_{SOC}^{sim} = 104.4558$ s. Besides, given the duration of each working cycle $\tau = 0.1$ s, the running time of the circuit experiment to complete the charge equalization for each test case above is estimated to range from 1.468 h to 4.289 h. Thus, the proposed algorithm can provide highly accurate estimation of the cell SOC evolution with little computational effort as compared to the iterative computer simulation and physical circuit experiment.

3.4 Calculation formulas for the battery charge equalization time

3.4.1 Analytical formulas to calculate the battery charge equalization time

While numerous battery charge equalizer designs and their associated control strategies have been proposed in recent years, the comparison of different designs is typically

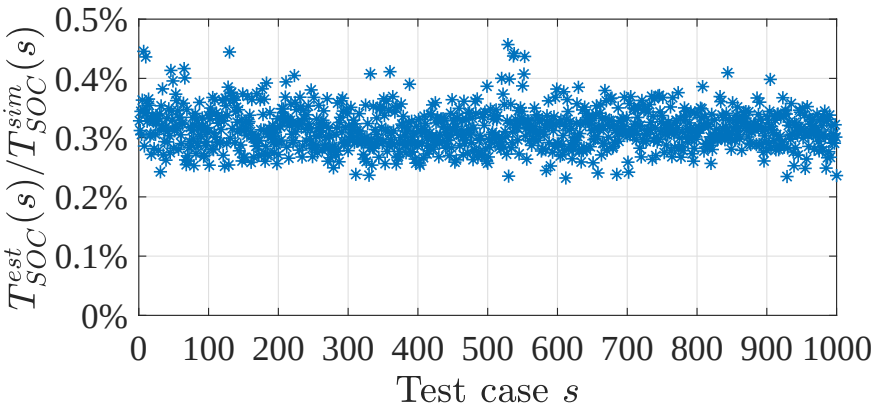

FIGURE 3.3.5: Computation time ratios of the proposed estimation algorithm to the iterative simulation based on (3.2.1)-(3.2.7) for 1000 randomly generated initial cell SOC test cases of a 64-cell module-based BCE system.

focused on circuit implementations. On the other hand, quantitative evaluation and systematic comparison of their key performance measures of charge equalization behavior are generally lacking. This is mainly due to the high demand of time and energy required by such experiments. Thus, computationally efficient tools to evaluate battery charge equalization performance are highly desired. Of all performance measures for battery charge equalization, one critical measure is the *battery charge equalization (BCE) time*, denoted by T_e and defined by the time needed for all battery cell SOCs to get equalized from their initial SOCs. In addition to indicating how soon the charge equalization can be achieved, the BCE time is also closely related to the energy and charge transfer efficiencies [72, 73, 74].

Clearly, using either iterative simulation of equations (3.2.1)-(3.2.7) formulated in Section 3.2 or the estimation algorithm derived in Section 3.3, we can construct the evolution of all cell SOCs and finally obtain the BCE time at the end of the charge equalization process. However, if the BCE time T_e can be directly estimated without

calculating the cell SOC evolution throughout the charge equalization process, the computational efficiency can be further improved. This is the goal of this section.

Again, we still view the module-based BCE system with M modules as $M+1$ independent subsystems. For the cell-level charge equalization, denote the BCE time of the m-th cell-level subsystem by $T_e^{cel}(m)$, $m \in \{1, 2, \ldots, M\}$. Then according to [42], $T_e^{cel}(m)$ can be calculated by

$$T_e^{cel}(m) = \max_{g \in \{1,\ldots,B-1\}} t^{cel}(m, g), \tag{3.4.1}$$

where

$$t^{cel}(m,g) = \begin{cases} \frac{(\bar{x}_{m,g}(0) - \bar{x}_{m,B}(0))\tau}{(\frac{1-l_c}{g} + \frac{l_c}{B})r_c}, & \text{if } \bar{x}_{m,g}(0) \geq \bar{x}_{m,B}(0), \\ \frac{(\bar{x}_{m,B}(0) - \bar{x}_{m,g}(0))\tau}{(\frac{1}{g} - \frac{l_c}{B})r_c}, & \text{if } \bar{x}_{m,g}(0) < \bar{x}_{m,B}(0), \end{cases}$$

$$\bar{x}_{m,g}(0) = \frac{1}{g} \sum_{i=(m-1)B+1}^{(m-1)B+g} x_i(0).$$

For the module-level charge equalization, denote the BCE time of the module-level subsystem by T_e^{mod}. Then, by extending the formulas from cell-level equalization to module-level equalization, T_e^{mod} can be calculated by

$$T_e^{mod} = \max_{g \in \{1,\ldots,M-1\}} t^{mod}(g), \tag{3.4.2}$$

where

$$t^{mod}(g) = \begin{cases} \frac{(\overline{X}_g(0) - \overline{X}_M(0))\tau}{(\frac{1-l_m}{g} + \frac{l_m}{M})Br_m}, & \text{if } \overline{X}_g(0) \geq \overline{X}_M(0), \\ \frac{(\overline{X}_M(0) - \overline{X}_g(0))\tau}{(\frac{1}{g} - \frac{l_m}{M})Br_m}, & \text{if } \overline{X}_g(0) < \overline{X}_M(0), \end{cases}$$

$$\overline{X}_g(0) = \frac{1}{g}\sum_{m=1}^{g} X_m(0),$$
$$X_m(t) = \sum_{i=(m-1)B+1}^{mB} x_i(t), \quad m \in \{1, 2, \ldots, M\},\ t \geq 0.$$

Clearly, for the original module-based BCE system, the overall system achieves charge equalization if and only if all $M + 1$ subsystems complete their own charge equalization. Thus, the BCE time of the entire system, denoted by T_e^{sys}, is equal to the longest one of all subsystems' BCE times, i.e.,

$$T_e^{sys} = \max\{T_e^{cel}(1), \ldots, T_e^{cel}(M), T_e^{mod}\}. \tag{3.4.3}$$

3.4.2 Calculation accuracy and computational efficiency of the proposed T_e calculation formulas

At this point, we have three methods to evaluate T_e:

(i) Iterative simulation of cell SOC evolution using (3.2.1)-(3.2.7);

(ii) Module-based SOC Estimation Algorithm proposed in Section 3.3;

(iii) Analytical calculation formulas of T_e, i.e., (3.4.1), (3.4.2), and (3.4.3).

To compare these three methods, we, again, use the $S = 1000$ test cases randomly generated for the 64-cell module-based BCE system in Subsection 3.3.3. Specifically, for the s-th test case, the BCE times obtained from methods 1), 2), and 3) are denoted by $T_e^{sim}(s)$, $T_e^{est}(s)$, and $T_e^{cal}(s)$, respectively. Accordingly, the computation times of these three methods are denoted by $T_{T_e}^{sim}(s)$, $T_{T_e}^{est}(s)$, and $T_{T_e}^{cal}(s)$, respectively.

Note that, from Fig. 3.3.2, we can see the BCE time obtained from the proposed Module-based SOC Estimation Algorithm, i.e., $T_e^{est}(s)$, is already verified by the experimental data. Besides, based on Fig. 3.3.4, the estimated cell SOC evolution and the BCE time are almost same to those obtained by the iterative simulation. Then, the BCE time obtained from the iterative simulation, i.e., $T_e^{sim}(s)$, is also verified by the experimental data. Thus, for the s-th test case, the accuracy of $T_e^{cal}(s)$ is evaluated based on the absolute percentage error defined by

$$\epsilon_{T_e}(s) = \frac{|T_e^{cal}(s) - T_e^{sim}(s)|}{T_e^{sim}(s)} \times 100\%, \ s \in \{1, 2, \ldots, S\}.$$

The results for the 1000 test cases are summarized in Fig. 3.4.1. As one can see, all absolute percentage errors are less than 0.35% with an average of 0.0854%. Thus, we claim that the BCE times calculated based on (3.4.1)-(3.4.3) are highly accurate.

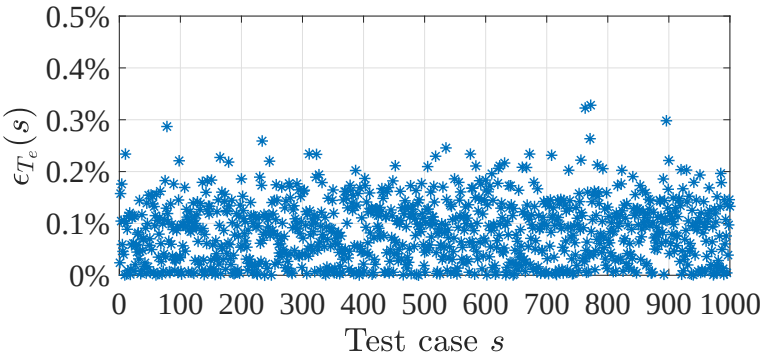

FIGURE 3.4.1: Absolute percentage errors of the T_e calculation for 1000 randomly generated initial cell SOC cases of a 64-cell module-based BCE system.

In addition to maintaining a high accuracy, numerical experiments show that the T_e calculation formulas (3.4.1)-(3.4.3) also have a clear advantage over the other two methods in terms of computational efficiency. As illustrated in Fig. 3.4.2, for each

test case, the computation time of the proposed T_e calculation formulas is less than 0.0012% of the iterative simulation's computation time, and less than 0.5% of the estimation algorithm's computation time. In addition, the average computation times of the three methods are $\overline{T}^{sim}_{T_e} = \overline{T}^{sim}_{SOC} = 104455.839\ ms$, $\overline{T}^{est}_{T_e} = \overline{T}^{est}_{SOC} = 331.485\ ms$, and $\overline{T}^{cal}_{T_e} = 0.469\ ms$. Therefore, we claim that formulas (3.4.1)-(3.4.3) provide a highly accurate and computationally efficient method for estimating the BCE time in module-based BCE systems.

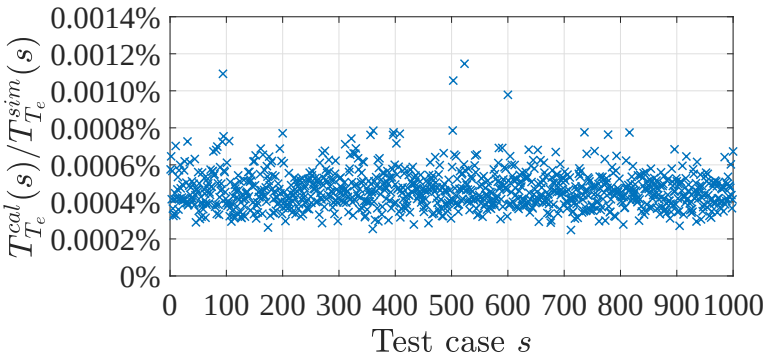

(A)

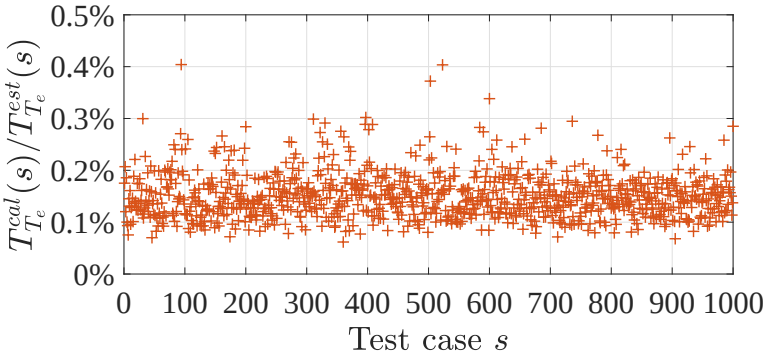

(B)

FIGURE 3.4.2: Computation time ratios for 1000 randomly generated test cases of a 64-cell module-based BCE system. (a) $T^{cal}_{T_e}(s)/T^{sim}_{T_e}(s)$. (b) $T^{cal}_{T_e}(s)/T^{est}_{T_e}(s)$.

3.5 Analysis of the charging/discharging process

So far, we have studied the charge equalization process without external charging or discharging, i.e., in the idle mode. In this section, we extend our analysis to the charging and discharging modes of module-based BCE systems.

3.5.1 Cell SOC evolution during charging/discharging

Since battery cells in a module-based BCE system are connected in series as shown in Fig. 3.2.3, they are charged or discharged with identical current when connected to an external power source or load. This implies that the charging/discharging process does not influence the charge imbalance among battery cells/modules and thus it does not affect the cell-level and module-level charge equalization processes. Then, the overall evolution of each cell's SOC can be viewed as the superposition of two components: the cell SOC evolution in the idle mode (i.e., charge equalization only), denoted by $x_i^{idle}(t)$, and the total charge gained/released through external charging/discharging, denoted by $x^{chg}(t)$. To formalize this, the overall evolution of the cell SOC in charging/discharging mode is given below,

$$x_i(t) = x_i^{idle}(t) + x^{chg}(t). \tag{3.5.1}$$

In (3.5.1), $x_i^{idle}(t)$ can be estimated by the proposed algorithm in Section 3.3, and $x_i^{chg}(t)$ can be calculated by

$$x^{chg}(t) = \sum_{j=1}^{n-1} r_g(j) + \frac{r_g(n)}{\tau}(t - t_{n-1}), \tag{3.5.2}$$

$$t \in (t_{n-1}, t_n],\ n \in \{1, 2, \ldots\},$$

where $r_g(n)$ denotes the battery cell's *charging rate*, i.e., the amount of charge gained by each cell during the n-th working cycle. Clearly, the cases of $r_g(n) > 0$, $r_g(n) = 0$, and $r_g(n) < 0$ indicate that the BCE system operates in the charging mode, idle mode, and discharging mode, respectively.

3.5.2 Estimation of charging time and discharging time

During the charging (discharging) process of a module-based BCE system, once the largest (smallest) cell SOC reaches its upper bound x_{ub} (lower bound x_{lb}), the charging (discharging) process needs to be terminated to avoid overcharging (overdischarging). The duration of the charging (discharging) process is referred to as the system's *charging* (*discharging*) *time* which is denoted by T_c (T_d).

Based on the cell SOC evolution estimated based on (3.5.1), (3.5.2), and the proposed estimation algorithm in Section 3.3, T_c (T_d) can be obtained by identifying the time instant when the largest (smallest) cell SOC reaches x_{ub} (x_{lb}). As an illustration, the evolutions of cell SOCs of a module-based BCE system under six different charging rates r_g's (denoted as $r_g^I, \ldots, r_g^{VI}$, and referred to as Case I to Case VI) are given in Fig. 3.5.1. For simplicity, we assume that $r_g(n)$ is time-invariant in each case and $x_{lb} = 0$, $x_{ub} = 1$. According to the cell SOC evolution, T_c or T_d can be quickly identified.

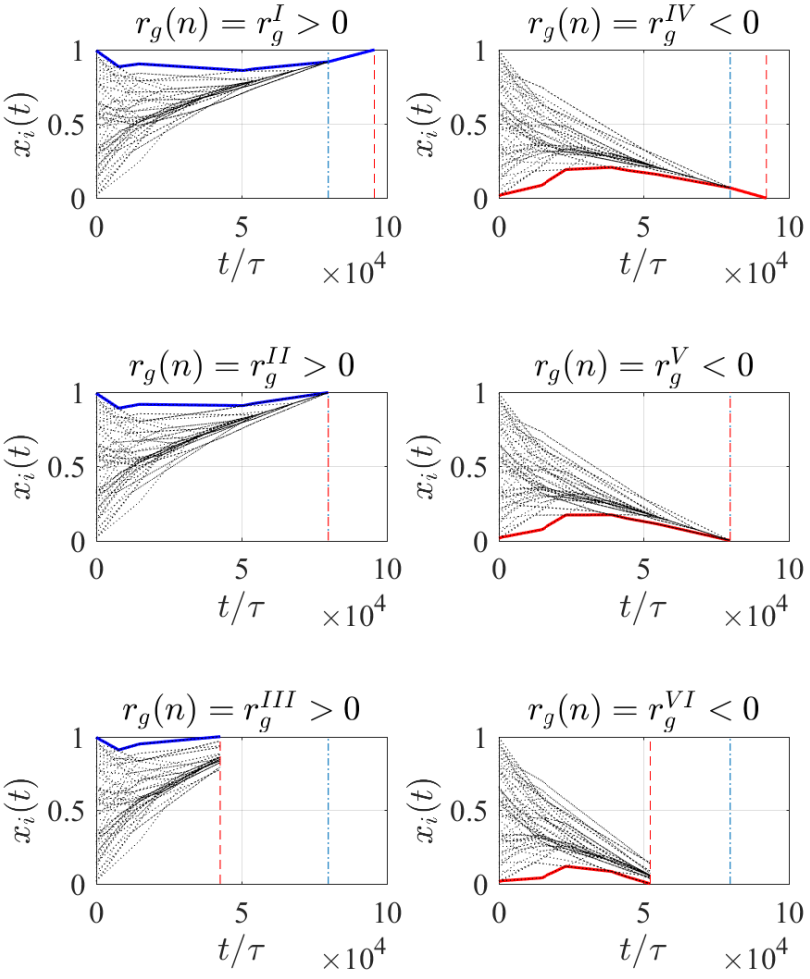

FIGURE 3.5.1: Cell SOC evolutions with six time-invariant charging rates $r_g^{VI} < r_g^V < r_g^{IV} < 0 < r_g^I < r_g^{II} < r_g^{III}$ for a 64-cell BCE system.

3.5.3 Charging rate range to have all cell SOCs get fully charged or fully discharged

Again, since all cells share the same charging profile $r_g(n)$, the charging/discharging process does not affect the two-level charge equalization process. Then, during the charging/discharging processes, the time needed for the system to reach equalization remains equal to the BCE time in the idle mode, i.e., T_e, which can be calculated

using (3.4.1)-(3.4.3). As shown in Fig. 3.5.1, for Cases I and IV, $|r_g|$ are selected relatively small such that the equalization process outpaces the charging/discharging process (i.e., $T_e < T_c$ for Case I and $T_e < T_d$ for Case IV). As a result, all cells reach equalization first, and then are charged/discharged together to x_{ub} or x_{lb}. In Cases II and V with larger $|r_g|$, the charge equalization is reached exactly when all cell SOCs are fully charged or fully discharged (i.e., $T_e = T_c$ in Case II and $T_e = T_d$ in Case V). Finally, in Cases III and VI, when the $|r_g|$ is further increased, the largest cell SOC reaches x_{ub} or the smallest cell SOC reaches x_{lb} before all cell SOCs get equalized (i.e., $T_e > T_c$ in Case III and $T_e > T_d$ in Case VI). As a consequence, the charging/discharging process has to be terminated prematurely before the cell SOC imbalance is completely eliminated, although there is still unused capacity/charge in some cells.

In order to have all SOCs get fully charged/discharged without overcharging and overdischarging, as shown in Fig. 3.5.1, the equalization process should be completed no later than the charging/discharging process, i.e., $T_e \leq T_c$ for charging, $T_e \leq T_d$ for discharging. Following this argument, we obtain:

Proposition 3.5.1. *Consider a module-based BCE system with $r_g(n) = r_g$, r_c and r_m satisfying (3.2.8), and $x_i(0) \in (x_{lb}, x_{ub})$, $i = 1, 2, \ldots, B \times M$. If no battery cell is overcharged and overdischarged before the charge equalization is reached, the charging rate r_g must fall into the following range,*

$$r_g^{-c} \leq r_g \leq r_g^{+c}, \tag{3.5.3}$$

where

$$r_g^{-c} = \frac{x_{lb} - \bar{x}(0)}{T_e}\tau + \frac{L_{net}}{MB}, \tag{3.5.4}$$

$$r_g^{+c} = \frac{x_{ub} - \bar{x}(0)}{T_e}\tau + \frac{L_{net}}{MB}, \tag{3.5.5}$$

$$\bar{x}(0) = \frac{1}{MB}\sum_{i=1}^{MB} x_i(0), \tag{3.5.6}$$

$$L_{net} = M(B-1)r_c l_c + (M-1)Br_m l_m. \tag{3.5.7}$$

Here, $\bar{x}(0)$ is the average initial cell SOC, and L_{net} is the net charge transfer loss during each working cycle.

Proof: See Subsection 7.2.2.

Proposition 3.5.1 presents a necessary condition but not a sufficient condition of $T_e \leq T_c, T_d$. Indeed, given a charging rate $r_g \in [r_g^{-c}, r_g^{+c}]$, during the charge equalization process, although the average cell SOC $\bar{x}(t) \in [x_{lb}, x_{ub}]$ can be guaranteed, some individual cell SOC is still possible to exceed x_{lb} or x_{ub}. Thanks to Proposition 3.5.1, to avoid such battery overcharging/overdischarging, we only need to search r_g within a very small range given by (3.5.3)-(3.5.7) instead of among all possible charging rates.

To define the feasible range of charging rate, let $r_g^{max} > 0$ and $r_g^{min} < 0$ denote the *critical charging rates* such that given any time-invariant charging rate $r_g \in [r_g^{min}, r_g^{max}]$, all battery cells can reach charge equalization at $t = T_e$ first and then gradually get fully charged at $t = T_c \geq T_e$ or fully discharged at $t = T_d \geq T_e$. In addition, once r_g^{min} and r_g^{max} are identified, given $r_g \in [r_g^{min}, r_g^{max}]$, the charging time T_c and discharging time T_d can be directly calculated based on Proposition 3.5.2.

Proposition 3.5.2. *For a module-based BCE system with $r_g(n) = r_g \in [r_g^{min}, r_g^{max}]$, r_c and r_m satisfying (3.2.8), and $x_i(0) \in (x_{lb}, x_{ub}),\ i = 1, 2, \ldots, B \times M$, the charging time T_c and discharging time T_d can be calculated as*

$$T_c = \frac{x_{ub} - \bar{x}(0)}{MBr_g - L_{net}} MB\tau, \text{ if } r_g \in (\frac{L_{net}}{MB}, r_g^{max}], \tag{3.5.8}$$

$$T_d = \frac{x_{lb} - \bar{x}(0)}{MBr_g - L_{net}} MB\tau, \text{ if } r_g \in [r_g^{min}, \frac{L_{net}}{MB}), \tag{3.5.9}$$

where $\bar{x}(0)$ and L_{net} are defined in (3.5.6) and (3.5.7), respectively.

Proof: See Subsection 7.2.3.

Clearly, given any charging rate $r_g \in [r_g^{min}, r_g^{max}]$, (3.5.8) and (3.5.9) provides a more efficient way to calculate T_c and T_d than using the cell SOC evolution derived in Subsection 3.5.2.

3.6 Summary

In this chapter we focus on the module-based BCE system and propose estimation methods for instantaneous cell SOCs and critical performance measures. Results from both circuit experiments and numerical simulations verify the estimation accuracy and computational efficiency of these methods. Particularly, the high computational efficiency of these proposed methods makes it possible to test, analyze, and optimize the module-based BCE system under various initial conditions, including those too costly and/or too time-consuming to be tested by circuit experiments.

Based on the proposed estimation algorithm for cell SOC evolution, we also analyze the charging and discharging processes of module-based BCE systems and derive

conditions under which the equalization process outpaces charging/discharging so that all cells can get fully charged/discharged without overcharging/overdischarging.

In the following study, using these proposed methods for the module-based BCE system, we will improve the system design such as reconfiguring the battery cells/modules for expedited charge equalization.

Chapter 4

Near-optimal battery system configuration for fast charge balance

4.1 Introduction

In all battery systems including multiple cells/modules/packs, one very common issue affecting system performance is the charge imbalance. As a consequence of charge imbalance among battery cells/modules/packs, the system performance deteriorates in terms of early termination of charging/discharging, increased energy loss, accelerated battery degradation, and even safety hazards, e.g., fire or explosion [16, 55, 62, 75]. To alleviate battery charge imbalance, typically two options are considered: (1) assigning larger charging (discharging) current to the batteries with lower (higher) charge, and (2) transferring charge from the higher-charge batteries to the lower-charge ones.

For the first option based on current assignment for charge balance, reconfigurable

battery systems are emerging as a promising solution since the connection topology of battery cells/modules/packs can be flexibly and adaptively reconfigured according to real-time system states and charging/discharging requirements [76, 77, 78]. Intuitively, a battery system can be reconfigured by rearranging battery cells or changing their wiring. While it is usually inefficient or infeasible to directly and frequently rearrange battery cells, it is possible to flexibly control the cell connection by switch operations. As summarized in [76], in most reconfigurable battery system designs reported so far, 2 to 6 controllable switches are usually connected to each battery cell and then flexible battery reconfiguration becomes achievable by controlling the operations of these switches [77, 78, 79, 80, 81]. Although battery reconfiguration needs extra computation effort and electric elements such as switches, it can bring plenty of benefits to battery systems. Adaptive or dynamic battery cell/module/pack reconfiguration frameworks have been shown to improve the system operating time and lifespan [78, 80, 81], energy efficiency [77], tolerance of cell failures [79], and utilization of battery capacity [80]. A few recent studies investigated how to improve battery charge balance by battery cell/module/pack reconfiguration. A reconfigurable and modular architecture was proposed to facilitate the operation of battery packs under unbalanced conditions in [82]. Battery pack reconfiguration was studied to mitigate battery charge imbalance for increased acceptable charge capacity during charging [83] and for increased deliverable charge capacity during discharging [84]. A reconfigurable battery management system was designed in [85] to alleviate charge imbalance by disconnecting the fully charged (discharged) cell during charging (discharging).

On the other hand, to apply the second option based on charge transfer to battery charge balance, a number of circuit designs and control strategies have been proposed in past decades [9, 15, 16, 55, 75]. Among these circuit designs, *cell-to-*

cell charge equalizers are widely used to balance the charge of two adjacent cells in series-connected battery systems. Based on such charge equalizers, different battery charge equalization (BCE) structures can be developed, such as series-based and module-based BCE structures.

Clearly, if the above two options can be combined, i.e., both battery reconfiguration and charge transfer can be performed in a battery system, the charge balance performance could be further improved and even optimized. Thus, in this chapter we will focus on studying the charge balance in *reconfigurable battery charge equalization (BCE) systems*.

To evaluate the performance of battery charge balance, one critical measure is the *battery charge equalization (BCE) time*. Not only does the BCE time indicate the time duration of battery charge equalization process, but it also has a close relation with the energy loss during charge equalization [72]. For series-connected battery cells, the external charging/discharging current passing through each cell is identical to each other. Then, during the discharging process, clearly, the deliverable charge capacity is restricted by the weakest cell (i.e., the cell with the lowest charge). The shorter the BCE time, the sooner all charge in the system becomes available to be delivered (i.e., all cells can be fully discharged). Similarly, for the charging process of series-connected battery cells, only after all cells reach charge equalization can all charging space in the system be completely utilized (i.e., all cells can be fully charged). The BCE time of a battery system depends on both the BCE structure applied and the configuration of all battery cells/modules/packs. Given the same BCE structure and parameter values, the battery configuration could significantly affects the BCE time. For example, for a module-based BCE system including 3 modules and 2 cells per module with initial cell SOCs, $\{0.72, 0.76, 0.78, 0.80, 0.73, 0.74\}$, the numerical

simulation results show that the BCE time could vary from 627.654 s to 1144.380 s with different battery cell/module configurations. Motivated by this, we aim to search the battery cell/module configuration leading to the fastest charge equalization, i.e., minimizing the BCE time by battery reconfiguration.

To optimize the battery cell/module configuration for fast charge equalization, the first constraint we have to consider is the reconfigurability level of battery systems. In a large-scale battery system, battery cells are typically grouped into a number of modules, and then the modules are further grouped into packs. For example, in the world's largest lithium-ion battery storage facility, 400,000 battery cells are installed in nearly 20,000 modules, and placed in 24 containers/packs [4]. For such large-scale systems, the reconfiguration could be performed on cell, module, or pack levels. Besides, depending on the reconfigurability of battery systems, the total number of cell/module/pack configurations is actually a permutation problem, and thus can easily reach an incredibly large number. For instance, even for a battery system including 20 reconfigurable cells connected in series, the total number of cell configurations can reach $20! = 2.433 \times 10^{18}$. This curse of dimensionality makes the search for the optimal cell-equalizer connection configuration an NP-hard combinatorial optimization problem itself. Thus, in this chapter we will develop computationally efficient algorithms to search the optimal battery cell/module configurations for fast charge equalization for series-based BCE systems in Section 4.2 and module-based BCE systems under different levels of reconfigurability in Section 4.3.

4.2 Near-optimal cell configuration in the series-based BCE system

4.2.1 Dependence of T_e on battery cell configuration

In multi-cell battery systems, battery cells are connected in different topologies to meet various requirements of charging/discharging current/voltage/capacity. To reconfigure a battery system, one can either relocate all battery cells or change their connection wiring. While it may not be feasible to frequently relocate battery cells, the connection topology could be flexibly adjusted through switching circuit designs. In some typical reconfigurable battery designs, six controllable switches are attached to each battery cell [78, 79] in order to facilitate series, parallel, or mixed connections of all battery cells. As a result, dynamic operation of individual battery cells becomes possible, which leads to higher efficiency and better reliability. The cost of switching circuit designs mainly depends on the number of switches applied. To further reduce the cost, two-switch [80] and single-switch [86] designs have also been developed. While the number of switches per cell is reduced for lower cost and system complexity, the level of system reconfigurability is compromised.

In this chapter, we focus on expediting the battery charge equalization process by battery reconfiguration. Thus, we first discuss the dependence of BCE time on the battery cell/module configuration. For the series-based BCE system, the calculation formulas for the BCE time are already introduced in Proposition 2.4.1. Here, to facilitate the analysis, we rewrite the BCE time calculation formulas as below:

$$T_e = t_{ideal}(g_e) = \max_{g \in \{1,\ldots,B-1\}} t_{ideal}(g), \tag{4.2.1}$$

$$t_{ideal}(g) = \begin{cases} \frac{(\bar{x}_g(0)-\bar{x}_B(0))\tau}{(\frac{1-l_e}{g}+\frac{1}{B}l_e)r_e}, & \text{if } \bar{x}_g(0) > \bar{x}_B(0), \\ \frac{(\bar{x}_B(0)-\bar{x}_g(0))\tau}{(\frac{1}{g}-\frac{1}{B}l_e)r_e}, & \text{if } \bar{x}_g(0) < \bar{x}_B(0), \end{cases} , g \in \{1, \ldots, B-1\}, \tag{4.2.2}$$

$$\bar{x}_g(t) = \frac{1}{g}\sum_{i=1}^{g} x_i(t), \ g = 1, 2, \ldots, B, \tag{4.2.3}$$

where $\bar{x}_g(t)$ is the average SOC of cell 1 to cell g at time instant t, and $t_{ideal}(g)$ is the shortest time needed for $\bar{x}_g(t)$ to reach $\bar{x}_B(t)$. In other words, the boundary battery group (BBG) consisting of cell 1 to cell g, $g < B$, has to be always discharged or charged by its neighboring cell, cell $g+1$, so that $\bar{x}_g(t)$ can reach $\bar{x}_B(t)$ at $t = t_{ideal}(g)$. In addition, the BBG consisting of cell 1 to cell g_e has the longest $t_{ideal}(g)$, which is equal to T_e.

From (4.2.1)-(4.2.3), we can see the BCE time T_e depends on not only the values of initial cell SOCs but also their permutation (i.e., cell configuration). Let vector $\mathbf{C_B}$ denote a cell configuration of a series-connected battery system, then the BCE time resulting from cell configuration $\mathbf{C_B}$ is denoted by $T_e(\mathbf{C_B})$. For instance, given the initial cell SOCs of a 3-cell system $\{0.3, 0.4, 0.5\}$, we have $3! = 6$ cell configurations in total, such as $\mathbf{C_B} = (0.3, 0.5, 0.4)$ or $\mathbf{C_B} = (0.4, 0.3, 0.5)$. In addition, given any cell configuration $\mathbf{C_B}$, we can get another cell configuration $\mathbf{C_B P_B}$ through a $B \times B$ permutation matrix $\mathbf{P_B} \in \mathbf{C_B}$, where S_B is the full set of all permutation matrices [87]. As a result, the new cell configuration $\mathbf{C_B P_B}$ will have a new BCE time $T_e(\mathbf{C_B P_B})$. Thus, based on (4.2.1), given any initial cell configuration $\mathbf{C_B}$, in order to obtain the minimum BCE time, we have to solve the following optimization problem:

$$\min_{\mathbf{P_B} \in \mathbf{S_B}} T_e(\mathbf{C_B P_B}) = \min_{\mathbf{P_B} \in \mathbf{S_B}} \max_{g \in \{1,\ldots,B-1\}} t_{ideal}(\mathbf{C_B P_B}, g). \tag{4.2.4}$$

This problem cannot be solved analytically since the maximization problem in (4.2.1) lacks analytical solution. On the other hand, solving this problem using exhaustive search is not practical since the number of cell configurations has a factorial growth. For example, for a system with only 10 cells, we have to perform 10!/2=1,814,400 calculations of T_e in the exhaustive search (only one test is needed for two configurations with inverse cell permutations since they result in identical T_e). In this case, it takes about 178 s to finish all exhaustive calculations of T_e using an exhaustive search on a computer server with Intel(R) Xeon(R) CPU 2.3 GHz. For a battery system with more cells, e.g., 15-cell battery series, the total number of configurations in the exhaustive search reaches 15!/2=653,837,184,000, and such exhaustive search is estimated to take more than two years. Thus, instead of performing exhaustive search for the minimum T_e, we will focus on analyzing the calculation of BCE time T_e to find the appropriate battery cell configuration which can result in a T_e close to the minimum T_e.

4.2.2 Two-stage cell reconfiguration algorithm

In this chapter, we will use a two-stage approach to solve the optimization problem (4.2.4). In the first stage, we construct an initial cell configuration that can lead to a relatively short BCE time. In the second stage, we perform iterative local search by relocating cells to achieve a shorter BCE time.

Stage 1: Construction of an initial cell configuration

It follows from (4.2.1) and (4.2.2) that if $\bar{x}_{g_e}(0) < \bar{x}_B(0)$, the BBG consisting of cell 1 to cell g_e is always charged during the equalization process, and is thus referred to

as the *charged BBG* (*CBBG*) of the battery system. Meanwhile, the BBG consisting of all remaining cells, from cell g_e+1 to cell B, is always discharged and is referred to as the *discharged BBG* (*DBBG*) of the system. Similarly, if $\bar{x}_{g_e}(0) > \bar{x}_B(0)$, the BBG consisting of cell 1 to cell g_e is the DBBG and all remaining cells form the CBBG. In other words, cell g_e and cell $g_e + 1$ mark the division of the battery system into the CBBG and the DBBG.

In practice, the charge transfer loss rate l_e between two cells is usually at a low level, e.g., $l_e = 5\%$ to 10% [24, 88, 89]. Thus, we start the analysis from a simplified case by neglecting the charge transfer loss, i.e., $l_e = 0$ in (4.2.1) and (4.2.2). Then based on (4.2.1)-(4.2.3), we obtain

$$\begin{aligned} T_e(l_e = 0) &= \max_{g\in\{1,\ldots,B-1\}} g\left|\bar{x}_g(0) - \bar{x}_B(0)\right| \frac{\tau}{r_e} \\ &= \max_{g\in\{1,\ldots,B-1\}} \left|\sum_{i=1}^{g} x_i(0) - g\bar{x}_B(0)\right| \frac{\tau}{r_e} \\ &= \max_{g\in\{1,\ldots,B-1\}} \left|\sum_{i=1}^{g} \left(x_i(0) - \bar{x}_B(0)\right)\right| \frac{\tau}{r_e} \\ &= \max_{g\in\{1,\ldots,B-1\}} \left|\sum_{i=1}^{g} d_i(0)\right| \frac{\tau}{r_e} \\ &= \left|\sum_{i=1}^{g_e} d_i(0)\right| \frac{\tau}{r_e}, \end{aligned} \tag{4.2.5}$$

where $d_i(0)$ is the ith cell's SOC deviation from all cells' average SOC at $t = 0$, i.e.,

$$d_i(0) \triangleq x_i(0) - \bar{x}_B(0),\ i = 1, 2, \ldots, B. \tag{4.2.6}$$

From (4.2.5) we can see, if we group a cell with large $d_i(0) > 0$ with a cell with small $d_j(0) < 0$, their SOC deviation will compensate each other to result in a $d_i + d_j$

close to 0. If this is applied to construct the CBBG or DBBG, the absolute summation term in (4.2.5) will be limited to a relatively low level. As a result, the BCE time may be shortened. Based on this idea, we propose the following method to initialize the battery cell configuration:

- *Step 1*: Put the cell with largest initial SOC and the cell with smallest initial SOC together to form a two-cell series, referred to as the *base string*.
- *Step 2*: Sort all remaining cells in descending order of their cell SOC deviations $|d_i(0)|$.
- *Step 3*: Pick the first N cells from the sorted remaining cells, and connect them with the base string to form an *augmented string*. This should result in a total of $(N+1)!$ possible permutations. If less than N cells are left, let all remaining cells form the augmented string. Calculate the T_e for each permutation and choose the one with the shortest T_e as the new *base string*.
- *Step 4*: If all cells are incorporated into the base string, stop and output the final base string as the cell configuration; otherwise, return to Step 3.

Note that, in Step 3, N is the number of cells attached during every update of cell string, which could vary from 1 to $B-2$. Particularly, if $N=1$, the remaining cells are attached to the base string one by one; if $N=B-2$, only one cell string update is needed, during which all $B-2$ remaining cells are attached. Given N, the total number of T_e calculations is approximately

$$\frac{B-2}{N}(N+1)! = (B-2)(N+1)(N-1)!.$$

Thus, a larger value of N requires more T_e calculations and longer computation time, but can lead to a cell configuration with shorter T_e.

Stage 2: Cell relocation-based local search of cell configuration

Once the initial cell configuration has been constructed, its corresponding $d_i(0)$'s, g_e, T_e, CBBG, and DBBG are all determined. Then, to carry out local search of cell configurations for further reduction of BCE time, "neighborhood" configurations have to be defined. Given a cell configuration, its neighborhood configuration is obtained by relocating only one of its cells. Note that some neighborhood configurations may result in longer equalization time than that of the original given cell configuration. Therefore, to improve the search efficiency, we propose these two cell relocation rules below to avoid those unpromising configurations during the local search:

- *Cell Relocation Rule 1*: Move a cell with $d_i(0) > 0$ from the DBBG to the CBBG.
- *Cell Relocation Rule 2*: Move a cell with $d_i(0) < 0$ from the CBBG to the DBBG.

It can be shown that these two rules can reduce the system BCE time $T_e(l_e = 0)$ under the condition given below:

Condition 1: The two cells connecting the charged and discharged BBGs before the cell relocation remain the boundary cells of the charged and discharged BBGs after the cell relocation.

Although these cell relocation rules are proposed assuming no charge transfer loss, i.e., $l_e = 0$, our simulation experiments indicate that these rules can also be applied

to reduce the BCE time when the charge transfer loss rate is small, e.g., $l_e = 5\%$. Finally, with Cell Relocation Rule 1 and Rule 2, we propose the following local search method to shorten the T_e of series-based charge equalization systems.

- *Step 1*: Given a cell configuration C_B^0, calculate its BCE time T_e^0 based on (4.2.1) and (4.2.2), and identify g_e, the CBBG, and the DBBG.

- *Step 2*: Find all cells with $d_i(0) > 0$ in the DBBG and all cells with $d_i(0) < 0$ in the CBBG excluding the two boundary cells: cell g_e and cell $g_e + 1$.

- *Step 3*: Perform local search of cell configuration at current configuration C_B^0 by relocating each eligible cell found in Step 2 to all its possible destination positions according to Cell Relocation Rule 1 or 2. Meanwhile, calculate the BCE times of all neighborhood configurations obtained.

- *Step 4*: If the minimum T_e obtained by Step 3 is less than T_e^0, set it as T_e^0, the corresponding cell configuration as C_B^0, and then return to Step 1. Otherwise, stop and output the final cell configuration C_B^0.

To illustrate the local search of neighborhood configurations performed in Step 3, we take a five-cell series $(c_1, c_2, c_3, c_4, c_5)$ as shown in Fig. 4.2.1 for an example. Assume that (c_1, c_2) is the charged BBG and (c_3, c_4, c_5) is the discharged BBG. Then, according to Step 3, only c_1, c_4, and c_5 may be eligible for relocation. If cell c_1 is to be relocated from BBG (c_1, c_2) to BBG (c_3, c_4, c_5), then it has three possible destination positions corresponding to three cell configurations: $(c_2, c_3, c_1, c_4, c_5)$, $(c_2, c_3, c_4, c_1, c_5)$, and $(c_2, c_3, c_4, c_5, c_1)$. Similarly, if c_4 is to be relocated, the possible cell configurations after relocation are $(c_4, c_1, c_2, c_3, c_5)$ and $(c_1, c_4, c_2, c_3, c_5)$.

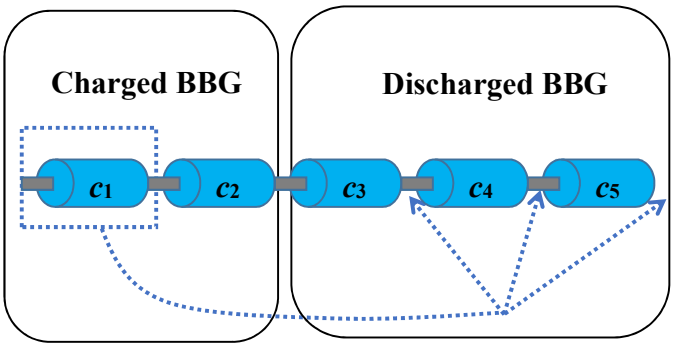

FIGURE 4.2.1: Illustration of the possible destination positions in cell relocation for a 5-cell system in series connection.

It should be noted that, Cell Relocation Rule 1 and Rule 2 can guarantee a reduced T_e only under Condition 1. Thus, we try to let Condition 1 hold in two ways: keeping the two boundary cells of the CBBG and the DBBG not moved in Step 2, and only moving one of all cells from the same cell configuration during each cell relocation in Step 3. Although these two ways still cannot guarantee Condition 1 to be satisfied and may lead to configurations with longer T_e after certain cell relocation, such cell configuration will not be selected in Step 4. Thus, The proposed cell relocation-based local search implemented via the two relocation rules can always guarantee an BCE time less than or equal to the BCE time of the original cell configuration.

Finally, to conclude this algorithm, we provide the flow chart of the proposed two-stage cell reconfiguration algorithm in Fig. 4.2.2. Next, we will evaluate the performance of the proposed algorithm by numerical simulations.

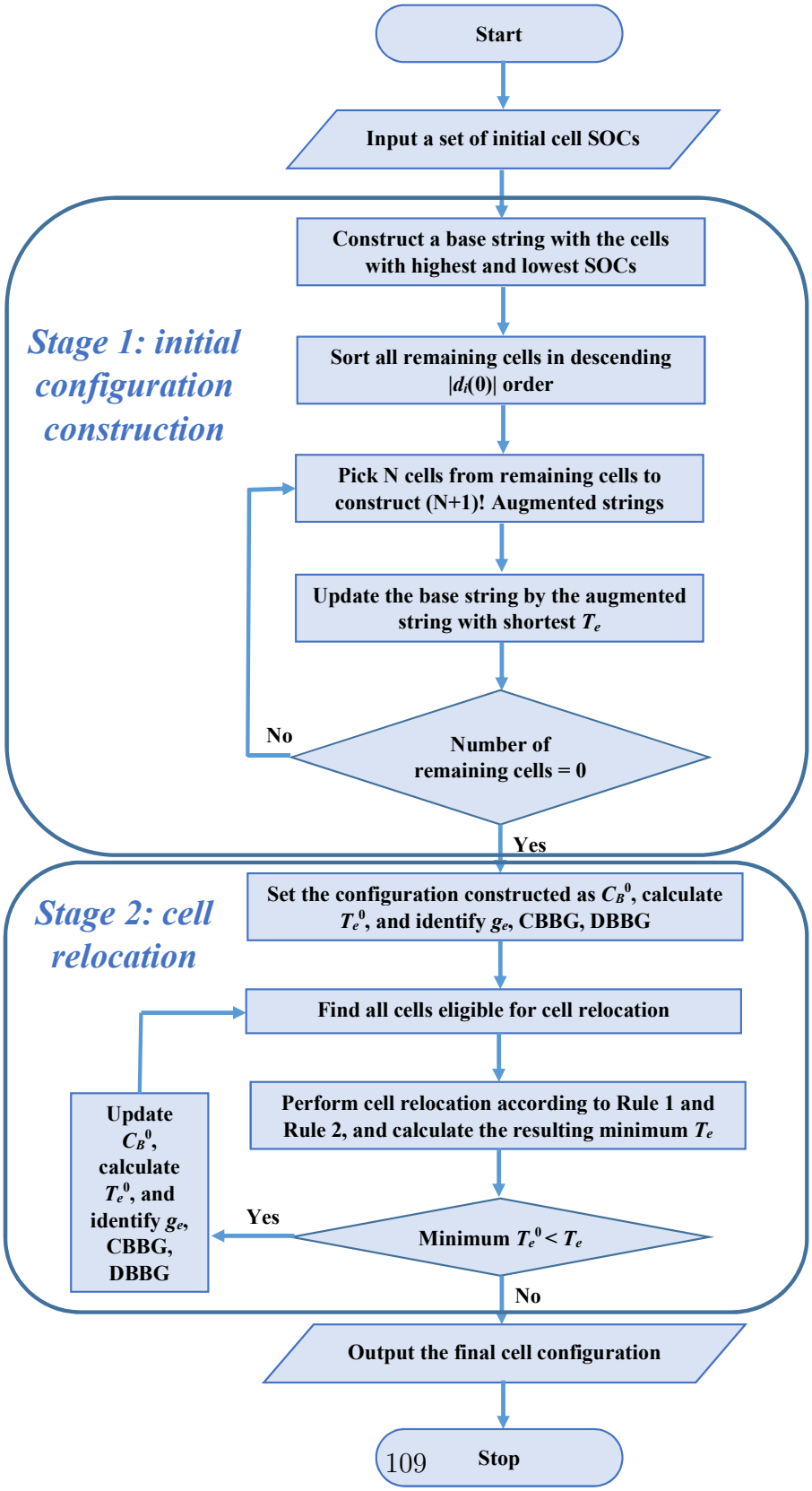

FIGURE 4.2.2: Two-stage cell reconfiguration algorithm for series-based charge equalization systems.

4.2.3 Performance evaluation of the cell reconfiguration algorithm

Experiment 1: Comparison with exhaustive search for 10-cell systems

The performance evaluation is composed of two steps: determining the cell configurations to be tested and evaluating their BCE times. In the first step, we will use the proposed algorithm to generate a cell configuration and also try all other possible cell configurations. This step only involves calculation or trials but no experiments. Then in the second step, for those cell configurations determined in the first step, their BCE times can be evaluated by circuit experiments, numerical simulations, or mathematical calculations. However, even for a small system, e.g., a 10-cell system, the total number of cell configurations is too large to be evaluated by circuit experiments since it is a factorial function of the number of cells, e.g., $10! = 3,628,800$. Besides, for larger systems, the model-based numerical simulation is also very time-consuming especially for a large number of cell configurations [41, 42]. Therefore, in the second step we will use the computationally efficient formula proposed in Chapter 2 to evaluate the BCE time. Note that this formula is based on a mathematical model which has shown high accuracy in recent papers. Thus, this validated model along with thoroughly mathematical analysis also verify the BCE time calculation in the second step of the performance evaluation.

To evaluate the efficacy and efficiency of the proposed algorithm under a large number of initial conditions, we first compare it with exhaustive search in series-connected battery systems consisting of 10 cells. Specifically, a total of $10,000$ test cases were created with each case having 10 initial cell SOCs randomly generated from uniform distribution $U(0,1)$. Then, for test case s, $s \in \{1, 2, \ldots, 10^4\}$, let

$\boldsymbol{T}(s)$ denote the set of the BCE times of all possible configurations obtained through exhaustive search. Among all T_e's $\in \boldsymbol{T}(s)$, the minimum and maximum values are denoted by $T_e^{min}(s)$ and $T_e^{max}(s)$, respectively. In addition, let $T_e^{rec}(s)$ denote the BCE time obtained using the proposed cell reconfiguration algorithm. To evaluate the effectiveness (i.e., optimality) of the cell configuration obtained by the proposed algorithm, we compare its BCE time with the total set of BCE times based on: normalized BCE time difference $\epsilon_d(s)$ defined in (4.2.7) and BCE time percentile $\epsilon_p(s)$ defined in (4.2.8).

$$\epsilon_d(s) = \frac{T_e^{rec}(s) - T_e^{min}(s)}{T_e^{max}(s) - T_e^{min}(s)} \times 100\%, \tag{4.2.7}$$

$$\epsilon_p(s) = \frac{\text{Number of } T_e\text{'s} \in \boldsymbol{T}(s) \text{ s.t. } T_e < T_e^{rec}(s)}{\text{Total number of } T_e\text{'s} \in \boldsymbol{T}(s)} \times 100\%. \tag{4.2.8}$$

For all $10,000$ test cases studied in this experiment, the mean and maximum values of these two measures are also calculated:

$$\bar{\epsilon}_d = \frac{1}{10^4} \sum_{s=1}^{10^4} \epsilon_d(s), \ \epsilon_d^{max} = \max_{s \in \{1,2,\ldots,10^4\}} \epsilon_d(s),$$

$$\bar{\epsilon}_p = \frac{1}{10^4} \sum_{s=1}^{10^4} \epsilon_p(s), \ \epsilon_p^{max} = \max_{s \in \{1,2,\ldots,10^4\}} \epsilon_p(s).$$

Clearly, smaller $\epsilon_d(s)$ and $\epsilon_p(s)$ indicate smaller difference between $T_e^{rec}(s)$ and the true optimum $T_e^{min}(s)$, and, thus, better optimality of the cell reconfiguration algorithm.

In addition to analyzing the optimality of T_e^{rec}, we also need to compare the running times of both approaches. For test case s, the running times of the exhaustive search and the proposed cell reconfiguration algorithm are denoted by $t_{exh}(s)$ and $t_{rec}(s)$, respectively. For all 10^4 initial cell SOC sets of the 10-cell system, the mean

values of these two measures are calculated as

$$\bar{t}_{exh} = \frac{1}{10^4}\sum_{s=1}^{10^4} t_{exh}(s),\ \bar{t}_{rec} = \frac{1}{10^4}\sum_{s=1}^{10^4} t_{rec}(s).$$

TABLE 4.2.1: Comparison of performance measures and running times between the exhaustive search and the proposed cell reconfiguration algorithm for 10^4 10-cell initial SOC test cases.

N	$\bar{\epsilon}_d$	ϵ_d^{max}	$\bar{\epsilon}_p$	ϵ_p^{max}	$\bar{t}_{exh}$ (s)	$\bar{t}_{rec}$ (s)
1	2.24%	15.33%	0.21%	4.37%	178.4224	0.2879
2	2.39%	18.03%	0.23%	6.53%	178.4224	0.2970
3	1.88%	10.93%	0.19%	6.50%	178.4224	0.2984
4	1.84%	13.37%	0.16%	6.31%	178.4224	0.3169
5	1.57%	9.40%	0.13%	4.65%	178.4224	0.3514
6	1.39%	8.89%	0.12%	4.96%	178.4224	0.6677
7	1.15%	8.82%	0.10%	3.89%	178.4224	4.2020
8	0.01%	2.17%	0.00%	0.92%	178.4224	37.5258

The simulation results are summarized in Table 4.2.1. As one can see, larger values of N (number of cells picked in each step of configuration initialization), in general, lead to better optimization performance, i.e., smaller $\bar{\epsilon}_d$, ϵ_d^{max}, $\bar{\epsilon}_p$, and ϵ_p^{max}. However, larger values of N also result in longer running time, $\bar{t}_{rec}$, due to more BCE time evaluations. Thus, the user needs to make a trade-off between the desired optimization quality and available computation time. For example, for the 10-cell system case, by setting $N = 6$, we can get a T_e very close to T_e^{min} ($\bar{\epsilon}_d < 1.39\%$ and $\bar{\epsilon}_p < 0.12\%$) within less than one second on average. If longer computation time is allowed, the BCE time can be further reduced. For example, by setting $N = 8$, we can get a near-minimum BCE time with $\bar{\epsilon}_d \approx 0.01\%$, $\bar{\epsilon}_p < 0.01\%$, $\epsilon_d^{max} < 2.2\%$, and $\epsilon_p^{max} < 1\%$, while the running time of the proposed cell reconfiguration algorithm is only about 21.22% of the exhaustive search's computation time.

Experiment 2: Comparison with random configuration for 20-cell systems

Although the exhaustive search can provide the BCE time for all cell configurations, including the shortest one, it takes a much longer running time than the proposed cell reconfiguration as shown in Table 4.2.1. Were one to study 10^4 test cases for 11-cell systems, the total computation time of exhaustive search would be estimated to exceed $(178.4224\text{ s} \times 11 \times 10^4)/(60 \times 60 \times 24\text{ s/day}) \approx 227$ days. Similar calculation suggests that the average computation time of exhaustive search on a single 15-cell test case would be over 2 years.

Therefore, to evaluate the performance of the proposed cell reconfiguration algorithm for battery systems with 20 cells, a different approach is used. Specifically, a total of 10^6 test cases are created with each case having the initial cell SOCs randomly generated from uniform distribution $U(0,1)$. Then, for each test case, we randomly generate a single cell configuration. For test case s in this experiment, $s \in \{1, 2, \ldots, 10^6\}$, let $T_e^{rec}(s)$ still denote the BCE time obtained from the proposed cell reconfiguration algorithm, and let $T_e^{ran}(s)$ denote the BCE time of randomly generated configuration. Then the relative difference in these BCE times is calculated as follows:

$$\epsilon_r(s) = \frac{T_e^{ran}(s) - T_e^{rec}(s)}{T_e^{ran}(s)} \times 100\%. \tag{4.2.9}$$

Clearly, larger value of $\epsilon_r(s)$ indicates better optimality of the proposed algorithm. Then, for all 10^6 test cases, we calculate the maximum, mean, and minimum of $\epsilon_r(s)$'s, denoted by ϵ_r^{max}, $\bar{\epsilon}_r$, and ϵ_r^{min}, respectively. Moreover, the fraction of test cases, in which the randomly generated configuration outperforms the one obtained by the

proposed algorithm, i.e., $T_e^{ran} < T_e^{rec}$, is also recorded and denoted as r_f:

$$r_f = \frac{\text{Number of test cases with } T_e^{rec}(s) > T_e^{ran}(s)}{\text{Total number of test cases}} \times 100\%. \tag{4.2.10}$$

Finally, the mean computation time of the cell reconfiguration algorithm for all test cases, $\bar{t}_{rec}$, is also measured. The results of this experiment are given in Table 4.2.2.

TABLE 4.2.2: Summary of all 10^6 $\epsilon_r(s)$'s with various values of N in the cell reconfiguration method.

N	ϵ_r^{max}	$\bar{\epsilon}_r$	ϵ_r^{min}	r_f	$\bar{t}_{rec}$ (s)
1	91.41%	67.60%	-27.17%	0.0050%	0.085
3	91.33%	67.98%	-34.46%	0.0030%	0.140
5	91.74%	68.27%	-13.12%	0.0028%	0.416

For these 20-cell battery systems, while it is too time consuming to get the minimum T_e by exhaustive search, the proposed cell reconfiguration algorithm can generate a configuration with sufficiently short BCE time, as shown in Table 4.2.2. The results indicate that the BCE time obtained by the proposed algorithm is, on average, 68% shorter than that of an configuration randomly generated. Note that there do exist cases that the proposed algorithm fails to generate a higher quality configuration than a randomly generated one. However, this occurs very rarely (at most 50 worse test cases out of a million when $N = 1$). In addition, for these 20-cell test cases, the proposed cell reconfiguration algorithm is still very computationally efficient with an average running time less than 0.5 s. Therefore, we claim that the proposal algorithm can effectively and efficiently generate a cell configuration with high charge equalization performance.

4.3 Near-optimal cell/module configuration in the module-based BCE system

4.3.1 Optimal battery cell/module reconfiguration for shortest BCE time

To shorten the BCE time of module-based BCE systems, significant research efforts have been directed to improve the circuit designs, connection topologies, and control strategies of battery charge equalizers. However, the influence of battery cell/module configuration on battery charge balance or equalization has not been well investigated so far. Indeed, for a module-based BCE system, the BCE time may vary dramatically if we only change the configuration of battery cells/modules. Motivated by this, in this subsection we formulate the optimization problems to minimize the BCE time of module-based BCE systems under two levels of battery cell/module reconfigurations.

In a module-based BCE system, both cell reconfiguration and module reconfiguration may be achievable through different circuit designs. In this chapter, we consider the following three types of battery reconfigurations:

- *Module reconfiguration*: The connecting sequence of battery modules can be flexibly changed.
- *Intra-module cell reconfiguration*: The connecting sequence of all cells in a single module can be arbitrarily adjusted. However, a cell is not allowed to be relocated from its original module to other modules.
- *Inter-module cell reconfiguration*: A cell can be reconfigured into any module, given that the total number of modules and the total number of cells per module do not change.

Clearly, while the intra-module cell reconfiguration only involves battery cells within one module, the inter-module cell reconfiguration is implemented among all battery cells and thus it requires more connection flexibility. In addition, it also leads to orders of magnitude greater number of possible configurations, which amounts to more complexity in optimizing the battery cell/module configuration for fast charge equalization. Thus, in this chapter, we consider two levels of reconfigurability in the module-based BCE system:

- *Bounded Reconfiguration*: Module reconfiguration and intra-module cell reconfiguration are allowed, but inter-module cell reconfiguration is forbidden;
- *Complete Reconfiguration*: Module reconfiguration, intra-module cell reconfiguration, and inter-module cell reconfiguration are all allowed.

As discussed in Chapter 3, the module-based BCE system consisting of M modules can be viewed as $M+1$ independently operating series-based BCE subsystems. Denote the configuration of the m-th subsystem by a vector $\mathbf{C}_\mathbf{B}^m$, $m \in \{1, \ldots, M+1\}$. Accordingly, the BCE time corresponding to the subsystem configuration $\mathbf{C}_\mathbf{B}^m$ is denoted by $T_e(\mathbf{C}_\mathbf{B}^m)$, $m \in \{1, \ldots, M+1\}$, which can be calculated using (3.4.1) or (3.4.2), i.e., the BCE time calculation formula for the series-based BCE system. Note that, here $\mathbf{C}_\mathbf{B}^m$ is a variable and $\mathbf{C}_\mathbf{B}^m \in \mathbf{S}_\mathbf{B}^m$, where $\mathbf{S}_\mathbf{B}^m$ is the set of all possible configurations of the m-th subsystem to be considered. Clearly, the BCE time depends on the system configuration. In order to evaluate the minimum BCE time of a module-based BCE system including M modules, based on the calculation formula of the BCE time

(3.4.3), the following optimization problem is formulated:

$$\min_{\substack{\mathbf{C}_\mathbf{B}^m \in \mathbf{S}_\mathbf{B}^m \\ m=1,\ldots,M+1}} T_e^{sys}(\mathbf{C}_\mathbf{B}^1,\ldots,\mathbf{C}_\mathbf{B}^{M+1}) = \min_{\substack{\mathbf{C}_\mathbf{B}^m \in \mathbf{S}_\mathbf{B}^m \\ m=1,\ldots,M+1}} \max_{i\in\{1,\ldots,M+1\}} T_e(\mathbf{C}_\mathbf{B}^i). \tag{4.3.1}$$

When performing the Bounded Reconfiguration, each battery cell or module is bounded within its original subsystem, i.e., the component cells/modules of each subsystem remain unchanged while their connection sequence can be reconfigured. Thus, the reconfiguration of each subsystem can be independently carried out. As a result, under the Bounded Reconfiguration, the optimization problem in (4.3.1) can be simplified to:

$$\begin{aligned}\min_{\substack{\mathbf{C}_\mathbf{B}^m \in \mathbf{S}_\mathbf{B}^m \\ m=1,\ldots,M+1}} T_e^{sys}(\mathbf{C}_\mathbf{B}^1,\ldots,\mathbf{C}_\mathbf{B}^{M+1}) &= \min_{\substack{\mathbf{C}_\mathbf{B}^m \in \mathbf{S}_\mathbf{B}^m \\ m=1,\ldots,M+1}} \max_{i\in\{1,\ldots,M+1\}} T_e(\mathbf{C}_\mathbf{B}^i) \\ &= \max_{i\in\{1,\ldots,M+1\}} \min_{\substack{\mathbf{C}_\mathbf{B}^m \in \mathbf{S}_\mathbf{B}^m \\ m=1,\ldots,M+1}} T_e(\mathbf{C}_\mathbf{B}^i) \\ &= \max_{i\in\{1,\ldots,M+1\}} \min_{\mathbf{C}_\mathbf{B}^i \in \mathbf{S}_\mathbf{B}^i} T_e(\mathbf{C}_\mathbf{B}^i). \end{aligned} \tag{4.3.2}$$

Then, in order to find the shortest BCE time of the entire system under the Bounded Reconfiguration, we only need to search for the shortest BCE time of each subsystem. Thus, according to (4.3.2), for a module-based BCE system including M modules and B cells per module, the total number of different configurations to be tested under the Bounded Reconfiguration for the shortest system BCE time is

$$N_{BR} = \frac{B!}{2} \times M + \frac{M!}{2}. \tag{4.3.3}$$

Note that, since a cell/module configuration and its reverse have the same BCE time,

we do not need to test the reverse configurations.

On the other hand, when the Complete Reconfiguration is carried out, battery cells can be relocated to any place in the battery series while the total number of modules in the system, i.e., M, and the total number of cells per module, i.e., B, do not change. This is more complicated than the Bounded Reconfiguration since the reconfiguration in one subsystem may affect those in other subsystems. The Complete Reconfiguration can be implemented in two steps: dividing all $M \times B$ battery cells evenly into M groups to form an *equal-size partition* of all battery cells denoted by P_{ar}, and then constructing the initial configurations of the M cell-level subsystems based on the M subsets of P_{ar} to perform the Bounded Reconfiguration. Note that, $P_{ar} \in S_P$ is a variable, where S_P is the full set of all cell partitions with M subsets and B cells per subset. Then, the m-th subsystem configuration constructed based on the subset of P_{ar} is denoted by $\mathbf{C}_{\mathbf{B}}^{m}(P_{ar})$, $m \in \{1, \ldots, M+1\}$. Thus, under the Complete reconfiguration, we need to solve the following problem for the minimum system BCE time:

$$\begin{aligned} &\min_{P_{ar} \in S_P} \quad \min_{\substack{\mathbf{C}_{\mathbf{B}}^{m} \in \mathbf{S}_{\mathbf{B}}^{m} \\ m = 1, \ldots, M+1}} \quad T_e^{sys}(\mathbf{C}_{\mathbf{B}}^{1}(P_{ar}), \ldots, \mathbf{C}_{\mathbf{B}}^{M+1}(P_{ar})) \\ &= \min_{P_{ar} \in S_P} \max_{i \in \{1, \ldots, M+1\}} \min_{\mathbf{C}_{\mathbf{B}}^{i} \in \mathbf{S}_{\mathbf{B}}^{i}} T_e(\mathbf{C}_{\mathbf{B}}^{i}(P_{ar})). \end{aligned} \tag{4.3.4}$$

According to (4.3.4), the total number of different configurations to be tested in the Complete Reconfiguration for the shortest system BCE time is

$$N_{CR} = \frac{(MB)!}{M!(B!)^M} \times \left(\frac{B!}{2} \times M + \frac{M!}{2} \right). \tag{4.3.5}$$

In order to evaluate the minimum BCE time of a module-based BCE system, a

straightforward way is to compare the BCE times of all possible cell/module configurations by exhaustive search. However, as one can easily see, as the system size increases, i.e., B and/or M increase, the total number of subsystem configurations grows very fast since they are functions of factorials. For example, for a system with $M = 6$ and $B = 8$, if the Complete Reconfiguration is performed, the total number of configurations can reach about 4.868×10^{35} according to (4.3.5). Even for Bounded Reconfiguration, the total number of configurations still goes to 121,320 according to (4.3.3). Thus, for moderate- to large-scale systems, it becomes too time-consuming to use the exhaustive search to identify the cell/module configuration with minimum BCE time. Therefore, computationally efficient battery reconfiguration algorithms are needed to achieve the minimum or near-minimum BCE time under different levels of reconfigurability. This will be studied in Subsections 4.3.2 and 4.3.3 for module-based BCE systems under the Bounded and Complete Reconfigurations, respectively.

4.3.2 Optimal cell/module configuration under the Bounded Reconfiguration

Module-based bounded reconfiguration algorithm

Consider a module-based BCE system under the Bounded Reconfiguration level, i.e., only intra-module cell reconfiguration and module reconfiguration are allowed. Then such a system can be viewed as $M + 1$ reconfigurable series-based BCE subsystems. According to the BCE time calculation formula (3.4.3), we can calculate the BCE time of each subsystem, and then select the longest one as the entire module-based BCE system's BCE time T_e^{sys}. Thus, to reach a shorter T_e^{sys}, we need to focus on the series-based BCE subsystem resulting in the longest BCE time. For such a

reconfigurable series-based BCE subsystem, the optimal battery cell reconfiguration algorithm for fast charge equalization developed in Subsection 4.2.2 can be adaptively applied, which is referred to as the *Series-based reconfiguration algorithm*. Then, we propose the *module-based bounded reconfiguration algorithm* to minimize the BCE time of module-based BCE systems as follows.

Module-based bounded reconfiguration algorithm:

Step 1 : From all $M+1$ series-based BCE subsystems in the module-based BCE system, select the one leading to the longest BCE time as the *critical subsystem*. The BCE time of each subsystem is calculated based on (3.4.1) or (3.4.2).

Step 2 : If any subsystem is selected as the critical subsystem for the second time, output the final cell/module configuration and terminate the algorithm. Otherwise, go to Step 3.

Step 3 : Apply the Series-based reconfiguration algorithm to the critical subsystem to minimize its BCE time. Then return to Step 1.

Optimality and computational efficiency

In order to illustrate the efficacy of the proposed module-based bounded reconfiguration algorithm, using the same test bed introduced in Subsection 3.3.3, we test a module-based BCE system composed of $M = 3$ modules and $B = 2$ cells per module. If each battery cell is represented by its initial SOC, the original cell configuration is given as [(0.78,0.80),(0.72,0.76),(0.73,0.74)]. After applying the proposed module-based bounded reconfiguration algorithm, the obtained configuration is [(0.72,0.76),(0.78,0.80),(0.73,0.74)]. Then, the cell SOC evolutions and BCE times

based on these two configurations are compared in Fig. 4.3.1. Clearly, after applying the proposed algorithm, the BCE time is dramatically reduced from about 1080 s to 605 s by about 44%, which verifies the efficacy of the proposed reconfiguration algorithm.

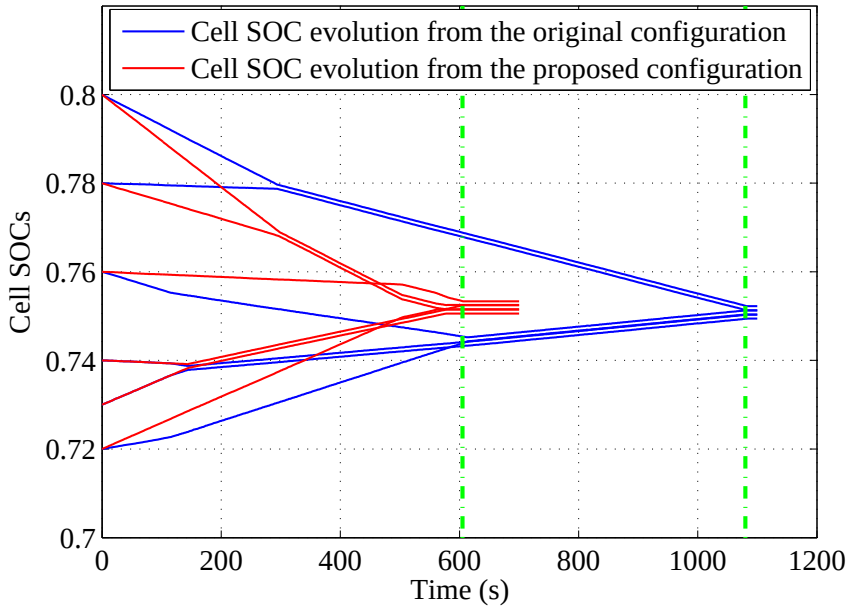

FIGURE 4.3.1: Comparison of the cell SOC evolution and BCE times between the original configuration and that obtained form the module-based bounded reconfiguration algorithm.

To evaluate the optimality of the proposed module-based bounded reconfiguration algorithm on larger systems under various initial cell/module configurations, we compare the BCE times obtained from the proposed algorithm and the exhaustive search by numerical experiments. Specifically, for a module-based BCE system with $M = 6$ modules and $B = 8$ cells per module, a total of S =10,000 initial cell SOC test cases are generated following the uniform distribution $U(0, 1)$.

As mentioned earlier, the exhaustive search method needs to test a total of 121,320

possible system configurations for each test case. Of all the BCE times of these configurations for the s-th test case, the minimum is denoted by $T_e^{exh}(s)$. On the other hand, for the s-th test case, the BCE time obtained by the proposed module-based bounded reconfiguration algorithm is denoted by $T_e^{BR}(s)$. Next, to evaluate the optimality of the proposed cell/module reconfiguration, we define the percentage difference of BCE time as well as its mean and maximum as follows.

$$\epsilon_d(s) = \frac{T_e^{BR}(s) - T_e^{exh}(s)}{T_e^{exh}(s)} \times 100\%, \quad s = 1, 2, \ldots, S,$$
$$\bar{\epsilon}_d = \frac{1}{S}\sum_{s=1}^{S} \epsilon_d(s),$$
$$\epsilon_d^{max} = \max_{s\in\{1,2,\ldots,S\}} \epsilon_d(s).$$

Besides, to quantify the success rate at which the proposed algorithm can identify the minimum BCE time, we define

$$r_{suc} = \frac{\text{Total \# of test cases with } T_e^{BR}(s) = T_e^{exh}(s)}{S}.$$

In addition to evaluating the optimality of the proposed reconfiguration algorithm, we also compare the running times of the exhaustive search and the proposed algorithm, which are denoted as $t_{exh}(s)$ and $t_{BR}(s)$, respectively. Their mean values are calculated by:

$$\bar{t}_{exh} = \tfrac{1}{S}\sum_{s=1}^{S} t_{exh}(s),\ \bar{t}_{BR} = \tfrac{1}{S}\sum_{s=1}^{S} t_{BR}(s).$$

Then, the comparison results between the proposed module-based bounded reconfiguration algorithm and the exhaustive search are given in Table 4.3.1. As we can

see, for such a module-based BCE system with 6 modules and 8 cells per module, the proposed algorithm can result in the minimum BCE time in 98.8% cases studied, while its average computation time is only 31.904% of the exhaustive search's average computation time. In addition, while the proposed algorithm fails to identify the configuration with the minimum BCE time for 1.2% test cases, the resulting BCE time is only 0.025% longer than the optimal one on average. Therefore, we claim that the proposed module-based bounded reconfiguration algorithm can lead to a minimum or near-minimum BCE time with much less computational efforts as compared to the exhaustive search.

TABLE 4.3.1: Comparison of BCE times and running times of the proposed reconfiguration algorithm and the exhaustive search for 10,000 test cases of a 48-cell module-based BCE system.

$\bar{\epsilon}_d$	ϵ_d^{max}	r_{suc}	$\bar{t}_{exh}$	$\bar{t}_{BR}$	$\bar{t}_{BR}/\bar{t}_{exh} \times 100\%$
0.025%	9.298%	98.800%	8.165 s	2.605 s	31.904%

4.3.3 Optimal cell/module reconfiguration under the Complete Reconfiguration

In the Complete Reconfiguration of a module-based BCE system, the battery cells can be reconfigured to any position of the battery string. As a result, the number of possible configurations is orders of magnitude larger than that under the Bounded Reconfiguration. Thus, the system performance such as BCE time has the potential to be further improved. Motivated by this, we extend our investigation to systems under the Complete Reconfiguration.

As discussed in Subsection 4.3.1, to generate a cell/module configuration by module reconfiguration and both intra- and inter-module cell reconfigurations, we can take

two steps. At the first step, all $M \times B$ battery cells are partitioned into M modules with each module having B cells. At this step, both the cell connection sequence in each module and module sequence in the system do not matter. Thus the resulting system from this step is an equal-size cell partition. Then, at the second step, for each equal-size cell partition, all cells are bounded within their assigned modules, and thus the module-based bounded reconfiguration algorithm proposed in Section 4.3.2 can be used to determine the cell order within each module and the module order. Therefore, next we will focus on the first step and discuss approaches to generate equal-size cell partitions.

Equal-size cell partition

Clearly, finding an equal-size cell partition of good quality is critical under Complete Reconfiguration. However, this is more challenging than the Bounded Reconfiguration. As shown in Subsection 4.3.1, for a system with M modules and B cells in each module, the total number of equal-size cell partitions is $\frac{(MB)!}{M!(B!)^M}$. As the system size increases, the total number of equal-size cell partitions grows very fast. For instance, given $M = 6$ and $B = 8$, the total number of equal-size cell partitions is 4.0129×10^{30}. Therefore, a computationally efficient method is necessary to help us quickly identify a high-quality equal-size cell partition.

According to (3.4.3), the BCE time of a module-based BCE system is the longest one of all its subsystems' BCE times. Intuitively, if all cell SOCs in the m-th module are closer to each other, we can get a smaller $T_e^{cel}(m)$. On the other hand, if the total cell SOCs of each module get closer to each other, T_e^{mod} will become smaller. Following this idea, we propose three approaches to construct the equal-size cell partition aiming

at shorter $T_e^{cel}(m)$ and/or T_e^{mod} as follows.

Approach 1 to reduce all cell-level BCE times $T_e^{cel}(m)$:

Sort all cells in descending SOC order and then assign the cell series consisting of the $((m-1)B+1)$-th cell to the mB-th cell into the m-th module, $m \in \{1, 2, \ldots, M\}$.

Approach 2 to reduce the module-level BCE time T_e^{mod}:

Step 1 : Sort all cells in descending SOC order and assign the m-th cell into the m-th module, $m \in \{1, 2, \ldots, M\}$.

Step 2 : Calculate each module's total cell SOC by summing up the SOCs of all cells already assigned to the module, and sort all modules by their total cell SOCs.

Step 3 : Pick up the first M cells from the remaining unassigned cells and assign the cell with the m-th largest SOC into the module with the m-th smallest total cell SOC, $m \in \{1, 2, \ldots, M\}$.

Step 4 : If all cells have been assigned into battery modules, terminate the algorithm. Otherwise, return to Step 2.

Approach 3 to balance $T_e^{cel}(m)$ and T_e^{mod}:

Step 1, 2, and 4 are same to those in Approach 2. Only replace Step 3 in Approach 2 by:

Step 3' : Pick up the first M cells from the remaining unassigned cells and assign the cell with the m-th largest SOC into the module with the m-th **largest** total cell SOC, $m \in \{1, 2, \ldots, M\}$.

To compare the performance of these three approaches, we test each of these approaches using the same S =10,000 initial cell SOC test cases randomly generated

in Subsection 4.3.2. For the s-th case, $s \in \{1, 2, \ldots, S\}$, the BCE times of the cell/module configurations with equal-size partition generated based on Approaches 1, 2, and 3 are denoted by $T_e^{app1}(s)$, $T_e^{app2}(s)$, and $T_e^{app3}(s)$, respectively. In addition, for the s-th case, the BCE time $T_e^{exh}(s)$ obtained from the exhaustive search under Bounded Reconfiguration in Subsection 4.3.2 is used here for reference. Then for the S =10,000 test cases, $T_e^{app1}(s)$, $T_e^{app2}(s)$, and $T_e^{app3}(s)$, are compared with $T_e^{exh}(s)$ in Figure 4.3.2.

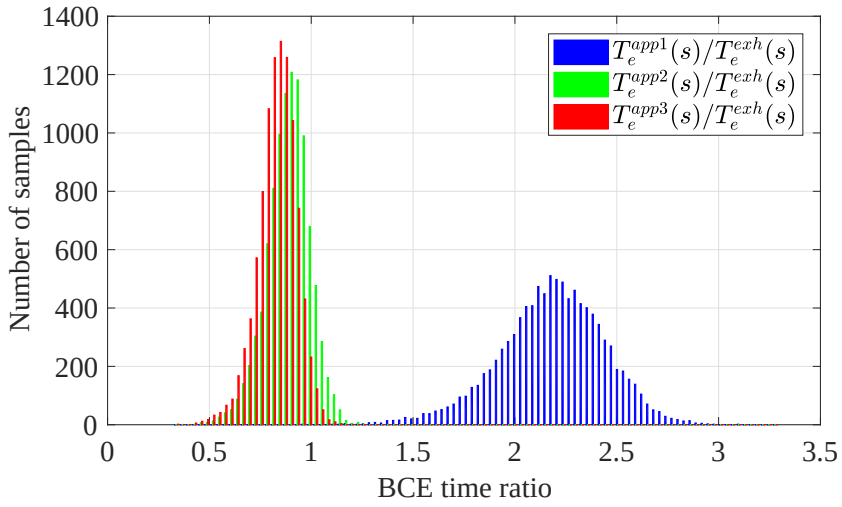

FIGURE 4.3.2: Comparison of the ratios of the BCE times based on three approaches to generate equal-size cell partitions and the BCE time obtained from the exhaustive search under the Bounded Reconfiguration.

Based on Figure 4.3.2 and the numerical simulation results, $\frac{T_e^{app1}(s)}{T_e^{exh}(s)} > 1$ in 99.97% of all cases studied, i.e., Approach 1 almost always fails to beat the optimal configuration under the Bounded Reconfiguration. On the other hand, $\frac{T_e^{app2}(s)}{T_e^{exh}(s)} < 1$ in 87.20% of all cases and $\frac{T_e^{app3}(s)}{T_e^{exh}(s)} < 1$ in 97.59% of all cases. In other words, it is highly likely that the BCE time can be improved if the inter-module cell reconfiguration based on Approach 2 or Approach 3 is applied. In addition, since the BCE times obtained from

Approach 3 are shorter than those from Approach 2 in 92.19% of all cases, we will apply Approach 3 to generate the equal-size cell partition in the subsequent analysis.

Optimality and computational efficiency

So far, for module-based BCE systems under the Complete Reconfiguration, we have developed the *module-based complete reconfiguration algorithm*, which consists of the Approach 3 of generating equal-size cell partitions as the first step and the module-based bounded reconfiguration algorithm proposed in Section 4.3.2 as the second step. To test its optimality, we need to compare the BCE time obtained from the proposed algorithm with the minimum BCE time. However, to evaluate the minimum BCE time in the presence of inter-module cell reconfiguration, exhaustive search becomes impractical when $M > 4$ and $B > 4$. Thus, we have to use other optimization tools such as the genetic algorithm (GA) to estimate the minimum BCE time. Although GA cannot guarantee a global minimum, it is commonly used to get some high-quality solutions to optimization problems [90].

To apply GA to the estimation of minimum BCE time, the initial population is generated randomly and a total of 60 individuals are generated for every generation. In addition, the GA is terminated if the resulting BCE time stays unimproved for 10^6 generations or it reaches the running time upper limit, i.e., 2 hours. For the module-based system with $M = 6$ modules and $B = 8$ cells in each module, we generate $S = 1000$ initial 48-cell SOC test cases following the uniform distribution $U(0, 1)$. For any configuration of each test case, the BCE time is calculated based on (3.4.1)-(3.4.3).

First, we investigate the optimality of the proposed module-based complete re-

configuration algorithm by comparing its BCE time with that obtained from GA. For the s-th test case, $s = 1, 2, \ldots, S$, the BCE times obtained from the module-based complete reconfiguration algorithm and GA are denoted by $T_e^{CR}(s)$ and $T_e^{GA}(s)$, respectively. For all these $S = 1000$ test cases, as shown in Fig. 4.3.3, the BCE time ratios $T_e^{CR}(s)/T_e^{GA}(s)$ ranges from 0.816 to 1.244 with the mean 1.038. Thus, for these 1000 randomly generated test cases, the BCE times obtained from the proposed module-based complete reconfiguration algorithm are similar to those minimum BCE times obtained from GA.

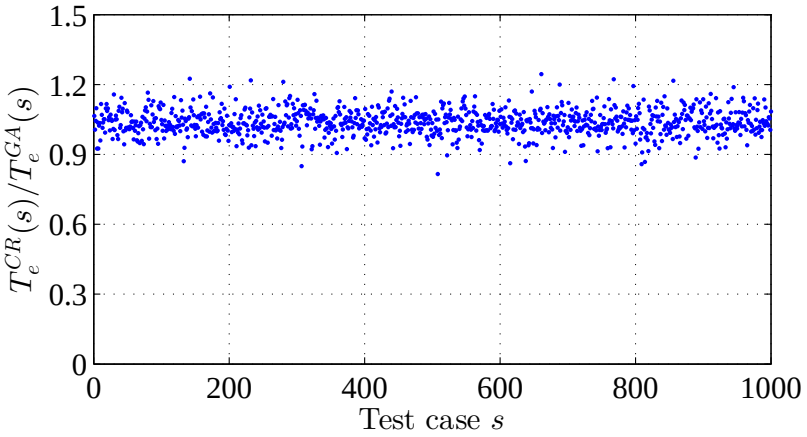

FIGURE 4.3.3: BCE time ratios of the proposed module-based complete reconfiguration algorithm and the GA for 1000 randomly generated initial cell SOC test cases of a module-based BCE system with 6 modules and 8 cells per module.

On the other hand, we compare the computation times of the proposed module-based complete reconfiguration algorithm and GA when they both reach the same BCE time level. For the 1000 test cases studied, the computation times of both methods reaching the same BCE time, i.e., the BCE time of the proposed reconfiguration algorithm, are shown in Fig. 4.3.4. According to the simulation results, with the given termination conditions, the GA succeeds in achieving the same BCE time of

the proposed reconfiguration in 81.2% of all cases. In addition, the average computation time of the proposed Complete Reconfiguration algorithm is 3.33 s while the GA takes 2,147.83 s on average. Thus, to reach the same BCE time level, the proposed module-based complete reconfiguration algorithm is much more computationally efficient than GA.

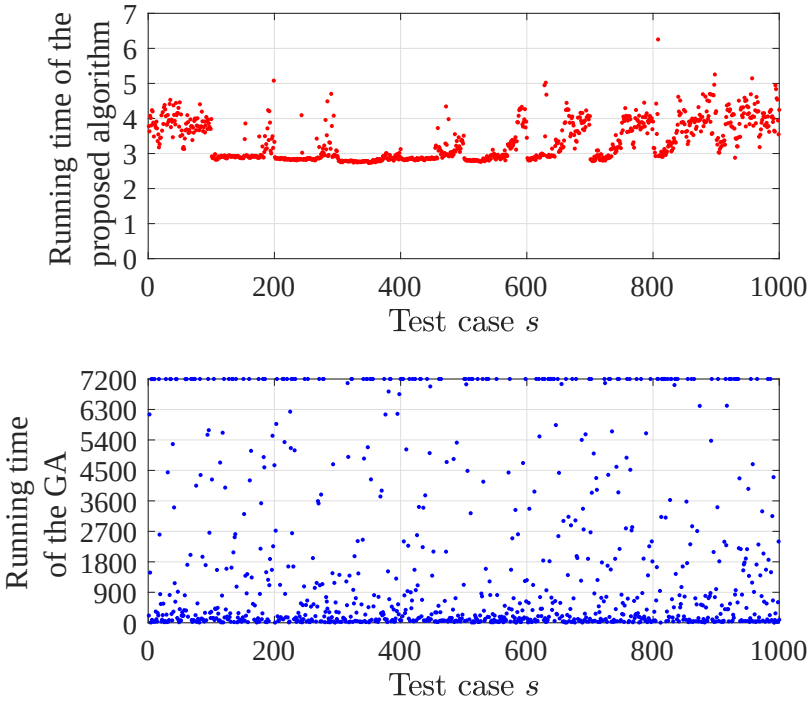

FIGURE 4.3.4: Comparison of the running times of the proposed module-based complete reconfiguration algorithm and GA when they reach the same BCE times for 1000 randomly generated initial cell SOC cases of a module-based BCE system with 6 modules and 8 cells per module.

Therefore, as compared to GA, the proposed module-based complete reconfiguration algorithm can provide an optimal or near-optimal BCE time with much less computation time.

4.4 Summary

In this chapter, we focus on analyzing the calculation formulas of the BCE time for series-based and module-based BCE systems and explore the influence of battery cell/module configuration on the speed of battery charge equalization. Then, we propose the battery reconfiguration algorithms for expedited battery charge equalization process, i.e., shorter BCE time T_e.

For the series-based BCE system, the simulation results show that the proposed cell reconfiguration algorithm can help achieve a T_e very close to its minimum for 10-cell systems and a T_e much shorter than that of the original cell configuration for 20-cell systems. Besides, using the proposed method, we can achieve the desired T_e with very short computation time.

For the module-based BCE system, as compared to the experimental data, exhaustive search, and genetic algorithm, these proposed algorithms demonstrate the capability of providing minimum or near-minimum BCE times with very high computational efficiency.

While we mainly discuss how to shorten the BCE time of BCE systems in this chapter, other important performance measures such as charge transfer efficiency will be investigated in our future work. Besides, in this chapter, the optimal cell/module configuration is determined and set up before the battery charge is balanced. We will extend our study to dynamic and adaptive cell/module reconfiguration during the charge balance for improved system performance.

Chapter 5

Parallel-connected battery power module system

5.1 Introduction

In order to maintain the charge balance or equalization among battery cells/modules, two important issues have to be considered, i.e., how to determine the battery state of charge (SOC) and how to balance battery SOCs. For the former, various estimation methods have been proposed and they are generally categorized into four classes in [91, 92, 93]: direct measurement, book-keeping estimation, adaptive systems, and hybrid methods. For the latter, a great number of circuit designs and control strategies have been developed for various battery system structures [14, 15, 16, 20, 21, 24, 25, 27, 41, 94, 95, 96]. In recent years, the technologies of battery power module (BPM) [97, 98, 99] and integrated battery building block [49, 100] have emerged to be promising solutions to battery charge balancing for possessing the capability of

independent control of each individual battery cell/module. Although these two technologies are different on the circuit level, both of them offer some similar functions on the system level. Therefore, in this chapter, with a slight abuse of notation, both will be referred to as *BPM* for simplicity. The diagrams of typical BPM systems are shown in Figure 5.1.1. As one can see, each BPM consists of a battery module and a DC/DC converter, and the BPMs can be connected either in series or parallel to be charged (discharged) by the charger (load). The BPM design has several advantages such as flexible individual module power or current control, better power protection, and easy installation and reconfiguration. On the other hand, as compared to conventional battery modules, BPMs usually cost more since they need extra converters [49]. This problem, however, is being offset thanks to the rapid advance in power electronics technology in recent years.

In a BPM system, by controlling the operation of each converter, each battery module's current can be individually adjusted. As a result, battery module charge imbalance in BPM systems can be alleviated by allocating different currents to each battery module. To reduce the battery charge imbalance in BPM systems during the charging (discharging) process, it is intuitive that battery modules with higher SOC should be charged (discharged) with smaller (larger) current. In recent studies, some heuristic methods for current or power allocation among battery cells or modules have been discussed. One class of current allocation method is to assign the discharging current of each module in proportion to its open circuit voltage (OCV) or SOC [99, 101, 102]. In this chapter, we refer to this method as *SOC-proportional* current allocation. Obviously, this method can help to improve the battery charge balance during the discharging process. On the other hand, it should be pointed out that this method lacks flexibility. Indeed, the allocated module currents will be fixed as

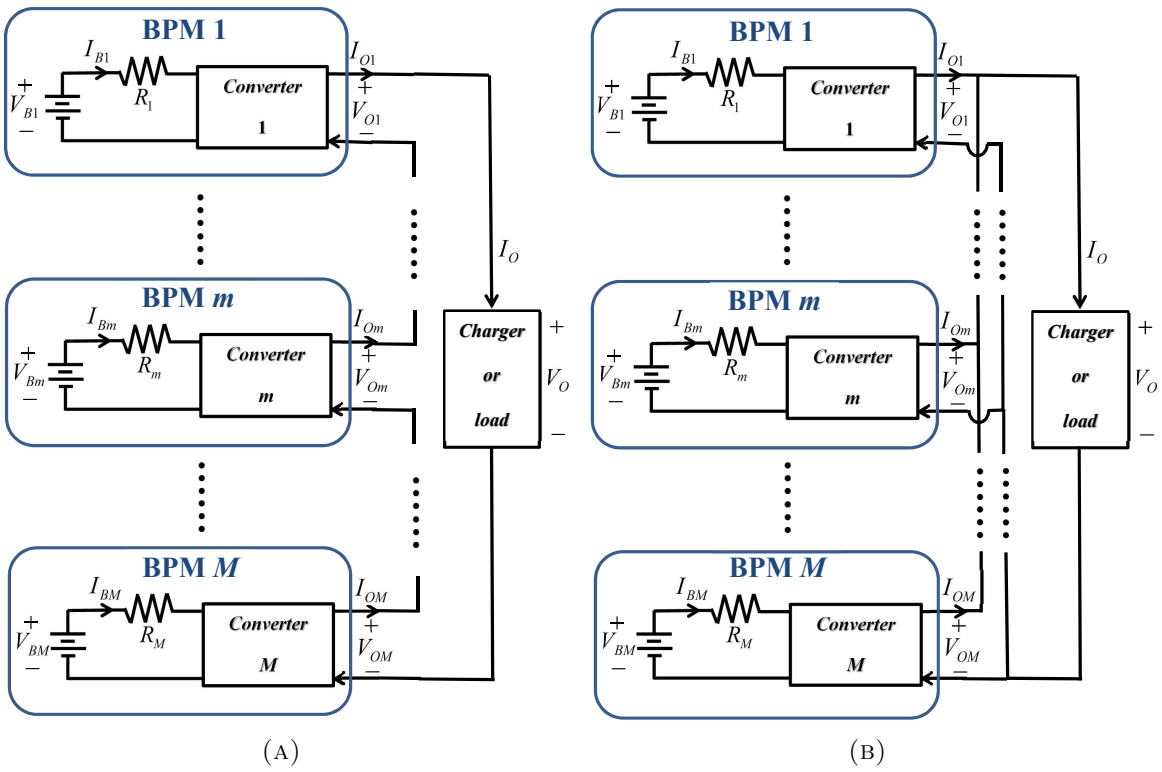

FIGURE 5.1.1: Equivalent circuits of BPM systems. (a) Series connection. (b) Parallel connection.

soon as the total power requirement on the load side is specified. To overcome this issue, we propose a new current allocation method, referred to as *charging/discharging space-based* (*CDS-based*) current allocation.

The major contributions of the proposed CDS-based current allocation and coordinated control algorithm are given as follows. First, different from the fixed system performance in SOC-proportional allocation, in the proposed CDS-based allocation we can flexibly tune the control parameters to achieve the desired time instant and SOC level at which all module SOCs will get equalized. Secondly, given the total power requirement in the CDS-based current allocation, a system performance control algorithm is developed to coordinate the module charge balance and total

power efficiency. It should be noted that, since all the subproblems in the proposed control algorithm have analytical solutions, the algorithm is very computationally efficient. This is of great importance for its application to large-scale battery systems. Lastly, it will be shown that the SOC-proportional method is simply a special case of the proposed CDS-based method. This also explains the superior performance of the proposed method in terms of higher control flexibility and coordinated system performance.

The remainder of the chapter is organized as follows. In Section 5.2, The effect of current allocation on charge balance in BPM systems is analyzed. Following the analysis, the CDS-based current allocation is proposed in Section 5.3. Then, the BPM system behavior under CDS-based current allocation with constant parameters is discussed in Section 5.4. Furthermore, in Section 5.5, an algorithm for system performance control is developed by considering the total power requirement, power loss constraint, and module charge balance. Next, simulation results are presented in Section 5.6 to illustrate the efficacy of the proposed current allocation. Finally, conclusions and future work are summarized in Section 5.7. All proofs are provided in Section 7.3.

5.2 Effect of current allocation on the charge balance in BPM systems

In this section, we will first introduce the modeling assumptions and notations for the BPM system under consideration. Then, based on these models, we will discuss the effect of current allocation on module charge balance and how to implement it in BPM circuits.

5.2.1 Modeling assumptions

Consider the BPMs connected in series (Figure 5.1.1a) or in parallel (Figure 5.1.1b). For each connection structure, the total number of BPMs in the system is denoted by M. Each BPM is composed of a battery module and a DC/DC converter. Each battery module may have one or more battery cells.

For the m-th BPM, assume that all the resistance parts of the battery module and DC/DC converter, such as the internal resistances of battery cells, the winding resistances of inductors, the conduction resistances of free-wheeling diodes and power MOSFETs, are lumped into an equivalent module resistance, denoted by R_m. This assumption is introduced in [98], where its feasibility was tested and analyzed based on circuit experiments. Note that, in practice, some resistance components of R_m may vary if operational conditions change, e.g., temperature, module SOC, or current. In this case, to obtain more accurate estimation of R_m, detailed circuit models of battery modules [103, 104] and converters can be used. Such extensions will be considered in future work.

In addition, we assume that all module voltages only change at discrete time instants in the model. The time interval between each pair of such time instants is referred to as a *control period* and denoted by τ_c. Thus, in the mathematical model, the module voltages are updated at the beginning of every control period and are assumed to be constants during this control period. Despite the fact that the voltage changes continuously in actual battery systems, this assumption does not lead to much discrepancy if τ_c is selected to be sufficiently small. For instance, in the numerical simulation discussed in Section 5.6, we select $\tau_c = 0.1$ s, which ensures that the maximum module voltage change during one control period is less than 10^{-4} V,

significantly smaller than a battery module's full voltage range of 4.8 V (from 12 V to 16.8 V).

Moreover, assume all battery modules are chosen to have identical rated charge capacity, denoted by Q_B. The battery module SOC is defined by the ratio of a battery module's present amount of charge to its rated charge capacity. Then, with identical rated charge capacity, the module SOC can directly characterize each module's amount of charge. Thus, in the following sections, we will study the battery module charge balance based on the module SOC.

5.2.2 Effect of current allocation on module charge balance

In this subsection, we consider the BPM systems shown in Figure 5.1.1 and defined by the above modeling assumptions. To facilitate the subsequent analyses, we first introduce necessary notations and then discuss the effect of current allocation on charge balance in BPM systems.

As shown in Figure 5.1.1, let $V_{Bm}(n)$ and $I_{Bm}(n)$ denote the average voltage and current of the battery module in the m-th BPM during the n-th control period, respectively. Here, the n-th control period refers to the time interval $t \in [(n-1)\tau_c, n\tau_c)$, $n = 1, 2, \ldots$. On the other side of the BPM, i.e., the charger or load side, let $V_{Om}(n)$, $I_{Om}(n)$, and $P_{Om}(n)$ denote the average voltage, current, and power of the m-th BPM during the n-th control period, respectively. Finally, let $V_O(n)$, $I_O(n)$, and $P_O(n)$ denote the average voltage, current, and power of the charger or load during the n-th control period, respectively.

Let $q_m(n)$ denote the amount of charge of the m-th BPM at the beginning of the

n-th control period. Then, we have

$$q_m(n+1) = q_m(n) \pm I_{Bm}(n)\tau_c,\ m \in \{1, 2, \ldots, M \tag{5.2.1}$$

where the "±" sign indicates the charging (+) or discharging (–) process. As a result, the charge difference between any two battery modules is

$$q_i(n+1) - q_j(n+1) = (q_i(n) - q_j(n)) \pm (I_{Bi}(n) - I_{Bj}(n))\,\tau_c, \tag{5.2.2}$$
$$i, j \in \{1, 2, \ldots, M\}.$$

From (5.2.2), we can see that, given the control period duration τ_c and initial module charge $q_i(n)$ and $q_j(n)$, the module charge difference at the end of a control period $q_i(n+1) - q_j(n+1)$ only depends on these two modules' average charging or discharging currents $I_{Bi}(n)$ and $I_{Bj}(n)$. Thus, if appropriate values of module currents can be allocated, the charge difference between any two modules can be gradually reduced. Then, to achieve charge balance or equalization of all battery modules in a BPM system, a system-wide module current allocation can be an effective solution.

5.2.3 Realization of current allocation in BPM systems

In each BPM, the voltage ratio from both sides of the converter is a function of the converter's duty ratio, i.e.,

$$\frac{V_{Om}(n)}{V_{Bm}(n) \pm I_{Bm}(n)R_m} = g(d_m(n)), \tag{5.2.3}$$

where, again, the "±" sign indicates the charging (+) or discharging (–) process, and $d_m(n)$ denotes the duty ratio of the m-th BPM's converter during the n-th control period. Function $g(\cdot)$ depends on the type of converter applied. For instance, $g(d_m(n)) = \frac{1}{1-d_m(n)}$ for a booster converter in the continuous conduction mode [98].

Then, according to power conservation and (5.2.3),

$$\frac{I_{Om}(n)}{I_{Bm}(n)} = \frac{1}{g(d_m(n))}. \tag{5.2.4}$$

If all BPMs are connected in series, we have

$$I_{Om}(n) = I_O(n) = \frac{P_O(n)}{V_O(n)},\ m \in \{1, 2, \ldots, M\}. \tag{5.2.5}$$

Combining (5.2.4) and (5.2.5) leads to

$$I_{Bm}(n) = g(d_m(n))\frac{P_O(n)}{V_O(n)}. \tag{5.2.6}$$

If all BPMs are connected in parallel,

$$V_{Om}(n) = V_O(n),\ m \in \{1, 2, \ldots, M\}. \tag{5.2.7}$$

Then, according to (5.2.3) and (5.2.7),

$$I_{Bm}(n) = \frac{\frac{V_O(n)}{g(d_m(n))} - V_{Bm}(n)}{\pm R_m}. \tag{5.2.8}$$

It follows from (5.2.6) and (5.2.8) that, since $V_O(n)$, $P_O(n)$, $V_{Bm}(n)$ and R_m are all constant during a given control period, the desired module current $I_{Bm}(n)$ can be

achieved by selecting appropriate duty ratio $d_m(n)$ of the converter.

Such converter duty ratio tuning-based module current allocation method has been applied in recent studies [49, 97, 98, 99, 100]. For example, as shown in the circuit experiments performed in [98, 99], the resultant module currents from tuning converter duty ratios can well match their expected design values.

From the analysis in this section, we have shown that the charge balance in BPM systems is directly affected by the currents allocated to battery modules, and that such current allocation can be realized by, for instance, tuning the converter duty ratios. In the following sections, we will focus on studying how to determine the exact currents to be allocated to each battery module in order to achieve the desired system performance.

5.3 Current allocation in BPM systems based on charging and discharging spaces

5.3.1 Charging and discharging spaces

The state of a battery module is usually characterized by its SOC. As mentioned in Section 5.1, in order to achieve charge balance among battery modules during the charging (discharging) process, the basic idea of all current allocation methods is to let the module with higher SOC be charged (discharged) with smaller (larger) current. To formulate the proposed current allocation method, first define parameters $C(n)$ and $F(n)$, referred to as the *ceiling level* and *floor level* of all battery module SOCs during the n-th control period. Note that, to facilitate the control, the values of $C(n)$ and $F(n)$ are not restricted by the module SOC's physical upper bound

(denoted by x_{ub}) and lower bound (denoted by x_{lb}), which are typically specified by battery manufacturers for safe operation. In other words, we allow $C(n) > x_{ub}$ and $F(n) < x_{lb}$.

Let $x_m(n)$ denote the m-th battery module's SOC at the beginning of the n-th control period. Then, the m-th battery module's *charging space* is defined by $C(n) - x_m(n)$, and its *discharging space* is defined by $x_m(n) - F(n)$. These are illustrated in Figure 5.3.1. Since control parameters $C(n)$ or $F(n)$ are shared by all battery modules, the charging or discharging spaces of all modules can be flexibly adjusted through $C(n)$ or $F(n)$, thus allowing different allocation options for the same distribution of module SOCs.

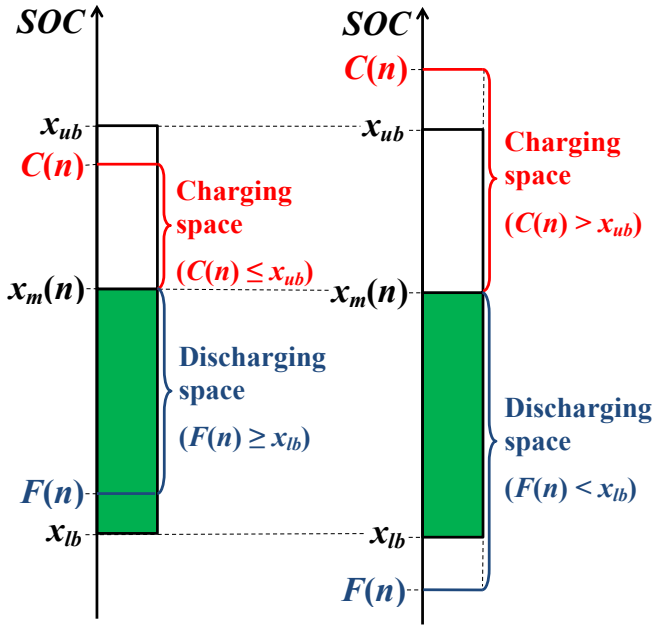

FIGURE 5.3.1: Illustration of charging and discharging spaces.

5.3.2 CDS-based current allocation model

According to the definitions of charging and discharging spaces, battery modules with higher SOCs will have smaller charging spaces and larger discharging spaces, which can be used as the basis for current allocation to each module. In order to achieve module charge balance, we let the module with larger charging (discharging) space be charged (discharged) with larger current. As a result, during the n-th control period of the charging (discharging) process, the module with the largest charging (discharging) space will have the largest module current, denoted by $I_B^{max}(n)$, i.e., $I_B^{max}(n) = \max_{m\in\{1,\ldots,M\}} I_{Bm}(n)$. Then, based on the charging and discharging spaces, we propose the following CDS-based current allocation method.

- For the charging process,

$$I_{Bm}(n) = \begin{cases} 0, & \text{if } x_m(n) = x_{ub}, \\ \alpha_m(n) I_B^{max}(n), & \text{if } x_m(n) < x_{ub}, \end{cases} \tag{5.3.1}$$

where

$$\alpha_m(n) = \frac{C(n) - x_m(n)}{C(n) - x_l(n)}, \tag{5.3.2}$$

$$C(n) \geq x_h(n), \tag{5.3.3}$$

$$x_h(n) = \max_{k\in\{1,\ldots,M\},\ x_k(n)<x_{ub}} x_k(n),$$

$$x_l(n) = \min_{k\in\{1,\ldots,M\},\ x_k(n)<x_{ub}} x_k(n).$$

- For the discharging process,

$$I_{Bm}(n) = \begin{cases} 0, & \text{if } x_m(n) = x_{lb}, \\ \alpha_m(n) I_B^{max}(n), & \text{if } x_m(n) > x_{lb}, \end{cases} \tag{5.3.4}$$

where

$$\alpha_m(n) = \frac{x_m(n) - F(n)}{x_h(n) - F(n)}, \tag{5.3.5}$$

$$F(n) \leq x_l(n), \tag{5.3.6}$$

$$x_h(n) = \max_{k \in \{1,\ldots,M\},\ x_k(n) > x_{lb}} x_k(n),$$

$$x_l(n) = \min_{k \in \{1,\ldots,M\},\ x_k(n) > x_{lb}} x_k(n).$$

As mentioned above, x_{ub} and x_{lb} are the module SOC's physical upper bound and lower bound, respectively. If any module's SOC reaches the upper bound x_{ub} (lower bound x_{lb}), the module is referred to as a *fully charged* (*fully discharged*) module. Clearly, during the charging (discharging) process, all fully charged (discharged) battery modules have to be disconnected from the system and their current should be set to zero. For all remaining battery modules, let $x_h(n)$ and $x_l(n)$ denote the highest SOC and lowest SOC among them, respectively. The currents allocated to these modules are based on $\alpha_m(n)$, which is the ratio of the m-th module's charging (discharging) space to the largest charging (discharging) space of all modules. Thus, $\alpha_m(n) \leq 1$. Moreover, in order to avoid circulating current among battery modules, we require $C(n) \geq x_h(n)$ during the charing process and $F(n) \leq x_l(n)$ during the discharging process, which results in $\alpha_m(n) \geq 0$. Thus, $0 \leq \alpha_m(n) \leq 1$. Particularly, if $C(n) = +\infty$ ($F(n) = -\infty$) or $x_h(n) = x_l(n)$, then $\alpha_m(n) = 1$, i.e., all non-fully-

charged (discharged) modules are charged (discharged) with identical current.

Therefore, based on the current allocation framework above, one can adjust the control parameters $C(n)$ and $I_B^{max}(n)$ during the charging process, or $F(n)$ and $I_B^{max}(n)$ during the discharging process, to flexibly control the system's behavior and performance.

5.3.3 Charge equalization under CDS-based current allocation

In order to evaluate the CDS-based current allocation's capability to reduce module charge imbalance, we study the evolution of module SOC range over time. Specifically, let $R_{SOC}(n)$ denote the SOC range of all battery modules that are not fully charged (discharged) at the beginning of the n-th control period of the charging (discharging) process, i.e.,

$$R_{SOC}(n) = x_h(n) - x_l(n). \tag{5.3.7}$$

Then, at the beginning of the $(n+1)$-th control period, the m-th battery module's SOC is updated by

$$x_m(n+1) = \begin{cases} x_m(n) + \frac{I_{Bm}(n)\tau_c}{Q_B}, & \text{for charging,} \\ x_m(n) - \frac{I_{Bm}(n)\tau_c}{Q_B}, & \text{for discharging,} \end{cases} \tag{5.3.8}$$

where, as defined in Section 5.2, Q_B is the rated module charge capacity, and τ_c is the duration of a control period. Based on (5.3.1), (5.3.2), (5.3.4), (5.3.5), (5.3.7), and (5.3.8), if module charge imbalance exists, i.e., $x_l(n) < x_h(n)$, the module SOC

range is updated by

$$R_{SOC}(n+1) = \begin{cases} \left(1 - \frac{I_B^{max}(n)\tau_c}{(C(n)-x_l(n))Q_B}\right) R_{SOC}(n), & \text{for charging,} \\ \left(1 - \frac{I_B^{max}(n)\tau_c}{(x_h(n)-F(n))Q_B}\right) R_{SOC}(n), & \text{for discharging.} \end{cases} \tag{5.3.9}$$

It follows immediately that $R_{SOC}(n+1) < R_{SOC}(n)$ if $x_l(n) < x_h(n)$. In other words, under CDS-based current allocation, the module SOC range always decreases over time as long as module charge imbalance exists.

5.3.4 Comparison with SOC-proportional current allocation

Consider the discharging case of the CDS-based current allocation with $F(n) = 0$. Then, each battery module's discharging space is exactly equal to its SOC, and the current allocation based on (5.3.4) and (5.3.5) becomes

$$I_{Bm}(n) = \frac{x_m(n)}{x_h(n)} I_B^{max}(n). \tag{5.3.10}$$

In this case, the total discharging current is given by

$$I_B^{total}(n) = \sum_{k=1}^{M} \frac{x_k(n)}{x_h(n)} I_B^{max}(n). \tag{5.3.11}$$

Combining (5.3.10) and (5.3.11), we have

$$I_{Bm}(n) = \frac{x_m(n)}{\sum_{k=1}^{M} x_k(n)} I_B^{total}(n). \tag{5.3.12}$$

Clearly, (5.3.12) indicates that each module current is allocated exactly in proportion to its SOC. In other words, the *SOC-proportional current allocation* discussed in [99, 101, 102] is actually a special case of the proposed *CDS-based current allocation with* $F(n) = 0$. However, it should be noted that, due to the elimination of parameter $F(n)$, there is only one control parameter $I_B^{max}(n)$ in the SOC-proportional current allocation. As a result, once a constraint is given, e.g., the total discharging power requirement, the only one control parameter $I_B^{max}(n)$ as well as the overall system performance will be uniquely determined. On the other hand, given one constraint, the proposed CDS-based current allocation still has one additional degree-of-freedom for control, which makes it possible to coordinate two system performance measures (see more details in Section 5.5).

5.4 CDS-based current allocation with constant parameters

In order to implement CDS-based current allocation, one needs to determine the values of two control parameters: $C(n)$ and $I_B^{max}(n)$ for the charging process, and $F(n)$ and $I_B^{max}(n)$ for the discharging process. In practice, these parameter values can be determined based on constraints and/or control objectives on system performance measures. In this section, we will first analyze the system behavior under CDS-based current allocation with constant control parameters, and study how to control module charge balance by assigning constant control parameters. In the next section, given the total charging or discharging power requirement, we will discuss how to select appropriate control parameters for each control period to obtain the desired system performance.

Proposition 5.4.1. *Consider the BPM system with initial module SOCs,* $x_m(1)$, $m = 1, \ldots, M$. *Assume constant control parameters are applied under CDS-based current allocation as long as* $x_l(n) < x_h(n)$, *i.e.,*

$$C(n) = C \geq x_h(1),\ F(n) = F \leq x_l(1),\ I_B^{max}(n) = I_B^{max}. \tag{5.4.1}$$

- *During charging, if* $x_m(n) < x_{ub}$ *and* $x_l(n) < x_h(n)$,

$$I_{Bm}(n) = I_{Bm}(1) = \frac{C - x_m(1)}{C - x_l(1)} I_B^{max}. \tag{5.4.2}$$

  In addition, if $C \leq x_{ub}$, *the SOCs of all modules with* $x_m(1) < x_{ub}$ *will reach* C *at the same time* $t = T_e$, *where*

$$T_e = \frac{(C - x_l(1))Q_B}{I_B^{max}}. \tag{5.4.3}$$

- *During discharging, if* $x_m(n) > x_{lb}$ *and* $x_l(n) < x_h(n)$,

$$I_{Bm}(n) = I_{Bm}(1) = \frac{x_m(1) - F}{x_h(1) - F} I_B^{max}. \tag{5.4.4}$$

  In addition, if $F \geq x_{lb}$, *the SOCs of all modules with* $x_m(1) > x_{lb}$ *will reach* F *at the same time* $t = T_e$, *where*

$$T_e = \frac{(x_h(1) - F)Q_B}{I_B^{max}}. \tag{5.4.5}$$

Proof: See Subsection 7.3.1.

In Proposition 5.4.1, T_e is referred to as the *equalization time* and C (F) is also

referred to as the *equalization SOC level* for the charging (discharging) process. From Proposition 5.4.1, we can see that, given constant parameters in the CDS-based current allocation, all modules that are not fully charged (discharged) always have *constant currents* during the charging (discharging) process until their SOCs get equalized at C (F) or reach the SOC upper (lower) bound. This implies that each module's SOC increases (decreases) linearly over time during the charging (discharging) process, i.e.,

$$x_m(n) = \begin{cases} x_m(1) + (n-1)\frac{(C - x_m(1))I_B^{max}\tau_c}{(C - x_l(1))Q_B}, & \text{for charging,} \\ x_m(1) - (n-1)\frac{(x_m(1) - F)I_B^{max}\tau_c}{(x_h(1) - F)Q_B}, & \text{for discharging.} \end{cases} \tag{5.4.6}$$

To illustrate this property, we take the charging process as an example and plot the module SOC evolutions in Figure 5.4.1 for a 3-module BPM system with $x_{ub} = 0.9$ and initial module SOCs at 0.3, 0.5, and 0.6. As we can see from Figure 5.4.1a, when C is selected at 0.8, which is smaller than x_{ub}, all module SOCs increase linearly and reach the equalization SOC level C at the equalization time $T_e = 4320$ s. Then, for $t > T_e$, it follows from (5.3.1) and (5.3.2) that, the current allocation does not depend on the value of parameter C and all modules are charged with identical current I_B^{max} until they are fully charged at x_{ub}. On the other hand, when $C > x_{ub}$, e.g., $C = 1$, as shown in Figure 5.4.1b, all module SOCs also increase linearly towards C but finally can only reach x_{ub} at different time instants.

Note that, Proposition 5.4.1 not only provides analytical formulas to calculate instantaneous module currents and module SOCs, but can also be used to calculate the constant parameter values of C, F, and I_B^{max}, which can lead to the desired charge equalization time and equalization SOC level. For example, consider a BPM system

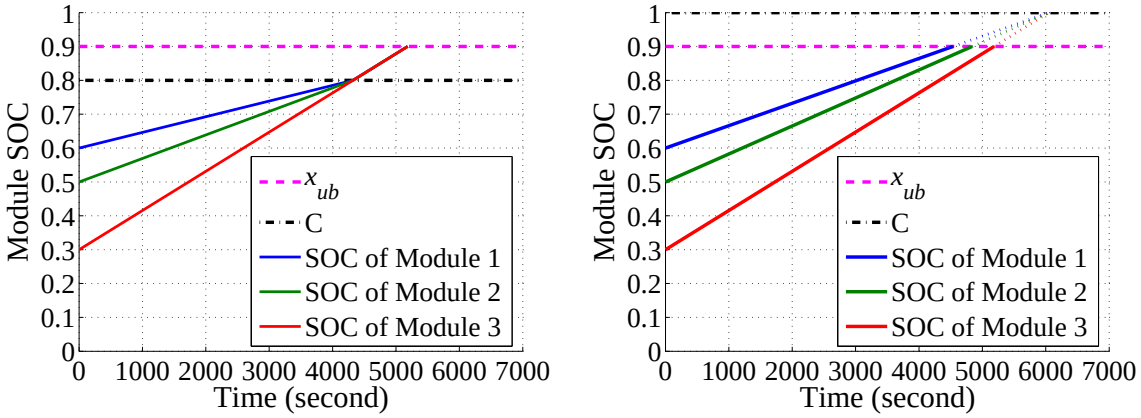

FIGURE 5.4.1: Simulation of module SOC evolution during the charging process under CDS-based current allocation with constant parameters. (a) $C \leq x_{ub}$. (b) $C > x_{ub}$.

with lowest initial module SOC $x_l(1) = 0.3$ and module charge capacity $Q_B = 10$ Ah. Assume that it is desired to charge all battery modules to SOC $= 0.9$ in 2 hours. Then, using the CDS-based current allocation, we need to set the equalization SOC level $C = 0.9$, and equalization time $T_e = 2$ h. Next, based on (5.4.3), we can determine the other parameter, $I_B^{max} = (0.9 - 0.3) \times 10$ Ah$/(2$ h$) = 3$ A.

5.5 Current allocation algorithm for system performance control

In many cases, e.g., in energy storage devices of solar panels or battery systems of electric vehicles, a battery system is required to endure (or provide) the desired real-time charging (or discharging) power. Apparently, such real-time power requirement may not always be satisfied through CDS-based current allocation with *constant parameters*. Thus, in this section, we will consider the real-time total power requirement

in the CDS-based current allocation, and discuss how to choose appropriate control parameters for each control period to meet the desired system performance including power efficiency and module charge balance.

5.5.1 Calculation of total power and total power loss

To simplify the analysis, assume that all BPMs have identical equivalent module resistance, denoted by R, i.e., $R_m = R$, $m = 1, \ldots, M$ [98]. During the n-th control period, denote the total power at the battery side by $P_B(n)$, and the total power loss caused by the equivalent module resistance by $P_L(n)$. In addition, define the following vectors:

$$\begin{aligned}
\mathbf{V}(n) &= [V_{B1}(n), V_{B2}(n), \ldots, V_{BM}(n)]\,, \\
\mathbf{X}(n) &= [x_1(n), x_2(n), \ldots, x_M(n)]\,, \\
\mathbf{J} &= [1, 1, \ldots, 1]_{1\times M}\,, \\
\boldsymbol{\alpha}(n) &= \begin{cases} \frac{C(n)\mathbf{J}-\mathbf{X}}{C(n)-x_l(n)}, & \text{for charging,} \\ \frac{\mathbf{X}-F(n)\mathbf{J}}{x_h(n)-F(n)}, & \text{for discharging.} \end{cases}
\end{aligned} \tag{5.5.1}$$

Since the following analysis will be focused on one control period, for simplicity, we will use $\mathbf{V}$, $\mathbf{X}$, and $\boldsymbol{\alpha}$ to represent $\mathbf{V}(n)$, $\mathbf{X}(n)$, and $\boldsymbol{\alpha}(n)$, respectively, in subsequent analysis.

According to the CDS-based current allocation formulated in (5.3.1)-(5.3.6), we

have

$$P_B(n) \triangleq P_B\left(C(n) \text{ or } F(n), I_B^{max}(n)\right) = \sum_{m=1}^{M} \left(V_{Bm}(n) I_{Bm}(n)\right) = \mathbf{V}\boldsymbol{\alpha}^T I_B^{max}(n), \tag{5.5.2}$$

$$P_L(n) \triangleq P_L\left(C(n) \text{ or } F(n), I_B^{max}(n)\right) = \sum_{m=1}^{M} \left(I_{Bm}(n)\right)^2 R = \boldsymbol{\alpha}\boldsymbol{\alpha}^T \left(I_B^{max}(n)\right)^2 R. \tag{5.5.3}$$

Thus, the total charging or discharging power is

$$P_O(n) \triangleq P_O\left(C(n) \text{ or } F(n), I_B^{max}(n)\right) = \begin{cases} P_B(n) + P_L(n), & \text{for charging,} \\ P_B(n) - P_L(n), & \text{for discharging.} \end{cases} \tag{5.5.4}$$

Again, as we can see from (5.5.1)-(5.5.4), $P_B(n)$, $P_L(n)$, and $P_O(n)$ are all functions of the two control parameters: $C(n)$ and $I_B^{max}(n)$ for the charging process, and $F(n)$ and $I_B^{max}(n)$ for the discharging process. In other words, given the values of the two control parameters, $P_B(n)$, $P_L(n)$, and $P_O(n)$ can be uniquely determined. In fact, it can be shown that, given the values of any two variables from $P_B(n)$, $P_L(n)$, $P_O(n)$, $C(n)$ or $F(n)$, and $I_B^{max}(n)$, all other three variables can be calculated. Thus, we can view each variable as a function of any two of the remaining variables (see (5.5.2)-(5.5.4)). For instance, $P_O\left(F(n) = x, P_L(n) = y\right)$ represents the total discharging power given $F(n) = x$ and total power loss $P_L(n) = y$. As a result, given the desired $P_O(n)$ and $P_L(n)$ in the CDS-based current allocation, the two control parameters can be reversely calculated. Note that, it is possible that the required total charging (discharging) power $P_O(n)$ may be too large to be accepted (provided) by

the BPM system. Thus, it is of critical importance for safe operations to know the feasible range of the total charging or discharging power $P_O(n)$ of the BPM system under current system states and constraints. This is carried out next.

5.5.2 Feasible range of total charging or discharging power

In BPM systems, the total charging or discharging power $P_O(n)$ is typically constrained by several factors. For instance, the circuit hardware often requires that the module current does not exceed a certain level, i.e.,

$$I_B^{max}(n) \leq I_B^{ub}. \tag{5.5.5}$$

In addition, to maintain desired working temperature in a packed multi-cell/module battery system, it is also necessary to limit the heat generated during system operation. In this chapter, this requirement is formulated as a constraint on the total power loss, i.e.,

$$P_L(n) \leq P_L^{ub}. \tag{5.5.6}$$

Without loss of generality, assume that

$$P_L^{ub} \leq M(I_B^{ub})^2 R \quad \text{or} \quad I_B^{ub} \geq \sqrt{\frac{P_L^{ub}}{MR}}. \tag{5.5.7}$$

Then, evaluating the feasible range of system power amounts to the maximization of total charging or discharging power $P_O(n)$, i.e.,

$$\max\ P_O(n),\ s.t.\ (5.3.3) \text{ or } (5.3.6), (5.5.1)\text{-}(5.5.4), (5.5.5), \text{ and } (5.5.6). \tag{5.5.8}$$

The solutions to problem (5.5.8) for charging and discharging processes are given in Proposition 5.5.1 and Proposition 5.5.2, respectively.

Proposition 5.5.1. *For the n-th control period of the charging process, given (5.5.7), the maximum total charging power based on (5.5.8) can be achieved at* $C(n) = +\infty$, *and* $I_B^{max}(n) = \sqrt{\frac{P_L^{ub}}{MR}}$.

Proof: See Subsection 7.3.2.

Proposition 5.5.1 indicates that to achieve the maximal system power during the charging process, all modules should be charged with identical current (since $C(n) = +\infty$), regardless of their individual SOCs. Then, the current should be selected as large as possible under the required constraints.

The discharging case is more complicated. To facilitate the discussion, introduce

$$\lambda(n) = \lambda\left(C(n) \text{ or } F(n)\right) = \frac{P_B^2(n)}{P_L(n)} = \frac{\left(\mathbf{V}\boldsymbol{\alpha}^T\right)^2}{\boldsymbol{\alpha}\boldsymbol{\alpha}^T R}. \tag{5.5.9}$$

Clearly, $\lambda(n)$ is only dependent on $C(n)$ or $F(n)$, but independent of the other control parameter $I_B^{max}(n)$. It is shown in Subsection 7.3.2 that $\lambda(F(n))$ is maximized at $F(n) = F^*(n)$,

$$F^*(n) = \frac{\mathbf{V}\mathbf{X}^T\mathbf{J}\mathbf{X}^T - \mathbf{V}\mathbf{J}^T\mathbf{X}\mathbf{X}^T}{M\mathbf{V}\mathbf{X}^T - \mathbf{V}\mathbf{J}^T\mathbf{X}\mathbf{J}^T}. \tag{5.5.10}$$

Consider now the three constraints (5.3.6), (5.5.5), and (5.5.6) in problem (5.5.8). If there exists an $F(n) \leq x_l(n)$, at which both constraint limits, I_B^{ub} and P_L^{ub}, can be hit, this $F(n)$ is denoted by $F^{int}(n)$. Otherwise, if only P_L^{ub} can be reached for

$F(n) \leq x_l(n)$, let $F^{int}(n) = x_l(n)$. Thus,

$$F^{int}(n) = \begin{cases} \frac{-rx_h(n)+\mathbf{X}\mathbf{J}^T-\sqrt{(rx_h(n)-\mathbf{X}\mathbf{J}^T)^2-(M-r)\left(\mathbf{X}\mathbf{X}^T-rx_h^2(n)\right)}}{M-r}, \\ \qquad \text{if } P_L(F(n)=x_l(n), I_B^{max}(n)=I_B^{ub}) \leq P_L^{ub}, \\ x_l(n), \text{ if } P_L(F(n)=x_l(n), I_B^{max}(n)=I_B^{ub}) > P_L^{ub}, \end{cases} \tag{5.5.11}$$

where $r = \dfrac{P_L^{ub}}{\left(I_B^{ub}\right)^2 R}$.

Next, introduce two conditions as below:

$$P_L^{ub} \leq \min\left\{\frac{\lambda(F(n)=x_l(n))}{4}, \frac{\lambda(F(n)=-\infty)}{4}\right\}, \tag{5.5.12}$$

$$I_B^{ub} < \frac{\mathbf{V}(x_h(n)\mathbf{J}-\mathbf{X})^T}{2R\mathbf{J}(x_h(n)\mathbf{J}-\mathbf{X})^T}. \tag{5.5.13}$$

The first condition (5.5.12) guarantees that the total power loss does not exceed the total discharging power, i.e., $P_L(n) \leq P_O(n)$. The second condition (5.5.13) ensures that, given $I_B^{max}(n) = I_B^{ub}$, the total discharging power $P_O(F(n), I_B^{max}(n) = I_B^{ub})$ decreases as $F(n)$ increases. Under these two conditions, the maximum total discharging power can be obtained by Proposition 5.5.2.

Proposition 5.5.2. *For the n-th control period of the discharging process, given (5.5.7), (5.5.12), and (5.5.13), the maximum total discharging power based on (5.5.8) is achieved at*

$$F(n) = \min\{F^*(n), F^{int}(n)\},$$

$$I_B^{max}(n) = \begin{cases} \sqrt{\frac{P_L^{ub}}{\boldsymbol{\alpha}\boldsymbol{\alpha}^T R}}, & \text{if } F^*(n) < F^{int}(n), \\ I_B^{ub}, & \text{if } F^*(n) \geq F^{int}(n). \end{cases}$$

Proof: See Subsection 7.3.2.

Although the optimal solution for the discharging process is not so straightforward as that for the charging process, from the optimal solution of $I_B^{max}(n)$ in Proposition 5.5.2, we can see that the maximum total discharging power is achieved at some constraint limit, either I_B^{ub} or P_L^{ub}. Accordingly, the optimal solution of $F(n)$ is $F^{int}(n)$ or $F^*(n)$.

Denote the maximum total charging or discharging power of the BPM system by $P_O^{max}(n)$. Then, $P_O^{max}(n)$ can be calculated by Propositions 5.5.1 and 5.5.2, and (5.5.1)-(5.5.4). Denote the required total charging or discharging power of the system by $P_O^{req}(n)$. Clearly, if $P_O^{req}(n) \geq P_O^{max}(n)$, the BPM system can at most accept (provide) $P_O^{max}(n)$ during the charging (discharging) process. Thus, in the following discussion, we will focus on the case with $P_O^{req}(n) < P_O^{max}(n)$ and study the system performance control under CDS-based current allocation.

5.5.3 System performance analysis

In many practical applications, accepting/providing the required power is typically a top priority for battery system operations. If only one condition, the total power requirement, is given in the CDS-based current allocation, i.e.,

$$P_O(n) = P_O^{req}(n) < P_O^{max}(n), \tag{5.5.14}$$

then multiple combinations of the two control parameters may be used to meet the same total power requirement $P_O^{req}(n)$. However, these different parameter combinations may result in different values of other system performance measures such as

power efficiency and module charge balance. Thus, given the total power requirement (5.5.14), one can still further improve other system performance measures by selecting appropriate control parameter combination.

Specifically, we first consider the system's total power loss, $P_L(n)$, which can be viewed as a measure of the system's power efficiency. Given $P_O^{req}(n) < P_O^{max}(n)$, it is possible to obtain the range of total power loss $[P_L^{min}(n), P_L^{max}(n)]$. This is accomplished by formulating two optimization problems as below and finding the optimal solutions as described in Propositions 5.5.3 and 5.5.4.

$$\min \ P_L(n) \quad s.t. \text{ (5.3.3) or (5.3.6), (5.5.1)-(5.5.6), and (5.5.14),} \tag{5.5.15}$$

$$\max \ P_L(n) \quad s.t. \text{ (5.3.3) or (5.3.6), (5.5.1)-(5.5.6), and (5.5.14).} \tag{5.5.16}$$

Proposition 5.5.3. *For the charging process, given (5.5.14) during the n-th control period, the solutions to problems (5.5.15) and (5.5.16) are*

$$P_L^{min}(n) = \left(\frac{2P_O^{req}(n)\sqrt{MR}}{\mathbf{V}\mathbf{J}^T + \sqrt{\mathbf{V}\mathbf{J}^T\mathbf{V}\mathbf{J}^T + 4P_O^{req}(n)MR}} \right)^2,$$

$$P_L^{max}(n) = \min\left\{ P_L^{ub}, P_L^{left}(n) \right\},$$

where

$$P_L^{left}(n) = \begin{cases} P_L(I_B^{max}(n) = I_B^{ub}, P_O(n) = P_O^{req}(n)), \\ \qquad\qquad \text{if } P_L(C(n) = x_h(n), P_O(n) = P_O^{req}(n)) > \\ \qquad\qquad P_L(C(n) = x_h(n), I_B^{max}(n) = I_B^{ub}), \\ P_L(C(n) = x_h(n), P_O(n) = P_O^{req}(n)), \ \text{otherwise,} \end{cases}$$

$P_L(C(n), I_B^{max}(n))$ is given in (5.5.3), and $P_L(C(n), P_O(n))$, $P_L\left(I_B^{max}(n), P_O(n)\right)$ are

calculated based on the formulas given in Subsection 7.3.3.

Proof: See Subsection 7.3.4.

Proposition 5.5.4. *For the discharging process, given (5.5.7), (5.5.12)-(5.5.14), and* $F^*(n) < x_l(n)$ *during the n-th control period, the solutions to problems (5.5.15) and (5.5.16) are*

$$P_L^{min}(n) = \begin{cases} P_L\left(F(n) = F^*(n), P_O(n) = P_O^{req}(n)\right), \\ \qquad\qquad \text{if } P_L\left(F(n) = F^*(n), P_O(n) = P_O^{req}(n)\right) \leq \\ \qquad\qquad P_L\left(F(n) = F^*(n), I_B^{max}(n) = I_B^{ub}\right), \\ P_L\left(I_B^{max}(n) = I_B^{ub}, P_O(n) = P_O^{req}(n)\right), \ \text{otherwise}, \end{cases}$$

$$P_L^{max}(n) = \min\left\{\max\left\{P_L(F(n) = -\infty, P_O(n) = P_O^{req}(n)), P_L^{right}(n)\right\}, P_L^{ub}\right\},$$

where

$$P_L^{right}(n) = \begin{cases} P_L(I_B^{max}(n) = I_B^{ub}, P_O(n) = P_O^{req}(n)), \\ \qquad\qquad \text{if } P_L(F(n) = x_l(n), P_O(n) = P_O^{req}(n)) > \\ \qquad\qquad P_L(F(n) = x_l(n), I_B^{max}(n) = I_B^{ub}), \\ P_L(F(n) = x_l(n), P_O(n) = P_O^{req}(n)), \text{otherwise}, \end{cases}$$

$P_L(F(n), I_B^{max}(n))$ *can be calculated based on (5.5.3), and* $P_L(F(n), P_O(n))$, $P_L\left(I_B^{max}(n), P_O(n)\right)$ *can be calculated based on the formulas in Subsection 7.3.3.*

Proof: See Subsection 7.3.4.

Therefore, given $P_O^{req}(n) < P_O^{max}(n)$, any total power loss $P_L(n) \in [P_L^{min}(n), P_L^{max}(n)]$ can be realized by assigning appropriate control parameters.

In addition to the total power loss $P_L(n)$, another important performance measure is the charge balance among battery modules, which is reflected by the module SOC

range $R_{SOC}(n)$ defined in (5.3.7). Clearly, smaller $R_{SOC}(n)$ indicates better module charge balance. From the system's perspective, can we reduce the module SOC range and total power loss simultaneously? Proposition 5.5.5 answers this question.

Proposition 5.5.5. *Given (5.5.14) for the n-th control period,*

- *for the charging process, as $C(n)$ increases from $x_h(n)$ to $+\infty$, $R_{SOC}(n+1)$ increases but $P_L(n)$ decreases.*
- *for the discharging process, as $F(n)$ decreases from $x_l(n)$ to $F^*(n)$, $R_{SOC}(n+1)$ increases but $P_L(n)$ decreases.*

Proof: See Subsection 7.3.5.

From Proposition 5.5.5, we can see that tuning control parameter values have opposite effects on module SOC range $R_{SOC}(n)$ and total power loss $P_L(n)$. Then, we are facing the trade-off between reducing $R_{SOC}(n)$ to achieve module charge balance and reducing $P_L(n)$ to improve power efficiency. If the module charge balance needs to be improved, instead of simply minimizing the total power loss, one has to choose a desired power loss between $P_L^{min}(n)$ and $P_L^{max}(n)$, which is denoted by $P_L^{des}(n)$. To realize the desired total power loss $P_L^{des}(n)$ under the total power requirement $P_O^{req}(n)$, we need to assign appropriate values to the control parameters in the CDS-based current allocation framework. This is accomplished by Proposition 5.5.6.

Proposition 5.5.6. *Given the total power $P_O(n) = P_O^{req}(n) < P_O^{max}(n)$ and total power loss $P_L(n) = P_L^{des}(n) \in [P_L^{min}(n), P_L^{max}(n)]$ under the CDS-based current allocation, the corresponding control parameters are calculated by*

$$C(n) = \frac{b(n) + \sqrt{b^2(n) - 4a(n)c(n)}}{-2a(n)}, \tag{5.5.17}$$

$$F(n) = \frac{b(n) - \sqrt{b^2(n) - 4a(n)c(n)}}{-2a(n)}, \tag{5.5.18}$$

$$I_B^{max}(n) = \begin{cases} \frac{P_O(n) - P_L(n)}{\mathbf{V}\boldsymbol{\alpha}^T}, & \textit{for charging}, \\ \frac{P_O(n) + P_L(n)}{\mathbf{V}\boldsymbol{\alpha}^T}, & \textit{for discharging}, \end{cases} \tag{5.5.19}$$

where

$$\begin{aligned} a(n) &= MR\lambda(n) - (\mathbf{V}\mathbf{J}^T)^2, \\ b(n) &= -2R\lambda(n)\mathbf{X}\mathbf{J}^T + 2\mathbf{V}\mathbf{X}^T\mathbf{V}\mathbf{J}^T, \\ c(n) &= R\lambda(n)\mathbf{X}\mathbf{X}^T - (\mathbf{V}\mathbf{X}^T)^2. \end{aligned}$$

Proof: See Subsection 7.3.6.

5.5.4 Algorithm for coordinated system performance control

In order to determine the desired total power loss $P_L^{des}(n)$ in Proposition 5.5.6 and to characterize its trade-off with the module SOC range, we introduce a normalizing parameter, referred to as the *loss reduction coefficient*, and denoted by $l_r(n)$, $l_r(n) \in [0, 1]$, such that

$$P_L(n) = P_L^{max}(n) - l_r(n)\left(P_L^{max}(n) - P_L^{min}(n)\right). \tag{5.5.20}$$

Here, $l_r(n)$ is a decision variable to be specified by the user. Particularly, if $l_r(n) = 1$, we pay all attention to the reduction of total power loss, i.e., $P_L(n)$ is minimized and $R_{SOC}(n)$ is maximized; if $l_r(n) = 0$, we only focus on the module charge balance, i.e., $R_{SOC}(n)$ is minimized and $P_L(n)$ is maximized. Thus, given $P_O^{req}(n) < P_O^{max}(n)$,

we can coordinate the total power loss $P_L(n)$ and module SOC range $R_{SOC}(n)$ by selecting appropriate $l_r(n)$.

Based on the above analysis, we formulate the algorithm for coordinated system performance control under CDS-based current allocation to meet the total power requirement $P_O^{req}(n)$ and to achieve the desired level of charge balance and power efficiency.

Algorithm 1:

Step 1: At the beginning of the n-th control period, update the voltage and SOC of each battery module, then calculate $P_O^{max}(n)$ based on Proposition 5.5.1 or 5.5.2.

Step 2: If $P_O^{req}(n) \geq P_O^{max}(n)$, let $P_O(n) = P_O^{max}(n)$, calculate the control parameters by Proposition 5.5.1 or 5.5.2, and then go to Step 5. Otherwise, let $P_O(n) = P_O^{req}(n)$, and go to Step 3.

Step 3: Calculate $P_L^{max}(n)$ and $P_L^{min}(n)$ by Proposition 5.5.3 or 5.5.4, then use (5.5.20) to determine the desired power loss level $P_L^{des}(n)$ by specifying $l_r(n)$.

Step 4: Based on the total power requirement $P_O(n) = P_O^{req}(n)$ determined in Step 2 and the desired total power loss $P_L(n) = P_L^{des}(n)$ determined in Step 3, calculate the control parameters by Proposition 5.5.6.

Step 5: Based on the calculated control parameters, determine each module's current by (5.3.1) and (5.3.2), or (5.3.4) and (5.3.5).

Note that, Algorithm 1 can be performed for battery systems with arbitrary initial SOCs, module numbers, and system parameters. Since the solutions of all subproblems in Algorithm 1 can be obtained by analytical formulas instead of numerical

search, it will be very computationally efficient to implement Algorithm 1 even for large-scale battery systems.

5.6 Illustration by simulation

To illustrate the efficacy of the results obtained in Section 5.5, a numerical simulation experiment is performed in this section. In this simulation, we use a battery system consisting of three parallel-connected BPMs with initial module SOCs (0.8, 0.6, 0.3). Each battery module is an Ultralife Lithium-ion battery UBBL10 [105] with rated charge capacity 14.4 Ah, which has display of its real-time SOC. The internal resistance of the battery is estimated in [106] to be about 0.145 Ω. Then, by incorporating the resistance components of converters, the equivalent resistance of each BPM is set to $R = 0.2\ \Omega$. During simulation, the battery module voltage is calculated at the beginning of each control period according to the OCV-SOC curve from the UBBL10 data sheet [105]. The system parameters used in this simulation are summarized in Table 5.6.1. In addition, the total discharging power profile for the battery system at hand is shown in Figure 5.6.1, which is adapted from [26] for four consecutive driving cycles of Highway Fuel Economy Test (HWFET).

TABLE 5.6.1: System parameters in the simulation.

Parameter	value
Number of modules M	3
Module charge capacity Q_B	14.4 Ah
Initial module SOCs	(0.8, 0.6, 0.3)
Module current upper bound I_B^{ub}	12 A
Equivalent module resistance R	0.2 Ω
Load voltage V_O	24 V
Control period τ_c	0.1 s

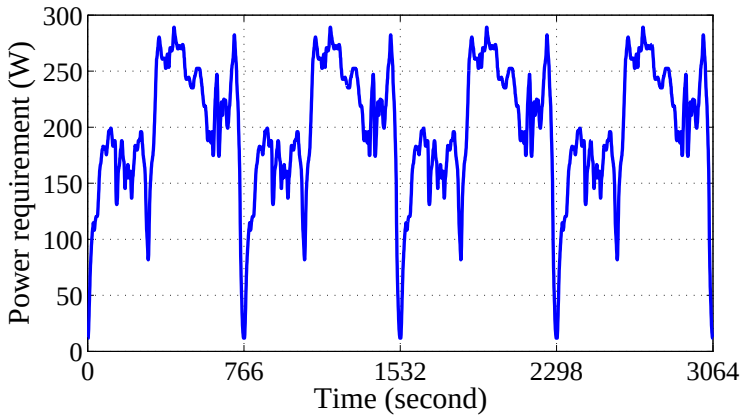

FIGURE 5.6.1: Total discharging power profile adapted from four consecutive HWFET driving cycles.

Given the data in Table 5.6.1 and Figure 5.6.1, two system performance measures of the BPM system under CDS-based current allocation and SOC-proportional current allocation are compared in Figure 5.6.2. Specifically, the two performance measures are module SOC range $R_{SOC}(n)$ defined in (5.3.7) and total power loss $P_L(n)$ defined in (5.5.3) and their evolutions are illustrated in Figure 5.6.2a and Figure 5.6.2b, respectively.

According to Subsection 5.5.4, if it is desired to reach module charge equalization as soon as possible, we need $l_r(n) = 0$ during each control period when performing the CDS-based current allocation. As shown in Figure 5.6.2a, this indeed results in the fastest way to reach zero module SOC range (i.e., all module SOCs get equalized). However, as shown in Figure 5.6.2b, $l_r(n) = 0$ also causes the largest power loss during each control period before all module SOCs get equalized.

On the other hand, if it is desired to reduce the total power loss to the least, we need $l_r(n) = 1$ during each control period when performing Algorithm 1. As shown in

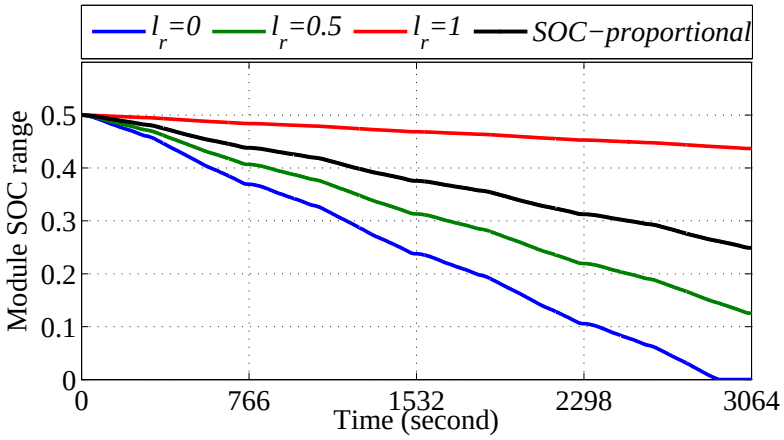

(A)

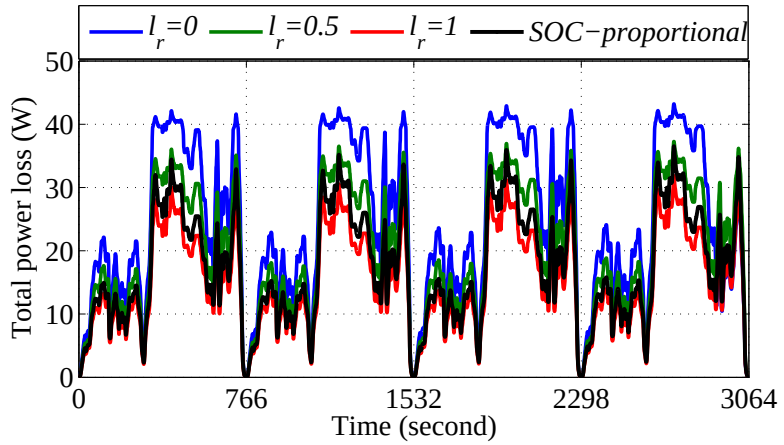

(B)

FIGURE 5.6.2: Comparison of system performance evolution with SOC-proportional and CDS-based current allocation methods. (a) Comparison of module SOC range evolution. (b) Comparison of total power loss evolution.

Figure 5.6.2b, by setting $l_r(n) = 1$, the total power loss during each control period is reduced to the minimum, while the module SOC range approaches zero at the slowest pace (see Figure 5.6.2a).

To get any desired system performance between the two cases above, we can pick

an intermediate loss reduction coefficient $l_r(n) \in (0, 1)$. For example, by simply setting $l_r(n) = 0.5$, the total power loss during each control period is exactly the average total power loss of the above two cases with $l_r(n) = 0$ and $l_r(n) = 1$ (see Figure 5.6.2b). Meanwhile, as shown in Figure 5.6.2a, the module SOC range also falls between the above two cases. Note that, it is desirable to vary the loss reduction coefficient over time to meet the real-time system performance requirement. The optimization of loss reduction coefficient over different control periods will be studied in future work.

Finally, as a special case of the CDS-based current allocation with $F(n) = 0$, the SOC-proportional current allocation can also alleviate module charge imbalance to some extent. As we can see from Figure 5.6.2, the module SOC range and total power loss of the SOC-proportional current allocation fall between those of the CDS-based current allocation cases with $l_r = 0.5$ and $l_r = 1$ (very close to the case with $l_r = 0.78$ in this simulation). However, as mentioned in Subsection 5.3.4, given the total power requirement, the system performance of the SOC-proportional current allocation cannot be changed any more. Therefore, given the total power requirement in both current allocation methods, the CDS-based current allocation outperforms the SOC-proportional current allocation for possessing the capability of flexible system performance control.

5.7 Summary

In this chapter, we propose the battery module current allocation method based on charging and discharging spaces for both series- and parallel-connected BPM systems.

Then by considering the total power requirement and total power loss constraint, we develop a control algorithm to achieve coordinated system performance between battery charge balance (i.e., reducing module SOC range) and power efficiency (i.e., reducing total power loss). Since the proposed system performance control algorithm is based on analytical solutions, it is very computationally efficient and can be applied to large-scale battery systems. In addition, it is shown that the SOC-proportional current allocation method, which was proposed and studied in recent literature, can be viewed as a special case of the proposed CDS-based current allocation with reduced control flexibility.

This chapter marks an initial step of analytical study of battery power module system control. In future research, we will test the applicability of these theoretical results on a complete hardware platform by incorporating some well-developed circuit designs of battery SOC estimation and BPM systems. In addition, we will also explore how to optimally adjust the loss reduction coefficient to meet time-varying system performance requirement.

Chapter 6

Conclusions and future work

In this thesis, the mathematical modeling, performance evaluation, and control of battery charge balance/equalization in series-based battery charge equalization (BCE) systems, module-based BCE systems, and battery power module (BPM) systems are studied.

For the series-based and module-based BCE systems, we first formulate the mathematical models to characterize the charge transfers between battery cells/modules for charge balance/equalization in one of the three operating modes: charging, discharging, or idle state. Based on the proposed mathematical model, we define two important concepts: merging point and merging battery group. Then, using their properties, we develop the algorithms to estimate the cell SOC evolution during the charge equalization process in idle/charging/discharging mode. Besides, analytical formulas are also derived to directly calculate some critical system performance measures such as the BCE time, charging time, and discharging time. A number of other system performance measures (e.g., total energy loss, range of SOCs) can be easily

evaluated based on these performance measures. The accuracy of these proposed estimation algorithms and calculation formulas has been validated by physical circuit experiments and extensive computer simulations.

To obtain statistically reliable performance evaluation results of the proposed designs or algorithms, a large number of system states or initial conditions need to be tested. To accomplish this in large-scale BCE systems, circuit experiments are not feasible since they usually cause high consumption in both energy and time. Besides, as the system scale becomes large, model-based computer simulations are facing the similar challenge since they could also consume a great amount of computation time and storage space. In this case, the proposed cell SOC estimation algorithms and performance evaluation formulas become good tools to achieve statistically reliable conclusions since the proposed methods demonstrate good estimation/evaluation accuracy and very high computational efficiency.

Moreover, the proposed analytical formulas for performance evaluation also incorporate the clues to improve the BCE system performance. A BCE system consists of two components: the series-connected battery cells/modules and the BCE structure applied to them. While the latter draws most research attentions, the former has been far less investigated. As observed in circuit experiments and computer simulations, a small change in the battery cell/module configuration may result in a dramatically different BCE time. Then, by analyzing the analytical formulas to calculate the BCE time, we develop the battery cell/module reconfiguration algorithms. Based on the test results of numerous initial conditions, we can claim that the battery cell/module configurations generated by these algorithms can lead to the shortest or near-shortest BCE time especially for large systems. Meanwhile, the emerging technique of reconfigurable battery systems also facilitates the implementation of these proposed

reconfiguration algorithms in real battery systems.

For the BPM systems, we base our study on the equivalent circuit models of both series- and parallel-connected BPM systems. At first, the charging and discharging spaces (CDSs) are defined. In order to reduce the charge imbalance among battery modules, the basic idea is to charge (discharge) the module having larger charging (discharging) space with larger current. Based on this idea, the CDS-based current allocation method is proposed, in which two control parameter values can be appropriately selected to drive the battery system towards the desired performance. Then considering the time-varying total power requirement and the power loss constraint, two important system performance measures, i.e., the cell SOC range indicating the charge balance and the total power loss reflecting the energy efficiency, can be adaptively and dynamically controlled and even optimized as the system states evolve.

Note that, the proposed current allocation algorithm can be performed for battery systems with various initial SOCs, module numbers, and system parameters. Besides, since the solutions of all subproblems in the proposed algorithm can be obtained by the proposed analytical formulas instead of numerical search, it is very computationally efficient to perform the proposed algorithm even for large-scale battery systems. In addition, we can show that the current allocation in proportion to battery cell/module SOCs, which is a very common heuristic applied in recent studies of the battery current allocation, can be viewed as a special case of the proposed CDS-based current allocation.

In the future study, a comprehensive hardware testbed will be set up to facilitate the validation of proposed system designs and control algorithms. Accordingly, based on the experimental test results, the modeling of BCE systems can be further extended by incorporating more detailed operating characteristics of battery cells and

circuit elements. The selection of appropriate BCE models depends on the system size and the research topic. For example, when studying the state of health, the model considering battery degradation will be used. Besides, in addition to the critical system performance measures investigated in this thesis such as the BCE time, charging time, and discharging time, other importance measures of interest will also be quantitatively evaluated by proposing some accurate and computationally efficient methods. In addition, the proposed coordinated performance control algorithm of BPM systems in this thesis is designed only for one single control period, multi-step optimal control using some model predictive control (MPC) tools will be further investigated in the future work.

Chapter 7

Proofs and calculation formulas

7.1 Proofs for Chapter 2

7.1.1 Proof of Proposition 2.3.2

For a battery system with B cells, let $D_i(t) = x_{i+1}(t) - x_i(t)$, $i \in \{1, \ldots, B-1\}$, then according to (2.2.1),

$$D_i(t) = D_i(t_{n-1}) + \frac{D_i(t_n) - D_i(t_{n-1})}{\tau}(t - t_{n-1}),\ t \in [t_{n-1}, t_n],\ n \in \{1, 2, \ldots\}. \quad (7.1.1)$$

Thus, during each time slot,

$$\min\{D_i(t_{n-1}), D_i(t_n)\} \leq D_i(t) \leq \max\{D_i(t_{n-1}), D_i(t_n)\},\ t \in [t_{n-1}, t_n],\ n \in \{1, 2, \ldots\}. \quad (7.1.2)$$

To facilitate the proof, introduce the dummy terms: $x_0(t) = x_1(t)$, $x_{B+1}(t) = x_B(t)$, and thus $D_0(t) = D_B(t) = 0$, $t \geq 0$. Based on the definition of $D_i(t)$ and (2.2.1),

$$\begin{aligned}
D_i(t_n) &= x_{i+1}(t_n) - x_i(t_n) \\
&= x_{i+1}(t_{n-1}) + \mathrm{sgnl}(x_{i+2}(t_{n-1}) - x_{i+1}(t_{n-1}), l_e)r_e \\
&\quad + \mathrm{sgnl}(x_i(t_{n-1}) - x_{i+1}(t_{n-1}), l_e)r_e - x_i(t_{n-1}) \\
&\quad - \mathrm{sgnl}(x_{i+1}(t_{n-1}) - x_i(t_{n-1}), l_e)r_e - \mathrm{sgnl}(x_{i-1}(t_{n-1}) - x_i(t_{n-1}), l_e)r_e \\
&= D_i(t_{n-1}) + \mathrm{sgnl}(D_{i+1}(t_{n-1}), l_e)r_e + \mathrm{sgnl}(-D_i(t_{n-1}), l_e)r_e \\
&\quad - \mathrm{sgnl}(D_i(t_{n-1}), l_e)r_e - \mathrm{sgnl}(-D_{i-1}(t_{n-1}), l_e)r_e, \\
&i \in \{1, \ldots, B-1\},\ n \in \{1, 2, \ldots\}.
\end{aligned}$$

Based on (2.2.3),

$$\mathrm{sgnl}(-D_i(t), l_e)r_e - \mathrm{sgnl}(D_i(t), l_e)r_e = \begin{cases} -(2 - l_e)r_e, & \text{if } D_i(t) > 0, \\ 0, & \text{if } D_i(t) = 0, \\ (2 - l_e)r_e, & \text{if } D_i(t) < 0, \end{cases}$$

$$(\mathrm{sgnl}(D_{i+1}(t_{n-1}), l_e)r_e - \mathrm{sgnl}(-D_{i-1}(t_{n-1}), l_e)r_e) \in [-(2 - l_e)r_e, (2 - l_e)r_e].$$

Thus,

$$D_i(t_n) \in \begin{cases} [D_i(t_{n-1}) - (4 - 2l_e)r_e, D_i(t_{n-1})], & \text{if } D_i(t_{n-1}) > 0, \\ [-(2 - l_e)r_e, (2 - l_e)r_e], & \text{if } D_i(t_{n-1}) = 0, \\ [D_i(t_{n-1}), D_i(t_{n-1}) + (4 - 2l_e)r_e], & \text{if } D_i(t_{n-1}) < 0. \end{cases} \tag{7.1.3}$$

Then, assume cells b_i and b_{i+1} merge together for the first time during the n_ith time slot, i.e., $t_{merge}(i) \in [t_{n_i-1}, t_{n_i})$, $i \in \{1, \ldots, B-1\}$. According to (7.1.1), $D_i(t)$ is a linear function of time t, connecting points $(t_{n-1}, D_i(t_{n-1}))$ and $(t_n, D_i(t_n))$ during each time slot $[t_{n-1}, t_n]$. If $D_i(t_{n_i-1}) < 0$, since $t_{merge}(i) \in [t_{n_i-1}, t_{n_i})$ and $D_i(t_{merge}(i)) = 0$, then $D_i(t_{n_i}) > 0$. Based on (7.1.3),

$$-(4-2l_e)r_e < D_i(t_{n_i}) - (4-2l_e)r_e \leq D_i(t_{n_i-1}) < 0,$$
$$0 < D_i(t_{n_i}) \leq D_i(t_{n_i-1}) + (4-2l_e)r_e < (4-2l_e)r_e.$$

Similarly, if $D_i(t_{n_i-1}) > 0$, we can prove that $0 < D_i(t_{n_i-1}) < (4-2l_e)r_e$ and $-(4-2l_e)r_e < D_i(t_{n_i}) < 0$. Otherwise, if $D_i(t_{n_i-1}) = 0$, i.e., $t_{n_i-1} = t_{merge}(i)$, then based on (7.1.3), $D_i(t_{n_i}) \in [-(2-l_e)r_e, (2-l_e)r_e]$. Thus, if cells b_i and b_{i+1} merge at $t = t_{merge}(i) \in [t_{n_i-1}, t_{n_i})$, then

$$D_i(t_{n_i-1}) \in (-(4-2l_e)r_e, (4-2l_e)r_e),\ D_i(t_{n_i}) \in (-(4-2l_e)r_e, (4-2l_e)r_e).$$

Based on (7.1.2),

$$-(4-2l_e)r_e < D_i(t) < (4-2l_e)r_e,\ t \in [t_{n_i-1}, t_{n_i}],\ t_{merge}(i) \in [t_{n_i-1}, t_{n_i}).$$

Next, assume $-(4-2l_e)r_e < D_i(t_k) < (4-2l_e)r_e$, $k = n_i, n_i+1, \ldots$, then, based on (7.1.3), by summarizing the results of $D_i(t_{k+1})$ from three cases: $-(4-2l_e)r_e < D_i(t_k) < 0$, $D_i(t_k) = 0$, and $0 < D_i(t_k) < (4-2l_e)r_e$, we can also obtain $-(4-2l_e)r_e < D_i(t_{k+1}) < (4-2l_e)r_e$. Based on (7.1.2), for $t \in [t_k, t_{k+1}]$, $-(4-2l_e)r_e < D_i(t) < (4-2l_e)r_e$, which completes the proof.

7.1.2 Proof of Proposition 2.3.4

Without loss of generality, we assume that the SOCs of any two adjacent cells are always unequal at the beginning of each time slot, i.e., $x_i(n\tau) \neq x_{i+1}(n\tau)$, $n = 0, 1, \ldots$, $i = 1, \ldots, B-1$.

During each time slot, the change of sum SOC of a battery group comes from two sources: the internal energy loss among the cells within the battery group and the external transfer to/from the neighboring cell(s) of the battery group. For battery group $BG(g, i)$, the former can be calculated as:

$$L_{(g,i)} = (g-1) l_e r_e. \tag{7.1.4}$$

The latter depends on the SOC difference between the boundary cell(s) of the battery group and its neighboring cell(s). According to the definition of external equalization time, the following equations hold for $0 < t < t_e^{ext}(g, i)$:

$$\begin{aligned}
&\text{If } i > 1\text{: } \operatorname{sgn}(x_i(t) - x_{i-1}(t)) = \operatorname{sgn}(x_i(0) - x_{i-1}(0));\\
&\text{If } i + g - 1 < B\text{: } \operatorname{sgn}(x_{i+g-1}(t) - x_{i+g}(t)) = \operatorname{sgn}(x_{i+g-1}(0) - x_{i+g}(0)),
\end{aligned}$$

where

$$\operatorname{sgn}(u) = \begin{cases} 1, & \text{if } u > 0, \\ 0, & \text{if } u = 0, \\ -1, & \text{if } u < 0. \end{cases} \tag{7.1.5}$$

Therefore, according to system model (2.2.1)-(2.2.3), during each time slot, the external charge transfer to/from the neighboring cell(s) from/to the battery group follows

a constant rate for $0 < t < t_e^{ext}(g,i)$:

$$C_{(g,i)} = \begin{cases} \text{sgnl}(x_{i+g}(0) - x_{i+g-1}(0), l_e)r_e, \text{ if } g < B,\ i = 1, \\ \text{sgnl}(x_{i-1}(0) - x_i(0), l_e)r_e + \text{sgnl}(x_{i+g}(0) - x_{i+g-1}(0), l_e)r_e, \\ \qquad\qquad\qquad\qquad\qquad \text{if } g < B,\ 1 < i < B - g + 1, \\ \text{sgnl}(x_{i-1}(0) - x_i(0), l_e)r_e, \qquad \text{if } g < B,\ i = B - g + 1, \\ 0, \qquad\qquad\qquad\qquad\qquad \text{if } g = B. \end{cases} \tag{7.1.6}$$

Combine both internal transfer energy loss and external charge transfers of a battery group, then we have

$$x_{(g,i)}(t) = x_{(g,i)}(0) + k_{(g,i)}t,\ t \le t_e^{ext}(g,i), \tag{7.1.7}$$

where

$$k_{(g,i)} = \frac{C_{(g,i)} - L_{(g,i)}}{\tau}. \tag{7.1.8}$$

Finally, the average SOC of the battery group can be calculated as

$$\begin{aligned} &\bar{x}_{(g,i)}(t) = \bar{x}_{(g,i)}(0) + \frac{k_{(g,i)}}{g}t, \\ &g \in \{1, \ldots, B\},\ i \in \{1, \ldots, B - g + 1\},\ t \in [0, t_e^{ext}(g,i)], \end{aligned} \tag{7.1.9}$$

where $k_{(g,i)}$ is given by (2.3.13) based on (7.1.4), (7.1.6), and (7.1.8).

7.1.3 Proof of Proposition 2.4.1

In the approximated equalization process generated by Algorithm 1 and (2.4.3), since after $\widehat{T}_e = t_m^{(S)}$, there is only one active MBG, i.e., the entirely equalized battery system, it follows from Algorithm 1 that

$$\hat{x}_j(t) = \bar{x}_{(B,1)}(t),\ t \geq \widehat{T}_e,\ j \in \{1, \ldots, B\}, \tag{7.1.10}$$

and

$$\hat{\bar{x}}_{(g,i)}(t) = \frac{1}{g} \sum_{j=i}^{g+i-1} \hat{x}_j(t) = \bar{x}_{(B,1)}(t), \tag{7.1.11}$$
$$t \geq \widehat{T}_e,\ g \in \{1, \ldots, B\},\ i \in \{1, \ldots, B-g+1\}.$$

Then, according to (2.3.7) and (7.1.11),

$$\bar{x}^l_{(g,i)}(\widehat{T}_e) \leq \bar{x}_{(B,1)}(\widehat{T}_e) \leq \bar{x}^u_{(g,i)}(\widehat{T}_e). \tag{7.1.12}$$

Substituting $\bar{x}^l_{(g,i)}(\widehat{T}_e)$, $\bar{x}^u_{(g,i)}(\widehat{T}_e)$, and $\bar{x}_{(B,1)}(\widehat{T}_e)$ with (2.3.4), (2.3.6), and (2.3.8), respectively, results in

$$\widehat{T}_e \geq t_{ideal}(g,i),\ g \in \{1, \ldots, B-1\},\ i \in \{1, \ldots, B-g+1\}, \tag{7.1.13}$$

where $t_{ideal}(g,i)$ is defined in (2.4.7).

Next, we will show that for some $BG(g,i)$, the equality in (7.1.13) can be achieved. Based on the analysis in Subsection 2.4.1, among all active MBGs between the last two merging points $t_m^{(S-1)}$ and $t_m^{(S)}$, there exists only one active MBG including cell

b_1. We denote this MBG as $BG(g_1, 1)$, $g_1 < B$. Clearly, $BG(g_1, 1)$ will merge with its neighboring MBG at $t = \widehat{T}_e$. Thus, given $x_i(0)$, $i \in \{1, \ldots, B\}$, and based on Proposition 2.3.4, we have

$$\hat{\bar{x}}_{(g_1,1)}(t) = \bar{x}_{(g_1,1)}(0) + \frac{(\text{sgnl}(x_{g_1+1}(0) - x_{g_1}(0), l_e) - (g_1 - 1)l_e)r_e}{g_1\tau} t, \ t \in [0, \widehat{T}_e]. \tag{7.1.14}$$

According to (7.1.11), $\hat{\bar{x}}_{(g_1,1)}(\widehat{T}_e) = \bar{x}_{(B,1)}(\widehat{T}_e)$, i.e., $\widehat{T}_e$ is the intersection time of $\hat{\bar{x}}_{(g_1,1)}(t)$ and $\bar{x}_{(B,1)}(t)$. Then, substituting $\hat{\bar{x}}_{(g_1,1)}(\widehat{T}_e)$ and $\bar{x}_{(B,1)}(\widehat{T}_e)$ with (7.1.14) and (2.3.8), respectively, yields

$$\widehat{T}_e = \frac{(\bar{x}_{(g_1,1)}(0) - \bar{x}_{(B,1)}(0))\tau}{-((\frac{1}{g_1} - \frac{1}{B})l_e + \frac{\text{sgnl}(x_{g_1+1}(0) - x_{g_1}(0), l_e)}{g_1})r_e}. \tag{7.1.15}$$

To take into account that $\widehat{T}_e > 0$, the sgnl$(\cdot)$ function in (7.1.15) is expanded to obtain:

$$\widehat{T}_e = \begin{cases} \frac{(\bar{x}_{(g_1,1)}(0) - \bar{x}_{(B,1)}(0))\tau}{-((\frac{1}{g_1} - \frac{1}{B})l_e - \frac{1}{g_1})r_e}, & \text{if } \bar{x}_{(g_1,1)}(0) > \bar{x}_{(B,1)}(0), \\ \frac{(\bar{x}_{(g_1,1)}(0) - \bar{x}_{(B,1)}(0))\tau}{-((\frac{1}{g_1} - \frac{1}{B})l_e + \frac{1-l_e}{g_1})r_e}, & \text{if } \bar{x}_{(g_1,1)}(0) < \bar{x}_{(B,1)}(0). \end{cases} \tag{7.1.16}$$

According to (2.4.7),

$$\widehat{T}_e = t_{ideal}(g_1, 1). \tag{7.1.17}$$

Therefore, by combining (7.1.13) and (7.1.17), the proposition is proved.

7.1.4 Proof of Proposition 2.5.1

In the approximated equalization process generated by Algorithm 1, the maximum cell SOC, $\max_{j \in \{1,\ldots,B\}} \hat{x}_j(t)$, is a piece-wise linear function of t described by several MBGs and their active periods. For $t \geq 0$, assume that $\max_{j \in \{1,\ldots,B\}} \hat{x}_j(t)$ consists of $M+1$ pieces

separated by M time instants (denoted as t^u_m, $m = 1, \ldots, M$). Clearly, $t^u_M = \widehat{T}_e$, and without loss of generality, let $t^u_0 = 0$, $t^u_{M+1} = \infty$. According to Algorithm 1, the mth piece during $[t^u_{m-1}, t^u_m)$, $m = 1, \ldots, M+1$, corresponds to an active MBG, denoted as $BG(g_m, i_m)$, such that at any time $t \in [t^u_{m-1}, t^u_m)$, $BG(g_m, i_m)$ is active and each cell in $BG(g_m, i_m)$ has the highest cell SOC. Thus, according to (2.3.15), for $t \in [t^u_{m-1}, t^u_m)$, the mth piece of $\max\limits_{j\in\{1,\ldots,B\}} \hat{x}_j(t)$ can be approximated as:

$$\max_{j\in\{1,\ldots,B\}} \hat{x}_j(t) = \hat{\bar{x}}_{(g_m,i_m)}(t) = \max_{\substack{g\,\in\,\{1,\ldots,\,B\}\\ i\,\in\,\{1,\ldots,\,B-g+1\}}} \hat{\bar{x}}_{(g,i)}(t),\ t \in [t^u_{m-1}, t^u_m). \tag{7.1.18}$$

Since $BG(g_m, i_m)$ merges with one of its neighboring cells at its external equalization time $t^{ext}_e(g_m, i_m) \geq t^u_m$, based on Proposition 2.3.4,

$$\hat{\bar{x}}_{(g_m,i_m)}(t) = \bar{x}_{(g_m,i_m)}(0) + \frac{k_{(g_m,i_m)}}{g_m} t,\ t \in [t^u_{m-1}, t^u_m). \tag{7.1.19}$$

According to (7.1.18), for $t \in [t^u_{m-1}, t^u_m)$, the charge is always transferred from $BG(g_m, i_m)$ to any of its neighboring cells. Thus,

$$k_{(g_m,i_m)} = -\frac{(g_m - 1) l_e r_e + \rho_{(g_m,i_m)} r_e}{\tau},\ t \in [t^u_{m-1}, t^u_m). \tag{7.1.20}$$

Based on (7.1.19), (7.1.20), and (2.3.4),

$$\hat{\bar{x}}_{(g_m,i_m)}(t) = \bar{x}^l_{(g_m,i_m)}(t),\ t \in [t^u_{m-1}, t^u_m). \tag{7.1.21}$$

Combining (7.1.21) and (7.1.18) yields

$$\bar{x}^l_{(g_m,i_m)}(t) = \hat{\bar{x}}_{(g_m,i_m)}(t) \geq \hat{\bar{x}}_{(g,i)}(t) \geq \bar{x}^l_{(g,i)}(t), \tag{7.1.22}$$

$$g \in \{1, \ldots, B\},\ i \in \{1, \ldots, B-g+1\},\ t \in [t^u_{m-1}, t^u_m).$$

Therefore,

$$\bar{x}^l_{(g_m,i_m)}(t) = \max_{\substack{g \in \{1,\ldots,B\} \\ i \in \{1,\ldots,B-g+1\}}} \bar{x}^l_{(g,i)}(t),\ t \in [t^u_{m-1}, t^u_m). \tag{7.1.23}$$

Next, combining (7.1.18), (7.1.21) and (7.1.23), we obtain

$$\max_{j\in\{1,\ldots,B\}} \hat{x}_j(t) = \max_{\substack{g \in \{1,\ldots,B\} \\ i \in \{1,\ldots,B-g+1\}}} \bar{x}^l_{(g,i)}(t),\ t \in [t^u_{m-1}, t^u_m). \tag{7.1.24}$$

Based on (2.3.4) and (2.3.8), it can be easily shown that if $\bar{x}_{(g,i)}(0) < \bar{x}_{(B,1)}(0)$, then $\bar{x}^l_{(g,i)}(t) < \bar{x}_{(B,1)}(t) \leq \max_{j\in\{1,\ldots,B\}} \hat{x}_j(t),\ t \geq 0$. Thus, we can narrow down the search zone to those BGs with $\bar{x}_{(g,i)}(0) \geq \bar{x}_{(B,1)}(0)$.

Finally, superpose the charging/discharging process to the approximated equalization process by adding $\frac{r_g}{\tau}t$ to the right hand side of (7.1.24), and combine all $M+1$ pieces, then (2.5.2) is obtained.

Using a similar approach, the approximate calculation formula of minimum cell SOC can be proved as well.

7.1.5 Proof of Lemma 2.5.2

According to Proposition 2.5.1 and equations (2.3.4) and (2.3.6),

$$\max_{j\in\{1,\ldots,B\}} \hat{x}_j(t) = \max_{\substack{g \in \{1,\ldots,B\} \\ i \in \{1,\ldots,B-g+1\} \\ \bar{x}_{(g,i)}(0) \geq \bar{x}_{(B,1)}(0)}} \{\bar{x}_{(g,i)}(0) + \bar{k}^l_{(g,i)}t\},$$

$$\bar{k}^l_{(g,i)} = \frac{r_g}{\tau} - \frac{\rho_{(g,i)} + (g-1)l_e}{g\tau} r_e, \tag{7.1.25}$$

$$\min_{j\in\{1,\ldots,B\}} \hat{x}_j(t) = \min_{\substack{g \in \{1,\ldots,B\} \\ i \in \{1,\ldots,B-g+1\} \\ \bar{x}_{(g,i)}(0) \le \bar{x}_{(B,1)}(0)}} \{\bar{x}_{(g,i)}(0) + \bar{k}^u_{(g,i)} t\},$$

$$\bar{k}^u_{(g,i)} = \frac{r_g}{\tau} + \frac{\rho_{(g,i)}(1-l_e) - (g-1)l_e}{g\tau} r_e. \tag{7.1.26}$$

If $r_g < \frac{B-1}{B} l_e r_e$, then for any $BG(g,i)$, $g \in \{1,\ldots,B\}$, $i \in \{1,\ldots,B-g+1\}$, equations (7.1.25) and (2.3.5) imply

$$\bar{k}^l_{(g,i)} < \frac{B-1}{B\tau} l_e r_e - \frac{\rho_{(g,i)} + (g-1)l_e}{g\tau} r_e = -\frac{l_e r_e}{B\tau} - \frac{\rho_{(g,i)} - l_e}{g\tau} r_e \le 0. \tag{7.1.27}$$

Therefore, the maximum cell SOC is always decreasing in time. Since $\bar{x}_{(g,i)}(0) < lim_u$, it is impossible for the maximum cell SOC to reach lim_u, i.e., $\widehat{T}_c$ does not exist. As time goes on, the SOC of certain cell(s) will reach lim_l, i.e., $\widehat{T}_d$ exists.

Similarly, if $r_g > \frac{B-1}{B} l_e r_e$, it can be shown that it is impossible for the minimum cell SOC to reach lim_l, i.e., $\widehat{T}_d$ does not exist and the system evolution will be terminated when the SOC of certain cell(s) reaches lim_u, i.e., $\widehat{T}_c$ exists.

Finally, if $r_g = \frac{B-1}{B} l_e r_e$, it can be shown using the same approach that the SOCs of all cells will not reach lim_l or lim_u but merge to a value in between and remain constant thereafter.

7.1.6 Proof of Proposition 2.5.3

First, we analyze the case of simultaneous equalization and charging processes with $r_e > 0$ and $r_g > \frac{(B-1)}{B} l_e r_e$. In this case, the approximated charging time $\widehat{T}_c$ is defined

as the solution to equation $\max\limits_{\substack{j \in \{1,\ldots,B\} \\ r_e > 0, r_g > \frac{B-1}{B} l_e r_e}} \hat{x}_j(\widehat{T}_c) = lim_u$.

Based on (2.5.2), at time t, the maximum cell SOC can be approximated by a particular battery group's $\bar{x}^l_{(g,i)}(t) + \frac{r_g}{\tau}t$. Denote the time t such that $\bar{x}^l_{(g,i)}(t) + \frac{r_g}{\tau}t = lim_u$ as $t_c^{(g,i)}$, then based on (2.3.4),

$$t_c^{(g,i)} = \frac{g(lim_u - \bar{x}_{(g,i)}(0))\tau}{gr_g - ((g-1)l_e + \rho_{(g,i)})r_e},\ g \in \{1,\ldots,B\},\ i \in \{1,\ldots,B-g+1\}. \quad (7.1.28)$$

Then, at $t = \widehat{T}_c$, based on (2.5.2), there exists a battery group, denoted as $BG(g_c, i_c)$, such that $\bar{x}_{(g_c,i_c)}(0) \geq \bar{x}_{(B,1)}(0)$ and

$$\begin{aligned} \bar{x}^l_{(g_c,i_c)}(\widehat{T}_c) + \frac{r_g}{\tau}\widehat{T}_c &= \max_{\substack{g \in \{1,\ldots,B\} \\ i \in \{1,\ldots,B-g+1\} \\ \bar{x}_{(g,i)}(0) \geq \bar{x}_{(B,1)}(0)}} \bar{x}^l_{(g,i)}(\widehat{T}_c) + \frac{r_g}{\tau}\widehat{T}_c \\ &= \max_{j \in \{1,\ldots,B\}} \hat{x}_j(\widehat{T}_c) \\ &= lim_u. \end{aligned}$$

In the above equation, substitute $\bar{x}^l_{(g_c,i_c)}(\widehat{T}_c)$ with (2.3.4) and use the denotation in (7.1.28), then

$$\begin{aligned} &\widehat{T}_c = \frac{g_c(lim_u - \bar{x}_{(g_c,i_c)}(0))\tau}{g_c r_g - ((g_c-1)l_e + \rho_{(g_c,i_c)})r_e} = t_c^{(g_c,i_c)}, \quad (7.1.29) \\ &\bar{x}_{(g_c,i_c)}(0) \geq \bar{x}_{(B,1)}(0),\ \bar{x}^l_{(g_c,i_c)}(\widehat{T}_c) = \max_{\substack{g \in \{1,\ldots,B\} \\ i \in \{1,\ldots,B-g+1\} \\ \bar{x}_{(g,i)}(0) \geq \bar{x}_{(B,1)}(0)}} \bar{x}^l_{(g,i)}(\widehat{T}_c). \end{aligned}$$

Since $t_c^{(g_c,i_c)} = \widehat{T}_c > 0$ and $lim_u > \bar{x}_{(g_c,i_c)}(0)$, according to (7.1.29), we obtain $g_c r_g > ((g_c-1)l_e + \rho_{(g_c,i_c)})r_e$. Thus, in order to obtain $\widehat{T}_c$, we need to search for $BG(g_c, i_c)$

among all the BGs with $\bar{x}_{(g,i)}(0) \geq \bar{x}_{(B,1)}(0)$ and $gr_g > ((g-1)l_e + \rho_{(g,i)})r_e$. Obviously, for any $BG(g,i)$ within the search scope of $BG(g_c, i_c)$, $\bar{x}^l_{(g,i)}(t) + \frac{r_g}{\tau}t$ is increasing in time t and

$$\bar{x}^l_{(g,i)}(\widehat{T}_c) + \frac{r_g}{\tau}\widehat{T}_c \leq \bar{x}^l_{(g_c,i_c)}(\widehat{T}_c) + \frac{r_g}{\tau}\widehat{T}_c = lim_u = \bar{x}^l_{(g,i)}(t_c^{(g,i)}) + \frac{r_g}{\tau}t_c^{(g,i)}.$$

Therefore, $\widehat{T}_c$ is upper bounded by $t_c^{(g,i)}$, i.e.,

$$\begin{aligned} &\widehat{T}_c \leq t_c^{(g,i)}, \\ &g \in \{1, \ldots, B\},\ i \in \{1, \ldots, B-g+1\}, \\ &\bar{x}_{(g,i)}(0) \geq \bar{x}_{(B,1)}(0),\ gr_g > ((g-1)l_e + \rho_{(g,i)})r_e. \end{aligned} \tag{7.1.30}$$

Since $r_g > \frac{(B-1)}{B}l_e r_e$ and $r_e > 0$, there exists at least one BG, $BG(B,1)$, satisfying the above constraints, i.e., the search scope of $BG(g_c, i_c)$ is non-empty. Finally, equation (2.5.6) is obtained by combining (7.1.29) and (7.1.30).

Using the same approach, equation (2.5.7) can also be proved.

7.2 Proofs for Chapter 3

7.2.1 Proof of Proposition 3.2.1

In each battery module of the module-based BCE system with initial cell SOCs $x_i(0) \in (x_{lb}, x_{ub})$, clearly, if the largest cell SOC always decreases or remain unchanged and the smallest cell SOC always increases or remain unchanged during each working cycle, finally all cells in each module and all modules in the system will reach charge

equalization before any cell is fully charged or fully discharged.

For the module-based BCE system without external charging and discharging, during each working cycle, the cell with the largest SOC in each battery module can release at least $r_c C_B$ units of charge when it has only one neighboring cell within the same module, and it can receive at most $2(1 - l_m)r_m C_B$ units of charge if it is charged by two neighboring modules. In order to ensure the largest cell SOC in each module not to increase during each working cycle, let $r_c C_B \geq 2(1 - l_m)r_m C_B$. Then, we obtain

$$r_m \leq \frac{r_c}{2(1 - l_m)}. \tag{7.2.1}$$

On the other hand, during each working cycle, the cell with the smallest SOC in each battery module can receive at least $(1 - l_c)r_c C_B$ units of charge when it has only one neighboring cell within the same module, and it can release at most $2r_m C_B$ units of charge if it is discharged by two neighboring modules. In order to ensure the smallest cell SOC in each module not to decrease during each working cycle, let $(1 - l_c)r_c C_B \geq 2r_m C_B$. Then, we obtain

$$r_m \leq \frac{(1 - l_c)r_c}{2}. \tag{7.2.2}$$

By combining (7.2.1) and (7.2.2), we obtain (3.2.8). Therefore, Proposition 3.2.1 is proved.

7.2.2 Proof of Proposition 3.5.1

Based on the model description (3.2.1)-(3.2.7) in Section 3.2, the charge transfer direction can only be updated at the beginning of each working cycle, i.e., some

discrete time instants. Then, without loss of generality, we can assume charge transfer always occurs between every two adjacent cells in the same module and between every two adjacent modules. As a result, for a module-based BCE system with M modules and B cells per module, the net charge transfer loss during each working cycle can be calculated by (3.5.7).

For a module-based BCE system, the evolution of total cell SOC depends on both the internal charge transfer loss and the external charging or discharging profile. Then, given a time-invariant charging rate $r_g(n) = r_g$, the evolution of total cell SOC is given below,

$$\sum_{i=1}^{MB} x_i(t) = \sum_{i=1}^{MB} x_i(0) - \frac{L_{net}}{\tau} t + \frac{MBr_g}{\tau} t. \tag{7.2.3}$$

For the charging process with $r_g(n) = r_g > \frac{L_{net}}{MB}$, if no cell is overcharged and overdischarged during the charge equalization, i.e., $T_e \leq T_c$, then at $t = T_c$ all cell SOCs are charged to x_{ub} together. Based on (7.2.3), we have

$$\sum_{i=1}^{MB} x_i(T_c) = \sum_{i=1}^{MB} x_i(0) - \frac{L_{net}}{\tau} T_c + \frac{MBr_g}{\tau} T_c = MBx_{ub}. \tag{7.2.4}$$

Thus, according to (7.2.4), (3.5.5), (3.5.6), and (3.5.7), given $T_e \leq T_c$, the time-invariant charging rate is

$$r_g = \frac{x_{ub} - \frac{1}{MB} \sum_{i=1}^{MB} x_i(0)}{T_c} \tau + \frac{L_{net}}{MB} \leq \frac{x_{ub} - \bar{x}_i(0)}{T_e} \tau + \frac{L_{net}}{MB} = r_g^{+c}. \tag{7.2.5}$$

For the discharging process with $r_g(n) = r_g < \frac{L_{net}}{MB}$, if all cell SOCs have already got equalized before any cell SOC reaches x_{lb}, i.e., $T_e \leq T_d$, we can also show $r_g \geq r_g^{-c}$ following the similar procedure. Therefore, Proposition 2 is proved.

7.2.3 Proof of Proposition 3.5.2

Based on Subsection 7.2.2, for the charging process with charge transfer rates satisfying (3.2.8), given any constant charging rate $r_g(n) = r_g \in (\frac{L_{net}}{MB}, r_g^{max}]$, all battery cells can reach charge equalization and finally get fully charged, i.e., $T_e \leq T_c$. As a result, we have (7.2.4). Then based on (7.2.4) and (3.5.6), the charging time T_c can be calculated by (3.5.8).

On the other hand, for the discharging process with charge transfer rates satisfying (3.2.8), given any constant charging rate $r_g(n) = r_g \in [r_g^{min}, \frac{L_{net}}{MB})$, all battery cells can reach charge equalization and finally get fully discharged, i.e., $T_e \leq T_d$. Then following the similar procedure, the discharging time T_d can be calculated by (3.5.9).

7.3 Proofs for Chapter 5

7.3.1 Proof of Proposition 5.4.1

For the charging process, at the beginning of the n-th control period, consider the case that charge imbalance exists among all non-fully-charged modules, i.e., $x_l(n) < x_h(n)$. Given constant parameters (5.4.1) under CDS-based current allocation, if the m-th battery module can still be charged, i.e., $x_m(n) < x_{ub}$, its SOC is updated based on (5.3.1), (5.3.2), (5.3.8), and (5.4.1), as below:

$$x_m(n+1) = x_m(n) + \frac{C - x_m(n)}{C - x_l(n)} \cdot \frac{I_B^{max} \tau_c}{Q_B}. \tag{7.3.1}$$

Next, from (5.3.1), (5.3.2), (5.4.1), and (7.3.1), we have

$$\begin{aligned}\frac{I_{Bm}(n+1)}{I_{Bm}(n)} &= \frac{C-x_m(n+1)}{C-x_l(n+1)} \cdot \frac{C-x_l(n)}{C-x_m(n)} \\ &= \frac{\left(C-x_m(n)-\frac{C-x_m(n)}{C-x_l(n)} \cdot \frac{I_B^{max}\tau_c}{Q_B}\right) \cdot \frac{C-x_l(n)}{C-x_m(n)}}{C-x_l(n)-\frac{C-x_l(n)}{C-x_l(n)} \cdot \frac{I_B^{max}\tau_c}{Q_B}} \\ &= 1. \end{aligned} \tag{7.3.2}$$

This implies that the charging current of any battery module is constant. Then based on (7.3.2), (5.3.1), (5.3.2), and (5.4.1), the constant module current in (5.4.2) is proved. Next, based on (5.3.8) and (5.4.2), the module SOC evolution in (5.4.6) is obtained. Finally, if the i-th and j-th modules with $x_i(1) < x_{ub}$, $x_j(1) < x_{ub}$, and $x_i(1) \neq x_j(1)$, $i, j \in \{1, \ldots, M\}$, have equal SOCs at the beginning of the n-th control period, i.e., $x_i(n) = x_j(n)$, then substituting $x_i(n)$ and $x_j(n)$ by (5.4.6) leads to

$$n = 1 + \frac{(C-x_l(1))Q_B}{I_B^{max}\tau_c}. \tag{7.3.3}$$

Thus, the equalization time of the i-th and j-th modules is

$$T_e = (n-1)\tau_c = \frac{(C-x_l(1))Q_B}{I_B^{max}}. \tag{7.3.4}$$

From (7.3.4) we can see that, T_e is independent of the i-th and j-th modules' initial SOCs, i.e., all module SOCs are equalized at the same time. Then, by substituting n with (7.3.3) in (5.4.6), we have $x_m(n) = C$, i.e., all module SOCs reach C at $t = T_e$.

For the discharging process, using the similar procedure, all results in Proposition 5.4.1 can also be proved.

7.3.2 Proof of Proposition 5.5.1 and Proposition 5.5.2

Based on (5.5.4) and (5.5.9), the total power is calculated by

$$P_O(n) = \begin{cases} \sqrt{\lambda(n)P_L(n)} + P_L(n), & \text{for charging,} \\ \sqrt{\lambda(n)P_L(n)} - P_L(n), & \text{for discharging.} \end{cases} \tag{7.3.5}$$

In addition, based on (5.5.3), (5.5.5), and (5.5.6), we have

$$P_L(n) \leq P_L^{top}(n) \triangleq \min\left\{P_L^{ub}, \boldsymbol{\alpha}\boldsymbol{\alpha}^T \left(I_B^{ub}\right)^2 R\right\}. \tag{7.3.6}$$

For the charging process, according to (5.5.1), (5.5.9), and (7.3.6), both $\lambda(n)$ and $P_L^{top}(n)$ are determined only by $C(n)$. Then, given any $C(n)$, based on (7.3.5), the total power $P_O(n)$ can be maximized at $P_L(n) = P_L^{top}(n)$, i.e.,

$$P_O(C(n), P_L(n) = P_L^{top}(n)) = \sqrt{\lambda(C(n))P_L^{top}(n)} + P_L^{top}(n). \tag{7.3.7}$$

Since $C(n) \geq x_h(n)$ based on (5.3.3), the maximum total power

$$P_O^{max}(n) = \max_{C(n)\geq x_h(n)} P_O(C(n), P_L(n) = P_L^{top}(n)). \tag{7.3.8}$$

By rewriting (5.3.2) as

$$\alpha_m(n) = 1 - \frac{x_m(n) - x_l(n)}{C(n) - x_l(n)}, \tag{7.3.9}$$

we can see that, as $C(n)$ increases from $x_h(n)$ to $+\infty$, $\alpha_m(n)$ increases for all modules except the module with the lowest SOC. Then, based on (7.3.6), as $C(n)$ increases, $P_L^{top}(n)$ does not decrease. Moreover, it can be shown that $\frac{d\lambda(C(n))}{dC(n)} > 0$, i.e., $\lambda(C(n))$

increases as $C(n)$ increases. Thus, based on (7.3.7) and (7.3.8), the maximum total power is achieved by

$$P_O^{max}(n) = P_O(C(n) = +\infty, P_L(n) = P_L^{top}(n)).$$

Finally, given $C(n) = +\infty$, and $P_L(n) = P_L^{top}(n)$, based on (5.5.3), (7.3.6), and (5.5.7), we have

$$I_B^{max}(n) = \sqrt{\frac{P_L^{top}(n)}{\boldsymbol{\alpha}\boldsymbol{\alpha}^T R}} = \min\left\{\sqrt{\frac{P_L^{ub}}{MR}}, I_B^{ub}\right\} = \sqrt{\frac{P_L^{ub}}{MR}}.$$

For the discharging process, based on (7.3.5) and (7.3.6), $P_O(n) = -\left(\sqrt{P_L(n)}\right)^2 + \sqrt{\lambda(n)}\sqrt{P_L(n)}$, where $\sqrt{P_L(n)} \leq \sqrt{P_L^{top}(n)}$. Then, given any $F(n) \in [-\infty, x_l(n)]$, based on (5.5.1), (5.5.9), and (7.3.6), both $\lambda(n)$ and $P_L^{top}(n)$ are determined. Thus, given any $F(n) \in [-\infty, x_l(n)]$, in order to maximize $P_O(n)$, we need to let

$$\sqrt{P_L(n)} = \sqrt{P_L^{opt}(F(n))} \triangleq \min\left\{\sqrt{P_L^{top}(F(n))}, \frac{\sqrt{\lambda(F(n))}}{2}\right\},$$

i.e.,

$$P_L^{opt}(F(n)) \triangleq \min\left\{P_L^{top}(F(n)), \frac{\lambda(F(n))}{4}\right\} = \min\left\{P_L^{ub}, \boldsymbol{\alpha}\boldsymbol{\alpha}^T \left(I_B^{ub}\right)^2 R, \frac{\lambda(F(n))}{4}\right\}. \tag{7.3.10}$$

Let $\frac{d\lambda(n)}{dF(n)} = 0$, then we have $F^*(n)$ shown in (5.5.10), such that $\frac{d\lambda(n)}{dF(n)}|_{F(n)=F^*(n)} = 0$. In addition, given $F(n) \leq x_l(n)$, it can also be shown that $\frac{d\lambda(n)}{dF(n)} > 0$ if $F(n) < F^*(n)$,

and $\frac{d\lambda(n)}{dF(n)} < 0$ if $F(n) > F^*(n)$. Thus,

$$\min_{F(n)\leq x_l(n)} \lambda(F(n)) = \min\left\{\lambda(F(n) = x_l(n)), \lambda(F(n) = -\infty)\right\},$$
$$\max_{F(n)\leq x_l(n)} \lambda(F(n)) = \lambda(F(n) = \min\left\{F^*(n), x_l(n)\right\}).$$

Based on (5.5.4), (5.5.6), and (5.5.9), given the condition (5.5.12), i.e., $P_L^{ub} \leq \frac{1}{4} \min_{F(n)\leq x_l(n)} \lambda(F(n))$, we have

$$P_L(n) \leq P_L^{ub} \leq \frac{\lambda(F(n))}{4} = \frac{\left(P_O(n) + P_L(n)\right)^2}{4P_L(n)} \implies P_L(n) \leq P_O(n).$$

Besides, given $P_L^{ub} \leq \frac{1}{4} \min_{F(n)\leq x_l(n)} \lambda(F(n))$, based on (7.3.10),

$$P_L^{opt}(F(n)) = \min\left\{P_L^{ub}, \boldsymbol{\alpha}\boldsymbol{\alpha}^T \left(I_B^{ub}\right)^2 R\right\}.$$

If $P_L(n) = P_L^{ub}$ for any $F(n) \leq x_l(n)$, based on (7.3.5),

$$P_O(n) = \sqrt{\lambda(n) P_L^{ub}} - P_L^{ub}.$$

Then, $P_O(n)$ is maximized when $\lambda(F(n))$ is maximized at $F(n) = \min\left\{F^*(n), x_l(n)\right\}$.

If $P_L(n) = \boldsymbol{\alpha}\boldsymbol{\alpha}^T \left(I_B^{ub}\right)^2 R$ for any $F(n) \leq x_l(n)$, i.e., $I_B^{max}(n) = I_B^{ub}$, based on (7.3.5), we have

$$\begin{aligned} P_O(n) &= P_O(F(n), I_B^{max}(n) = I_B^{ub}) \\ &= \sqrt{\lambda(n) P_L(F(n), I_B^{max}(n) = I_B^{ub})} - P_L(F(n), I_B^{max}(n) = I_B^{ub}). \end{aligned}$$

Based on (5.5.1)-(5.5.4), let $\frac{\partial P_O(F(n),I_B^{max}(n)=I_B^{ub})}{\partial F(n)}=0$, then

$$F^{**}(n)=\frac{(2I_B^{ub}R\mathbf{X}-x_h(n)\mathbf{V})(x_h(n)\mathbf{J}-\mathbf{X})^T}{(2I_B^{ub}R\mathbf{J}-\mathbf{V})(x_h(n)\mathbf{J}-\mathbf{X})^T}, \tag{7.3.11}$$

such that $\frac{\partial P_O(F(n),I_B^{ub})}{\partial F(n)}|_{F(n)=F^{**}(n)}=0$. From (7.3.11) we can see that, $F^{**}(n)$ approaches $-\infty$ or $+\infty$ if I_B^{ub} is equal to

$$I_B^{ub0}=\frac{\mathbf{V}(x_h(n)\mathbf{J}-\mathbf{X})^T}{2R\mathbf{J}(x_h(n)\mathbf{J}-\mathbf{X})^T}>0. \tag{7.3.12}$$

It can be proved that, given $I_B^{ub}\in(0,I_B^{ub0})$, $P_O(F(n),I_B^{max}(n)=I_B^{ub})$ decreases as $F(n)$ increases from $-\infty$ to $x_l(n)$.

Rewrite (5.3.2) as

$$\alpha_m(n)=1-\frac{x_h(n)-x_m(n)}{x_h(n)-F(n)}, \tag{7.3.13}$$

then $\alpha_m(n)$ decreases as $F(n)$ increases. As a result,
$P_L(F(n),I_B^{max}(n)=I_B^{ub})=\boldsymbol{\alpha}\boldsymbol{\alpha}^T\left(I_B^{ub}\right)^2R$, decreases as $F(n)$ increases.

If P_L^{ub} falls within the range of the total power loss $P_L(F(n)\le x_l(n),I_B^{max}(n)=I_B^{ub})$, there exists an $F(n)\in[-\infty,x_l(n)]$, denoted by $F^{int}(n)$, such that

$$P_L^{ub}=P_L(F(n)=F^{int}(n),I_B^{max}(n)=I_B^{ub}).$$

Based on (5.5.3), $F^{int}(n)$ is given in (5.5.11). Note that, at $F(n)=F^{int}(n)$, we also have

$$P_O(F(n)=F^{int}(n),I_B^{max}(n)=I_B^{ub})=P_O(F(n)=F^{int}(n),P_L(n)=P_L^{ub}).$$

Then, given (5.5.12), based on (7.3.10), we can obtain

$$P_L^{opt}(F(n)) = \begin{cases} P_L^{ub}, & F(n) \in [-\infty, F^{int}(n)], \\ P_L(F(n), I_B^{max}(n) = I_B^{ub}), & F(n) \in [F^{int}(n), x_l(n)]. \end{cases}$$

If $F^*(n) \leq F^{int}(n)$, we have

$$\begin{aligned} \max_{-\infty \leq F(n) \leq F^{int}(n)} P_O(n) &= P_O\left(F(n) = F^*(n), P_L(n) = P_L^{ub}\right) \\ &\geq P_O\left(F(n) = F^{int}(n), P_L(n) = P_L^{ub}\right) \\ &= P_O(F(n) = F^{int}(n), I_B^{max}(n) = I_B^{ub}) \\ &= \max_{F^{int}(n) \leq F(n) \leq x_l(n)} P_O(n). \end{aligned}$$

Thus, if $F^*(n) \leq F^{int}(n)$, to get the maximum total power, we need to let $F(n) = F^*(n) = \min\{F^*(n), F^{int}(n)\}$ and $I_B^{max}(n) = \sqrt{\frac{P_L^{ub}}{\boldsymbol{\alpha}\boldsymbol{\alpha}^T R}}$ based on (5.5.3). On the other hand, if $F^*(n) > F^{int}(n)$, we have

$$\begin{aligned} \max_{-\infty \leq F(n) \leq F^{int}(n)} P_O(n) &= P_O\left(F(n) = F^{int}(n), P_L(n) = P_L^{ub}\right) \\ &= P_O\left(F(n) = F^{int}(n), I_B^{max}(n) = I_B^{ub}\right) \\ &= \max_{F^{int}(n) \leq F(n) \leq x_l(n)} P_O(n). \end{aligned}$$

Thus, if $F^*(n) > F^{int}(n)$, to get the maximum total power, we need to let $F(n) = F^{int}(n) = \min\{F^*(n), F^{int}(n)\}$ and $I_B^{max}(n) = I_B^{ub}$.

Finally, if $P_L^{ub} < P_L(F(n), I_B^{max}(n) = I_B^{ub})$ for any $F(n) \leq x_l(n)$, we let $F^{int}(n) = x_l(n)$. Then under condition (5.5.12), we have $P_L^{opt}(F(n)) = P_L^{ub}$ based on (7.3.10). Thus, to get the maximum total power, we need to let $F(n) = \min\{F^*(n), F^{int}(n)\}$

and $I_B^{max}(n) = \sqrt{\frac{P_L^{ub}}{\boldsymbol{\alpha}\boldsymbol{\alpha}^T R}}$ based on (5.5.3). This completes the proof of Proposition 5.5.2.

7.3.3 Calculation formulas of total power loss

For the charging process, given $C(n)$ and $P_O(n)$, based on (5.5.4) and (5.5.9), the total power loss can be calculated by

$$P_L(C(n), P_O(n)) = \frac{1}{4}\left(\sqrt{\lambda(C(n)) + 4P_O(n)} - \sqrt{\lambda(C(n))}\right)^2,$$

where $\lambda(C(n))$ is defined in (5.5.9).

For the discharging process, given $F(n)$ and $P_O(n)$, based on (5.5.4) and (5.5.9), the total power loss can be calculated by

$$P_L(F(n), P_O(n)) = \frac{1}{4}\left(\sqrt{\lambda(F(n))} - \sqrt{\lambda(F(n)) - 4P_O(n)}\right)^2,$$

where $\lambda(F(n))$ is defined in (5.5.9).

For the charging process, given $I_B^{max}(n)$ and $P_O(n)$, the total power loss $P_L(I_B^{max}(n), P_O(n))$ can be calculated by (5.5.3), in which $I_B^{max}(n)$ is given and $C(n)$ is calculated based on (5.5.1)-(5.5.4), i.e.,

$$\begin{aligned}
C(n) =& \frac{-bb(n) + \sqrt{bb^2(n) - 4aa(n)cc(n)}}{2aa(n)},\\
aa(n) =& \mathbf{V}\mathbf{J}^T I_B^{max}(n) + M\left(I_B^{max}(n)\right)^2 R - P_O(n),\\
bb(n) =& -2\mathbf{X}\mathbf{J}^T\left(I_B^{max}(n)\right)^2 R - \mathbf{X}\mathbf{V}^T I_B^{max}(n) - x_l(n)\mathbf{V}\mathbf{J}^T I_B^{max}(n) + 2x_l(n)P_O(n),\\
cc(n) =& x_l(n)\mathbf{X}\mathbf{V}^T I_B^{max}(n) + \mathbf{X}\mathbf{X}^T\left(I_B^{max}(n)\right)^2 R - x_l^2(n)P_O(n).
\end{aligned}$$

For the discharging process, given $I_B^{max}(n)$ and $P_O(n)$, $P_L\left(I_B^{max}(n), P_O(n)\right)$ can be calculated by (5.5.3), in which $I_B^{max}(n)$ is given and $F(n)$ is calculated based on (5.5.1)-(5.5.4),

$$\begin{aligned}
F(n) =& \frac{-bb(n) - \sqrt{bb^2(n) - 4aa(n)cc(n)}}{2aa(n)}, \\
aa(n) =& \mathbf{V}\mathbf{J}^T I_B^{max}(n) - M\left(I_B^{max}(n)\right)^2 R - P_O(n), \\
bb(n) =& 2\mathbf{X}\mathbf{J}^T\left(I_B^{max}(n)\right)^2 R - \mathbf{X}\mathbf{V}^T I_B^{max}(n) - x_h(n)\mathbf{V}\mathbf{J}^T I_B^{max}(n) + 2x_h(n)P_O(n), \\
cc(n) =& x_h(n)\mathbf{X}\mathbf{V}^T I_B^{max}(n) - \mathbf{X}\mathbf{X}^T\left(I_B^{max}(n)\right)^2 R - x_h^2(n)P_O(n).
\end{aligned}$$

7.3.4 Proof of Proposition 5.5.3 and Proposition 5.5.4

For the charging process, based on (7.3.5),

$$\begin{aligned}
\sqrt{P_L(n)} &= \frac{-\sqrt{\lambda(C(n))} + \sqrt{\lambda(C(n)) + 4P_O(n)}}{2} \\
&= \frac{2P_O(n)}{\sqrt{\lambda(C(n))} + \sqrt{\lambda(C(n)) + 4P_O(n)}}.
\end{aligned} \tag{7.3.14}$$

Given $P_O(n) = P_O^{req}(n)$, $P_L(C(n), P_O(n) = P_O^{req}(n))$ decreases as $\lambda(n)$ increases. It has been shown in Subsection 7.3.2 that $\lambda(C(n))$ increases as $C(n)$ increases. Thus, $P_L(C(n), P_O(n) = P_O^{req}(n))$ decreases as $C(n)$ increases.

Given $I_B^{max}(n) = I_B^{ub}$, based on (7.3.9) and (5.5.3), the total power loss $P_L(C(n),$ $I_B^{max}(n) = I_B^{ub})$ increases as $C(n)$ increases. If P_L^{ub} falls within the range of $P_L(C(n),$ $I_B^{max}(n) = I_B^{ub})$, all possible cases of $P_L(C(n), P_O(n) = P_O^{req}(n))$ with various $P_O^{req}(n)$'s are shown in Figure 7.3.1. For the three cases, the minimum and maximum total power loss satisfying (5.3.3), (5.5.5), (5.5.6), and (5.5.14), are denoted by $P_L^{min}(C(n), P_O(n) = P_O^{req}(n))$ and $P_L^{max}(C(n), P_O(n) = P_O^{req}(n))$, respectively, and

they are given in Table 7.3.1. By combining the results of all cases, if P_L^{ub} falls within the range of $P_L(C(n), I_B^{max}(n) = I_B^{ub})$, the calculation formulas for $P_L^{min}(C(n), P_O(n) = P_O^{req}(n))$ and $P_L^{max}(C(n), P_O(n) = P_O^{req}(n))$ in Proposition 5.5.3 are obtained. Otherwise, if P_L^{ub} falls outside the range of $P_L(C(n), I_B^{max}(n) = I_B^{ub})$, given (5.5.7), it can also be shown that the formulas for $P_L^{min}(C(n), P_O(n) = P_O^{req}(n))$ and $P_L^{max}(C(n), P_O(n) = P_O^{req}(n))$ in Proposition 5.5.3 still hold.

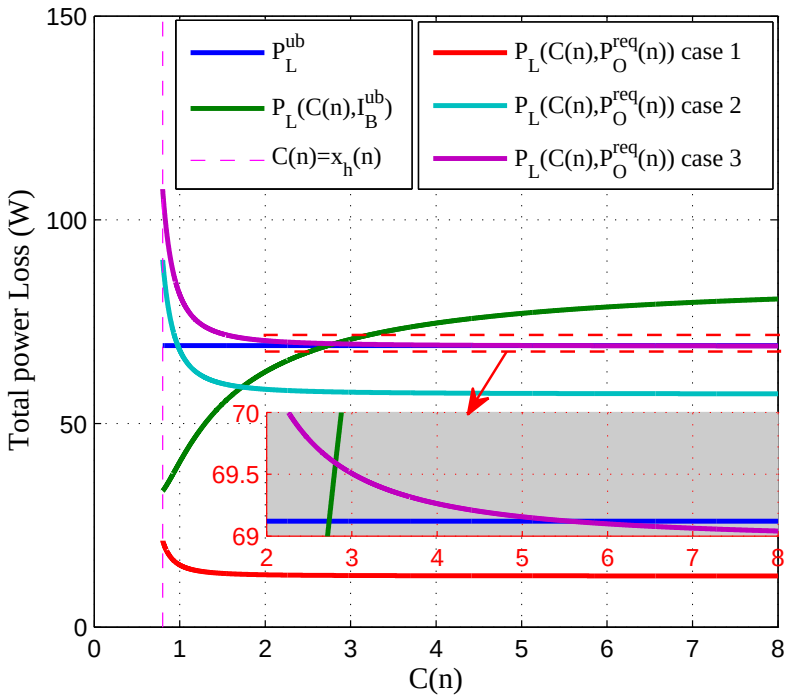

FIGURE 7.3.1: Illustration of the total power loss upper bound P_L^{ub}, the total power loss with module current upper bound $P_L(C(n), I_B^{max}(n) = I_B^{ub})$, and the total power losses given different total power requirements $P_L(C(n), P_O(n) = P_O^{req}(n))$.

For the discharging process, based on (7.3.5), $P_L(n) = \left(\frac{\sqrt{\lambda(n)} \pm \sqrt{\lambda(n) - 4P_O(n)}}{2}\right)^2$.

TABLE 7.3.1: Minimum and maximum $P_L(C(n), P_O(n) = P_O^{req}(n))$'s satisfying (5.3.3), (5.5.5), (5.5.6), and (5.5.14) for the three cases shown in Figure 7.3.1.

Case	$P_L^{min}(C(n), P_O(n) = P_O^{req}(n))$	$P_L^{max}(C(n), P_O(n) = P_O^{req}(n))$
Case 1	$P_L(C(n) = +\infty, P_O(n) = P_O^{req}(n))$	$P_L(C(n) = x_h(n), P_O(n) = P_O^{req}(n))$
Case 2	$P_L(C(n) = +\infty, P_O(n) = P_O^{req}(n))$	$P_L(I_B^{max}(n) = I_B^{ub}, P_O(n) = P_O^{req}(n))$
Case 3	$P_L(C(n) = +\infty, P_O(n) = P_O^{req}(n))$	P_L^{ub}

Given (5.5.12), $P_L(n) \leq \left(\frac{\sqrt{\lambda(n)}}{2}\right)^2$, then we select

$$\begin{aligned} P_L(n) &= \left(\frac{\sqrt{\lambda(F(n))} - \sqrt{\lambda(F(n)) - 4P_O(n)}}{2}\right)^2 \\ &= \left(\frac{2P_O(n)}{\sqrt{\lambda(F(n))} + \sqrt{\lambda(F(n)) - 4P_O(n)}}\right)^2. \end{aligned} \tag{7.3.15}$$

Given $P_O(n) = P_O^{req}(n)$, $P_L(F(n), P_O(n) = P_O^{req}(n))$ decreases as $\lambda(n)$ increases. It has been shown in Subsection 7.3.2 that $\lambda(F(n))$ is an increasing function for $-\infty \leq F(n) \leq F^*(n)$ and a decreasing function for $F^*(n) \leq F(n) \leq x_l(n)$. Thus, $P_L(F(n), P_O(n) = P_O^{req}(n))$ decreases as $F(n)$ increases from $-\infty$ to $F^*(n)$, and $P_L(F(n), P_O(n) = P_O^{req}(n))$ increases as $F(n)$ increases from $F^*(n)$ to $x_l(n)$.

Given $I_B^{max}(n) = I_B^{ub}$, it follows (7.3.13) and (5.5.3) that, the total power loss $P_L(F(n), I_B^{max}(n) = I_B^{ub})$ decreases as $F(n)$ increases. Then using the similar procedure for charging process, we consider all possible cases during the discharging process and combine the minimum and maximum total power losses of all cases to get the results shown in Proposition 5.5.4.

7.3.5 Proof of Proposition 5.5.5

For the charging process, based on the analysis in Subsection 7.3.4, given (5.5.14), $P_L(C(n), P_O(n) = P_O^{req}(n))$ decreases as $C(n)$ increases for $C(n) \in [x_h(n), +\infty]$. On the other hand, it follows (7.3.9) that, $\alpha_m(n)$ increases as $C(n)$ increases. Then, given (5.5.14), based on (5.5.3), $I_B^{max}(n) = \sqrt{\frac{P_L(n)}{\boldsymbol{\alpha}\boldsymbol{\alpha}^T R}}$ decreases as $C(n)$ increases for $C(n) \in [x_h(n), +\infty]$. Thus, given (5.5.14), based on (5.3.9), $R_{SOC}(n+1)$ increases as $C(n)$ increases for $C(n) \in [x_h(n), +\infty]$.

Similarly, for the discharging process, based on the analysis in Subsection 7.3.4, given (5.5.14), $P_L(F(n), P_O(n) = P_O^{req}(n))$ increases as $F(n)$ increases from $F^*(n)$ to $x_l(n)$. Then based on (7.3.13), (5.5.3), and (5.5.14), we can show that $I_B^{max}(n) = \sqrt{\frac{P_L(n)}{\boldsymbol{\alpha}\boldsymbol{\alpha}^T R}}$ increases as $F(n)$ increases for $F(n) \in [F^*(n), x_l(n)]$. Thus, given (5.5.14), based on (5.3.9), $R_{SOC}(n+1)$ decreases as $F(n)$ increases for $F(n) \in [F^*(n), x_l(n)]$.

7.3.6 Proof of Proposition 5.5.6

Given $P_O(n) = P_O^{req}(n) < P_O^{max}(n)$ and $P_L(n) \in [P_L^{min}(n), P_L^{max}(n)]$ in the CDS-based current allocation, $P_B(n)$ can be obtained by (5.5.4) and then $\lambda(n)$ can be calculated by (5.5.9). For the charging process, based on (5.5.1) and (5.5.9), using $\lambda(n) = \frac{\left(\mathbf{v}\boldsymbol{\alpha}^T\right)^2}{\boldsymbol{\alpha}\boldsymbol{\alpha}^T R}$, we get a quadratic equation of $C(n)$:

$$a(n)C^2(n) + b(n)C(n) + c(n) = 0, \tag{7.3.16}$$

where $a(n)$, $b(n)$, and $c(n)$ are given in Proposition 5.5.6. Then the square root of (7.3.16) satisfying (5.3.3) is selected as $C(n)$, shown in (5.5.17). Similarly, for the discharging process, we can obtain $F(n)$ as shown in (5.5.18). Based on the $C(n)$

(or $F(n)$) obtained in (5.5.17) (or (5.5.18)), using (5.5.1) and (5.5.3), $I_B^{max}(n)$ can be calculated by (5.5.19).

Bibliography

[1] "Global energy storage database," 2017.

[2] X. Hu, C. Zou, C. Zhang, and Y. Li, "Technological developments in batteries: A survey of principal roles, types, and management needs," *IEEE Power Energy Mag.*, vol. 15, pp. 20–31, Sept 2017.

[3] T. Morstyn, A. Savkin, B. Hredzak, and V. Agelidis, "Multi-agent sliding mode control for state of charge balancing between battery energy storage systems distributed in a dc microgrid," *IEEE Trans. Smart Grid*, vol. PP, no. 99, pp. 1–9, 2017.

[4] "SDG&E unveils worlds largest lithium ion battery storage facility," 2017.

[5] W. F. Bentley, "Cell balancing considerations for lithium-ion battery systems," in *Proc. 12th Annu. Battery Conf. Appl. Adv.*, pp. 223–226, Jan. 1997.

[6] H. S. Park, C. H. Kim, K. B. Park, G. W. Moon, and J. H. Lee, "Design of a charge equalizer based on battery modularization," *IEEE Trans. Veh. Technol.*, vol. 58, pp. 3216–3223, Sept. 2009.

[7] S. Chen, C. C. Chen, H. P. Huang, and C. C. Hwu, "Implementation of cell balancing with super-capacitor for robot power system," in *Proc. 9th World Congr. Intell. Control Autom.*, pp. 468–473, June 21-25, 2011.

[8] J. Kim, J. Shin, C. Chun, and B. H. Cho, "Stable configuration of a li-ion series battery pack based on a screening process for improved voltage/soc balancing," *IEEE Trans. Power Electron.*, vol. 27, pp. 411–424, Jan. 2012.

[9] J. Cao, N. Schofield, and A. Emadi, "Battery balancing methods: A comprehensive review," in *IEEE Veh. Power Propulsion Conf.*, pp. 1–6, Sept. 2008.

[10] L. Lu, X. Han, J. Li, J. Hua, and M. Ouyang, "A review on the key issues for lithium-ion battery management in electric vehicles," *Journal of Power Sources*, vol. 226, pp. 272–288, 2013.

[11] N. Kutkut and D. Divan, "Dynamic equalization techniques for series battery stacks," in *Proc. IEEE 18th INTELEC*, pp. 514–521, Oct. 1996.

[12] K. Nishijima, H. Sakamoto, and K. Harada, "A pwm controlled simple and high performance battery balancing system," in *31st IEEE Annual Power Electronics Specialists Conference (PESC'00)*, vol. 1, pp. 517–520, 2000.

[13] S. W. Moore and P. J. Schneider, "A review of cell equalization methods for lithium ion and lithium polymer battery systems," tech. rep., SAE Technical Paper, 2001.

[14] Z. G. Kong, C. B. Zhu, R. G. Lu, and S. K. Cheng, "Comparison and evaluation of charge equalization technique for series connected batteries," in *Proc. IEEE Power Electron. Spec. Conf.*, pp. 1–6, June 2006.

[15] M. Daowd, N. Omar, P. Van den Bossche, and J. Van Mierlo, "Passive and active battery balancing comparison based on matlab simulation," in *Proc. IEEE Vehicle. Power Propulsion Conf.*, pp. 1–7, Sept. 2011.

[16] J. Gallardo-Lozano, E. Romero-Cadaval, M. I. Milanes-Montero, and M. A. Guerrero-Martinez, "Battery equalization active methods," *J. Power Sources*, vol. 246, pp. 934–949, Jan. 2014.

[17] H. Shen, W. Zhu, and W. Chen, "Charge equalization for series connected lithium-ion batteries," in *Proc. IEEE ICEMI Conf.*, pp. 4–1032–4–1037, Aug. 2009.

[18] B. Dong and Y. Han, "A new architecture for battery charge equalization," in *IEEE Energy Conversion Congress and Exposition*, pp. 928–934, Sept. 2011.

[19] C. H. Kim, M. Y. Kim, H. S. Park, and G. W. Moon, "A modularized two-stage charge equalizer with cell selection switches for series-connected lithium-ion battery string in an HEV," *IEEE Trans. Power Electron.*, vol. 27, pp. 3764–3774, Aug. 2012.

[20] W. Han, L. Zhang, and Y. Han, "Mathematical modeling, performance analysis and control of battery equalization systems: Review and recent developments," in *Advances in Battery Manufacturing, Services, and Management Systems* (J. Li, S. Zhou, and Y. Han, eds.), ch. 12, pp. 281–301, New York: Wiley-IEEE Press, 2016.

[21] Y. S. Lee and M. W. Cheng, "Intelligent control battery equalization for series connected lithium-ion battery strings," *IEEE Trans. Ind. Electron.*, vol. 52, pp. 1297–1307, Oct. 2005.

[22] D. Zhang, S. Qiu, G. Zhu, Y. Ma, W. Chen, and S. Wong, "Balancing control strategy for li-ion batteries string based on balanced point," in *IEEE Veh. Power Propulsion Conf.*, pp. 1–5, Oct. 2013.

[23] L. R. Yu, Y. C. Hsieh, W. C. Liu, and C. S. Moo, "Balanced discharging for serial battery power modules with boost converters," in *ICSSE*, pp. 449–453, July 2013.

[24] J. Yan, Z. Cheng, G. Xu, H. Qian, and Y. Xu, "Fuzzy control for battery equalization based on state of charge," in *2010 IEEE 72nd VTC*, pp. 1–7, Sept. 2010.

[25] M. Samadi and M. Saif, "Nonlinear model predictive control for cell balancing in li-ion battery packs," in *American Control Conference, 2014*, pp. 2924–2929, June 2014.

[26] D. D. Quinn and T. T. Hartley, "Design of novel charge balancing networks in battery packs," *Journal of Power Sources*, vol. 240, pp. 26–32, 2013.

[27] M. Einhorn, W. Roessler, and J. Fleig, "Improved performance of serially connected li-ion batteries with active cell balancing in electric vehicles," *IEEE Trans. Veh. Technol.*, vol. 60, pp. 2448–2457, July 2011.

[28] Y. Guo, R. Lu, G. Wu, and C. Zhu, "A high efficiency isolated bidirectional equalizer for lithium-ion battery string," in *IEEE Veh. Power Propulsion Conf.*, pp. 962–966, Oct. 2012.

[29] M. Tang and T. Stuart, "Selective buck-boost equalizer for series battery packs," *IEEE Transactions on Aerospace and Electronic Systems*, vol. 36, no. 1, pp. 201–211, 2000.

[30] L. Yuang-Shung, M.-W. Cheng, Y. Shun-Ching, and H. Co-Lin, "Individual cell equalization for series connected lithium-ion batteries," *IEICE transactions on communications*, vol. 89, no. 9, pp. 2596–2607, 2006.

[31] P. A. Cassani and S. S. Williamson, "Feasibility analysis of a novel cell equalizer topology for plug-in hybrid electric vehicle energy-storage systems," *IEEE Transactions on Vehicular Technology*, vol. 58, no. 8, pp. 3938–3946, 2009.

[32] M.-Y. Kim, J.-W. Kim, C.-H. Kim, S.-Y. Cho, and G.-W. Moon, "Automatic charge equalization circuit based on regulated voltage source for series connected lithium-ion batteries," in *8th IEEE International Conference on Power Electronics and ECCE Asia (ICPE & ECCE)*, pp. 2248–2255, 2011.

[33] C.-H. Lin, C.-M. Wang, H.-Y. Chao, and M.-H. Hung, "Dual-balancing control for improving imbalance phenomenon of lithium-ion battery packs," in *3rd IEEE International Conference on Sustainable Energy Technologies (ICSET)*, pp. 229–234, Sept 2012.

[34] R. Ling, Y. Dong, H. Yan, M. Wu, and Y. Chai, "Fuzzy-PI control battery equalization for series connected lithium-ion battery strings," in *Power Electronics and Motion Control Conference (IPEMC), 2012 7th International*, vol. 4, pp. 2631–2635, June 2012.

[35] Y. Yuanmao, K. Cheng, and Y. Yeung, "Zero-current switching switched-capacitor zero-voltage-gap automatic equalization system for series battery

string," *IEEE Transactions on Power Electronics*, vol. 27, no. 7, pp. 3234–3242, 2012.

[36] M. Baric and F. Borrelli, "Decentralized robust control invariance for a network of storage devices," *IEEE Transactions on Automatic Control*, vol. 57, pp. 1018–1024, April 2012.

[37] C. Danielson, F. Borrelli, D. Oliver, D. Anderson, M. Kuang, and T. Phillips, "Balancing of battery networks via constrained optimal control," in *American Control Conference (ACC)*, pp. 4293–4298, June 2012.

[38] M. Preindl, C. Danielson, and F. Borrelli, "Performance evaluation of battery balancing hardware," in *European Control Conference (ECC)*, pp. 4065–4070, 2013.

[39] C. Danielson, F. Borrelli, D. Oliver, D. Anderson, and T. Phillips, "Constrained flow control in storage networks: Capacity maximization and balancing," *Automatica*, vol. 49, no. 9, pp. 2612–2621, 2013.

[40] M. Caspar and S. Hohmann, "Optimal cell balancing with model-based cascade control by duty cycle adaption," in *19th IFAC World Congress*, pp. 10311–10318, 2014.

[41] H. Chen, L. Zhang, and Y. Han, "System-theoretic analysis of a class of battery equalization systems: Mathematical modeling and performance evaluation," *IEEE Trans. Veh. Technol.*, vol. 64, pp. 1445–1457, April 2015.

[42] W. Han, L. Zhang, and Y. Han, "Computationally efficient methods for state of charge approximation and performance measure calculation in series-connected

battery equalization systems," *Journal of Power Sources*, vol. 286, no. 0, pp. 145 – 158, 2015.

[43] F. Ju, W. Deng, and J. Li, "Modularized global equalization of battery cells for electric vehicles," in *IEEE International Conference on Robotics and Automation (ICRA)*, pp. 1681–1686, May 2014.

[44] S. Yarlagadda, T. Hartley, and I. Husain, "A battery management system using an active charge equalization technique based on a DC/DC converter topology," *IEEE Transactions on Industry Applications*, vol. 49, pp. 2720–2729, Nov 2013.

[45] F. Ju, J. Wang, J. Li, G. Xiao, and S. Biller, "Virtual battery: A battery simulation framework for electric vehicles," *IEEE Transactions on Automation Science and Engineering*, vol. 10, no. 1, pp. 5–15, 2013.

[46] M. Daowd, M. Antoine, N. Omar, P. Lataire, P. Van Den Bossche, and J. Van Mierlo, "Battery management systembalancing modularization based on a single switched capacitor and bi-directional dc/dc converter with the auxiliary battery," *Energies*, vol. 7, no. 5, pp. 2897–2937, 2014.

[47] H.-S. Park, C.-H. Kim, K.-B. Park, G.-W. Moon, and J.-H. Lee, "Design of a charge equalizer based on battery modularization," *IEEE Transactions on Vehicular Technology*, vol. 58, pp. 3216–3223, Sept 2009.

[48] C.-H. Kim, M.-Y. Kim, and G.-W. Moon, "A modularized charge equalizer using a battery monitoring ic for series-connected li-ion battery strings in electric vehicles," *IEEE Transactions on Power Electronics*, vol. 28, no. 8, pp. 3779–3787, 2013.

[49] Y. Li and Y. Han, "Power electronics integration on battery cells," in *IEEE 29th Applied Power Electronics Conference and Exposition*, pp. 3318–3322, March 2014.

[50] J. Xu, S. Li, C. Mi, Z. Chen, and B. Cao, "SOC based battery cell balancing with a novel topology and reduced component count," *Energies*, vol. 6, no. 6, pp. 2726–2740, 2013.

[51] R. Ling, Q. Dan, J. Zhang, and G. Chen, "A distributed equalization control approach for series connected battery strings," in *26th Chinese Control and Decision Conference (2014 CCDC)*, pp. 5102–5106, May 2014.

[52] J. W. Kim, J. W. Shin, and J. I. Ha, "Cell balancing control using adjusted filters in flyback converter with single switch," in *IEEE Energy Conversion Congress and Exposition*, pp. 287–291, Sept. 2013.

[53] N. T. T. Ngoc, "Adaptive Neuro-Fuzzy Control Circuit for Cell Equalization in Battery Management System," Master's thesis, Ulsan National Institute of Science and Technology, South Korea, 2014.

[54] Y. Zheng, M. Ouyang, L. Lu, J. Li, X. Han, and L. Xu, "On-line equalization for lithium-ion battery packs based on charging cell voltages: Part 2. fuzzy logic equalization," *Journal of Power Sources*, vol. 247, pp. 460–466, 2014.

[55] S. Wen, "Cell balancing buys extra run time and battery life," *Analog Applications Journal*, pp. 14–18, 2009.

[56] Q. Ouyang, J. Chen, J. Zheng, and Y. Hong, "SOC estimation-based quasi-sliding mode control for cell balancing in lithium-ion battery packs," *IEEE Trans. Ind. Electron.*, vol. 65, pp. 3427–3436, April 2018.

[57] M. B. Ketzer, A. M. N. Lima, A. C. Oliveira, and C. B. Jacobina, "Evaluating circuit topologies for battery charge equalization," in *39th Annu. Conf. of the IEEE Ind. Electron. Soc.*, pp. 743–748, Nov 2013.

[58] Q. Ouyang, J. Chen, J. Zheng, and H. Fang, "Optimal cell-to-cell balancing topology design for serially connected lithium-ion battery packs," *IEEE Trans. Sustain. Energy*, vol. 9, pp. 350–360, Jan 2018.

[59] V. Johnson, "Battery performance models in ADVISOR," *J. Power Sources*, vol. 110, no. 2, pp. 321–329, 2002.

[60] R. Tichy, "Use cell balancing to enable large-scale li-ion batteries," 2009.

[61] D. Rosewater, S. Ferreira, D. Schoenwald, J. Hawkins, and S. Santoso, "Battery energy storage state-of-charge forecasting: Models, optimization, and accuracy," *IEEE Trans. Smart Grid*, vol. PP, no. 99, pp. 1–10, 2018.

[62] Y. Barsukov, "Battery cell balancing: What to balance and how," in *Portable Power Design Seminar, Texas Instruments*, 2006.

[63] C. Mikolajczak, M. Kahn, K. White, and R. T. Long, *Lithium-ion batteries hazard and use assessment*. Springer Science & Business Media, 2012.

[64] C. Zhou and L. Zhang, "Modeling and computationally efficient algorithms for analysis of battery equalization systems," in *12th World Congress on Intelligent Control and Automation*, pp. 344–349, June 2016.

[65] J. Rivera-Barrera, N. Muoz-Galeano, and H. Sarmiento-Maldonado, "SoC estimation for lithium-ion batteries: Review and future challenges," *Electron.*, vol. 6, p. 102, Nov 2017.

[66] M. Hannan, M. Lipu, A. Hussain, and A. Mohamed, "A review of lithium-ion battery state of charge estimation and management system in electric vehicle applications: Challenges and recommendations," *Renewable Sustain. Energy Rev.*, vol. 78, pp. 834 – 854, 2017.

[67] L. Y. Wang, C. Wang, G. Yin, F. Lin, M. P. Polis, C. Zhang, and J. Jiang, "Balanced control strategies for interconnected heterogeneous battery systems," *IEEE Trans. Sustain. Energy*, vol. 7, no. 1, pp. 189–199, 2016.

[68] C. Zhang, L. Y. Wang, X. Li, W. Chen, G. G. Yin, and J. Jiang, "Robust and adaptive estimation of state of charge for lithium-ion batteries," *IEEE Trans. Ind. Electron.*, vol. 62, pp. 4948–4957, Aug 2015.

[69] C. Zou, C. Manzie, D. Nei, and A. G. Kallapur, "Multi-time-scale observer design for state-of-charge and state-of-health of a lithium-ion battery," *J. Power Sources*, vol. 335, pp. 121 – 130, 2016.

[70] C. Zou, X. Hu, S. Dey, L. Zhang, and X. Tang, "Nonlinear fractional-order estimator with guaranteed robustness and stability for lithium-ion batteries," *IEEE Trans. Ind. Electron.*, vol. 65, pp. 5951–5961, July 2018.

[71] X. Lin, A. G. Stefanopoulou, Y. Li, and R. D. Anderson, "State of charge imbalance estimation for battery strings under reduced voltage sensing," *IEEE Trans. Control Syst. Technol.*, vol. 23, no. 3, pp. 1052–1062, 2015.

[72] W. Han and L. Zhang, "Charge transfer and energy transfer analysis of battery charge equalization," in *IEEE Int. Conf. Automation Science and Engineering*, pp. 1137–1138, Aug 2015.

[73] W. Han and L. Zhang, "Charging and discharging spaces-based current allocation in parallel-connected battery systems," in *IEEE Int. Conf. Automation Science and Engineering*, pp. 1209–1214, Aug 2016.

[74] W. Han and L. Zhang, "Mathematical analysis and coordinated current allocation control in battery power module systems," *J. Power Sources*, vol. 372, pp. 166 – 179, 2017.

[75] Z. G. Kong, C. B. Zhu, R. G. Lu, and S. K. Cheng, "Comparison and evaluation of charge equalization technique for series connected batteries," in *Proc. IEEE Power Electron. Spec. Conf.*, pp. 1–6, June 2006.

[76] S. Ci, N. Lin, and D. Wu, "Reconfigurable battery techniques and systems: A survey," *IEEE Access*, vol. 4, pp. 1175–1189, 2016.

[77] L. He, L. Gu, L. Kong, Y. Gu, C. Liu, and T. He, "Exploring adaptive reconfiguration to optimize energy efficiency in large-scale battery systems," in *2013 IEEE 34th Real-Time Systems Symposium*, pp. 118–127, Dec 2013.

[78] S. Ci, J. Zhang, H. Sharif, and M. Alahmad, "A novel design of adaptive reconfigurable multicell battery for power-aware embedded networked sensing systems," in *IEEE Global Telecommunications Conference*, pp. 1043–1047, Nov 2007.

[79] H. Kim and K. G. Shin, "On dynamic reconfiguration of a large-scale battery system," in *15th IEEE Real-Time and Embedded Technology and Applications Symposium*, pp. 87–96, April 2009.

[80] T. Kim, W. Qiao, and L. Qu, "Series-connected self-reconfigurable multicell battery," in *26th Annual IEEE Applied Power Electronics Conference and Exposition (APEC)*, pp. 1382–1387, March 2011.

[81] H. Kim and K. G. Shin, "Scheduling of battery charge, discharge, and rest," in *30th IEEE Real-Time Systems Symposium*, pp. 13–22, Dec 2009.

[82] G. Wang, J. Pou, and V. G. Agelidis, "Reconfigurable battery energy storage system for utility-scale applications," in *Annu. Conf. IEEE Ind. Electron. Soc.*, pp. 004086–004091, Nov 2015.

[83] L. He, L. Kong, S. Lin, S. Ying, Y. J. Gu, T. He, and C. Liu, "RAC: Reconfiguration-assisted charging in large-scale lithium-ion battery systems," *IEEE Trans. Smart Grid*, vol. 7, pp. 1420–1429, May 2016.

[84] L. He, Z. Yang, Y. Gu, C. Liu, T. He, and K. G. Shin, "SoH-aware reconfiguration in battery packs," *IEEE Trans. Smart Grid*, vol. PP, no. 99, pp. 1–1, 2017.

[85] J. Cabrera, A. Vega, F. Tobajas, V. Dniz, and H. A. Fabelo, "Design of a reconfigurable li-ion battery management system (BMS)," in *Technol. Appl. Electron. Teaching*, pp. 1–6, June 2014.

[86] T. Kim, W. Qiao, and L. Qu, "Power electronics-enabled self-x multicell batteries: A design toward smart batteries," *IEEE Trans. Power Electron.*, vol. 27, pp. 4723–4733, Nov 2012.

[87] E. W. Weisstein, "Permutation matrix."

[88] Z. Zhang and S. Cuk, "A high efficiency 1.8 kw battery equalizer," in *8th Annual Applied Power Electronics Conference and Exposition*, pp. 221–227, Mar 1993.

[89] M. Y. Kim, J. H. Kim, and G. W. Moon, "Center-cell concentration structure of a cell-to-cell balancing circuit with a reduced number of switches," *IEEE Trans. Power Electron.*, vol. 29, pp. 5285–5297, Oct 2014.

[90] M. Mitchell, *An Introduction to Genetic Algorithms*. MIT press, 1996.

[91] W.-Y. Chang, "The state of charge estimating methods for battery: A review," *ISRN Applied Mathematics*, vol. 2013, 2013.

[92] N. Watrin, B. Blunier, and A. Miraoui, "Review of adaptive systems for lithium batteries State-of-Charge and State-of-Health estimation," in *IEEE Transportation Electrification Conference and Expo (ITEC)*, pp. 1–6, June 2012.

[93] V. Prajapati, H. Hess, E. J. William, V. Gupta, M. Huff, M. Manic, F. Rufus, A. Thakker, and J. Govar, "A literature review of state of-charge estimation techniques applicable to lithium poly-carbon monoflouride (li/cfx) battery," in *India International Conference on Power Electronics 2010 (IICPE2010)*, pp. 1–8, Jan 2011.

[94] W. Han and L. Zhang, "Charging and discharging spaces-based current allocation in parallel-connected battery systems," in *IEEE International Conference on Automation Science and Engineering (CASE)*, pp. 1209–1214, Aug 2016.

[95] M. Einhorn, W. Guertlschmid, T. Blochberger, R. Kumpusch, R. Permann, F. V. Conte, C. Kral, and J. Fleig, "A current equalization method for serially connected battery cells using a single power converter for each cell," *IEEE Tran. Veh. Technol.*, vol. 60, pp. 4227–4237, Nov 2011.

[96] N. Nguyen, S. K. Oruganti, K. Na, and F. Bien, "An adaptive backward control battery equalization system for serially connected lithium-ion battery packs," *IEEE Tran. Veh. Technol.*, vol. 63, pp. 3651–3660, Oct 2014.

[97] C.-S. Moo, K. S. Ng, and Y.-C. Hsieh, "Parallel operation of battery power modules," *IEEE Tran. Energy Convers.*, vol. 23, pp. 701–707, June 2008.

[98] K.-H. Lin, L.-R. Yu, C.-S. Moo, and C.-Y. Juan, "Analysis on parallel operation of boost-type battery power modules," in *10th IEEE International Conference on Power Electronics and Drive Systems (PEDS)*, pp. 809–813, April 2013.

[99] K.-H. Lin, "Operation of boost-type battery power modules in parallel," Master's thesis, National Sun Yat-sen University, Taiwan, 2013.

[100] Y. Li and Y. Han, "Control of input-series and output-independent power converter building block system based on buck converter topology," in *IEEE Applied Power Electronics Conference and Exposition (APEC)*, pp. 422–429, March 2015.

[101] E. Kim, K. Shin, and J. Lee, "Real-time battery thermal management for electric vehicles," in *ACM/IEEE International Conference on Cyber-Physical Systems (ICCPS)*, pp. 72–83, April 2014.

[102] B.-Y. Choi, S.-R. Lee, J.-W. Kang, and C.-Y. Won, "Battery balancing algorithm for parallel operation of single phase ups inverters," in *IEEE Conference and Expo Transportation Electrification Asia-Pacific (ITEC Asia-Pacific)*, pp. 1–6, Aug 2014.

[103] L. Lam, P. Bauer, and E. Kelder, "A practical circuit-based model for li-ion battery cells in electric vehicle applications," in *33rd IEEE International Telecommunications Energy Conference (INTELEC)*, pp. 1–9, Oct 2011.

[104] J. Jaguemont, L. Boulon, and Y. Dub, "Characterization and modeling of a hybrid-electric-vehicle lithium-ion battery pack at low temperatures," *IEEE Tran. Veh. Technol.*, vol. 65, pp. 1–14, Jan 2016.

[105] "Ultralife UBBL10 technical datasheet," 2010.

[106] J. Li, M. Mazzola, J. Gafford, and N. Younan, "A new parameter estimation algorithm for an electrical analogue battery model," in *27th IEEE Applied Power Electronics Conference and Exposition (APEC)*, pp. 427–433, Feb 2012.